University of Alberta
Department of Civil &
Environmental Engineering

Structural Engineering Report No. 256

CFRP Sheets Application to Masonry Shear Walls with Openings

by

Honglan Miao

A.E. Elwi

J.J.R. Cheng

February, 2005

CFRP Sheets Application to Masonry Shear Walls with Openings

by

Honglan Miao

A.E. Elwi

J.J.R. Cheng

Structural Engineering Report 256

Department of Civil and Environmental Engineering

University of Alberta

Edmonton, Alberta

February 2005

Acknowledgements

Financial support for the research was provided by the Network of Intelligent Sensing for Innovative Structures (ISIS), The Alberta Masonry Contractor Association, The Natural Sciences and Engineering Research Council of Canada (NSERC) and the University of Alberta.

ABSTRACT

This thesis described an experimental program that investigated strengthening of masonry shear walls with openings using externally bonded Carbon Fiber Reinforced Polymer (CFRP) Sheets carried out at University of Alberta. Four wall specimens were designed and tested under combined uniformly distributed constant vertical load and monotonic in-plane lateral load. The variables in this test included the amount and layout of CFRP Sheets. This thesis analyzed the general shear wall behavior based on lateral load-top displacement curves, cracking patterns and the action of the CFRP Sheets to walls. The test results showed that the lateral load capacity and displacement ability of strengthened walls with CFRP Sheets were increased remarkably. Moreover, CFRP Sheets were effective in enhancing the stiffness of walls in the later loading stage. Finally, several mechanical models were presented to estimate the shear contribution of CFRP Sheets to the perforated masonry shear walls. Four methods to predict wall stiffness were also discussed.

TABLE OF CONTENTS

LIST OF TABLES

LIST OF FIGURES

LIST OF PHOTOS

LIST OF ABBREVIATIONS AND SYMBOLS

Abbreviation

ASTM	American Society for Testing and Materials
ACI	American Concrete Institute
ASCE	American Society of Civil Engineers
CFRP	Carbon Fibre Reinforced Polymer
CSA	Canadian Standards Association
GFRP	Glass Fibre Reinforced Polymer
FRP	Fibre Reinforced Polymer
HSS	Hollow Structural Section
kN	Kilo Newton
LVDT	Linear Variable Differential Transformer
m	Meter
mm	Millimeter
MPa	Mega Pascal
MSJC	Masonry Standards Joint Committee
MTS	Material Testing System
N	Newton
TMS	The Minerals, Metals & Materials Society
W	Wide Flange Beam Designation
URM	Unreinforced Masonry

Symbols

A = wall cross-sectional area, (mm^2)

A_e = effective cross-sectional area of wall, (mm^2)

A_g = gross cross-sectional area of wall, (mm^2)

A_f = cross-sectional area of the FRP reinforcement, (mm^2)

A_v = cross-sectional area of web reinforcement, (mm^2)

b = width of pier, (mm)

d = effective depth of pier, (mm)

d_i = distance from the i^{th} FRP rod to the furthest corner of the wall which carries maximum compression, (mm)

d_1 = moment arm of F_1, (mm)

d_2 = moment arm of F_3, (mm)

d_3 = moment arm of uniformly distributed gravity load, (mm)

E = modulus of elasticity of steel bars, (MPa)

E_c = calculated modulus of elasticity of coupon CFRP composite, (MPa)

E_e = Tested modulus of elasticity of coupon CFRP composite, (MPa)

E_f = modulus of elasticity of fibre, (MPa)

E_{frp} = modulus of elasticity of FRP composite, (MPa)

E_m = modulus of elasticity of masonry, (MPa)

E_m' = modulus of elasticity of epoxy, (MPa)

F_1 = force developed by vertical CFRP strips around opening, (kN)

F_1' = Force developed in the FRP rod farthest from the bottom compression zone, (kN)

F_2 = Force developed by horizontal CFRP strips at the bottom of opening , (kN)

F_3 = Force developed by vertical CFRP strips in the middle of the pier, (kN)

F_v = Allowable shear stress of wall, (MPa)

$F_{v,v}$ = contribution of the vertical FRP reinforcement to shear stress, (kN)

f_f = assumed tensile stress in the FRP reinforcement, (MPa)

f_m' = compressive strength of masonry, (MPa)

f_y = Yield stress in steel reinforcement, (MPa)

f_v = Calculated shear stress of wall, (MPa)

G_m = modulus of rigidity of the masonry, (MPa)

H = height of wall, (mm)

h_1 = moment arm of V_f, (mm)

h_2 = moment arm of F_2, (mm)

h_w = pier height, (mm)

I = second moment area of wall, (mm^4)

i = 1 to m

K = wall stiffness, (N/mm)

k_i = stiffness of the i^{th} pier, (N/mm)

L = length of wall, (mm)

L_w = length of pier, (mm)

M/(Vd) = shear span

M_0 = Moment of point O, (kN.m)

m = total number of vertical FRP rods

n = number of FRP rods crossing the cracks

P' = factored gravity load, (kN)

P_u = load capacity of walls, (kN)

q = uniformly distributed gravity load, (kN/m)

$\dot{q}$ = aspect ratio of the pier

r' = aspect ratio of the top spandrel

s = spacing of shear reinforcement measured parallel to the longitudinal axis of the member, (mm)

s' = aspect ratio of the bottom spandrel

t = nominal thickness of the wall, (mm)

V = shear force applied on wall, (kN)

V' = shear force applied on pier, (kN)

$V_{F.H}$ = horizontal FRP reinforcement contribution to shear strength, (kN)

V_f = ultimate load carried by pier, (kN)

V_f = volume fraction of the fibre

V_{frp} = shear resistance of FRP, (kN)

V_m = shear strength contributed by masonry, (kN)

$V_{m'}$ = volume fraction of the epoxy

$V_{m,v}$ = shear capacity of wall without FRP reinforcement, (kN)

V_s = shear resistance of shear reinforcement, (kN)

Δ = total wall deflection, (mm)

Δi = deflection of the i^{th} pier, (mm)

Δ_m = moment deflection, (mm)

Δ_u = lateral displacement capacity of wall, (mm)

Δ_v = shear deflection, (mm)

$\varepsilon_{frp.e}$ = effective FRP strain

$\varepsilon_{frp,u}$ = ultimate tensile strain of FRP

Φ_m = resistance factor for masonry

Φ_s = resistance for reinforcing bars

ρ_E = mechanical ratio

ρ_{frp} = area fraction of FRP reinforcement

ρ_h = area faction of horizontally placed FRP reinforcement

γ = a reinforcement efficiency factor

γ_{frp} = partial safety factor for FRP reinforcement

γ_g = a factor to account for partially grouting walls

σ_u = yield strength of steel bars, (MPa)

σ_y = ultimate tensile strength of steel bars, (MPa)

1. INTRODUCTION

1.1 Background

A building structure must have the ability to resist horizontal loads, such as wind or seismic loads, and transfer them to the foundation. A shear wall is one type of lateral-load-resisting element used to transfer lateral forces. In masonry construction, this element often forms a part of a bearing wall system. The presence of stiff shear walls limits deformation and damage during extreme lateral loads and decreases the nonstructural damage. Significant amount of researches were carried out to study the behavior of masonry shear walls. Most of the researches were on solid shear walls despite of the fact that shear walls with openings (called "perforated walls") are the typical walls in real buildings. Moreover, masonry shear walls with openings were shown to be the most frequently damaged structural elements in past during earthquakes.

1.2 Problem Statement

Many old masonry shear walls are at risk of suffering severe damage because of structural deficiency, including insufficient in-plane stiffness, flexural and shear strength and /or ductility during a strong earthquake. In addition to these factors, deterioration of the structural elements or new demands resulted in the need of upgrading or strengthening many masonry structures including masonry shear walls.

Recent studies have shown that Fibre Reinforced Polymers (FRP) is effective in upgrading or strengthening existing structural elements. Most researches reported the use of FRP in upgrading reinforced concrete columns and beams. At the University of Alberta an ongoing research program since 1999 investigates rehabilitation of masonry structures with FRP Sheets by Albert *et al.* (1998) and Kuzik *et al.* (1999). Walls have been investigated for out-of plane flexure and eccentric axial compression. There is very limited information regarding the use of FRP for masonry shear walls with openings.

1.3 Objectives and Scope

The main objective of this research is to investigate the behaviour of a masonry shear wall with a central opening when strengthened with externally epoxy-bonded Carbon Fibre Reinforced Polymers (CFRP) under monotonic in-plane load and constant vertical load. The effects of parameters such as the amount and layout of the CFRP on the strength, stiffness and ductility are examined. This experimental program is also helpful in understanding the behaviour of perforated masonry shear walls subjected to in-plane loads.

The scope of this study involved testing and analysis of four full-scale reinforced concrete masonry shear walls with central openings: one was a reference wall without CFRP sheets and the other three walls were strengthened with CFRP sheets whose amount and layout are different from each wall.

1.4 Thesis Organization

Chapter 2 presents a literature review of the research studies with respect to the structural elements strengthened with FRP. Chapter 3 explains the experimental program of this research. It includes a description of the materials, the test specimens, loading system, instrumentations and general testing procedures. Chapter 4 describes the main testing observation and results, including the lateral load-displacement behaviour, strain behaviour, failure modes and crack patterns. A comparative analysis of the test results is provided in Chapter 5. In this chapter, a comparison between analytically predicted and experimental results is also discussed. Finally, the summary and conclusion of this research as well as the recommendations for further research studies are presented in Chapter 6.

2. LITERATURE REVIEW

2.1 Introduction

Fibre Reinforced Polymers (FRP) has been utilized in a variety of industries including aerospace, automobile and sport industries for several decades. Nowadays there is an increasing interest in investigating the use of FRP in structural applications; especially, the use of FRP for externally bonded reinforcement to repair and strengthen existing structures. The advantages of using FRP as an alternative to traditional retrofitting materials include high strength-to-weight ratio and very high resistance to corrosion and fatigue, perfect adaptability to the original shape of the structural element that needs to be reinforced, stiffened, and/or integrated, simple application methods, non-invasive application, durability, time saving flexibility, low labour costs and low tooling and machinery costs. There is another appealing characteristic of fibrous composites: fibrous reinforcement may be orientated in such a way as to provide the greatest strength and stiffness in the direction in which it is needed.

Because of these advantages over conventional materials, FRP can effectively be utilized in the construction, rehabilitation, and strengthening of structures. While the use of FRP reinforcement as an external overlay for the strengthening of concrete beams and slabs in flexure and for the confinement of circular column has been successfully demonstrated, little attention has been given to the use of composite in enhancing the in-plane shear capacity of masonry shear walls. Especially there is no available information on the use of FRP as a strengthening material for perforated masonry shear walls. This chapter will mainly outline the shear strengthening of masonry structures with FRP.

2.2 Literature Review

2.2.1 Valluzzi *et al.* (2002)

This research was aimed to investigate the efficiency of FRP laminates as an alternative shear reinforcement technique for unreinforced masonry panels. The testing program consisted of a series of nine unreinforced masonry panels and 24 strengthened panels by different FRP materials. In order to study the influence of the eccentricity of the strengthening, the strips were applied on both sides or only at one side of panels. The FRP thickness was double in the latter case to maintain the FRP amount constant. There were two configurations of the reinforced system: strips as grid arrangement or application of diagonal strips orthogonal to the loaded diagonal. The same reinforcement amount was used for the two different configurations and for each kind of reinforced material to maintain the "stiffness by mechanical ratio", ρ_E in the two arrangements. The design reinforcement criterion of FRP amount was based on expectation of an increase of 50% of the URM ultimate shear strength by applying the principle tensile stress limitation, so each test condition is characterized by a different width of the strips and different number of layers to be glued because of the different mechanical characteristics of the fibres.

All the test specimens were subjected to diagonal compression test, which simulated the combination of in-plane shear force and vertical load. The tests showed several failure modes: de-lamination (or debonding) of FRP strips, FRP tensile rupture and diagonal splitting. All the unreinforced specimens and single-side reinforced panels presented brittle failure due to splitting along the loaded diagonal while wider cracks that appeared in single-side strengthening case provided sufficient signals well before collapse. A clear bending deformation was measured in single-side strengthening case and bending behavior caused a lower average failure loads than the reference value defined by the average failure loads of plane panels. That bending deformation was caused by a noticeable difference on the opposite side as a result of the asymmetrical reinforcements. In double-side strengthening cases, the failure mode consisted in sudden loss of bond between reinforcements and substrate because of either peeling of the masonry or rupture

of the FRP strips. The ultimate strength significantly increased. The URM typical sudden failure was noticeably corrected by the FRP application.

Valluzzi *et al.* (2002) also discussed formulas to evaluate the shear strength of URM shear walls strengthened with FRP. But the authors pointed out that the application to available codes required further calibrations. Current codes are based on the linear superposition, which provides a lower bound of plastic stress redistribution. Redistribution-derived theories are not applicable because the FRP's up-to-failure continues to show elastic behaviour. The formula doesn't consider the arrangement of FRP, but the experiment results show the shear strength differed by more than 40% in the two configurations.

Test conclusions are summarized as follows:

1) Asymmetrical applications (single-side reinforcement) to masonry panels offer a limited effectiveness.

2) The diagonal configuration is more efficient in enhancing the shear capacity than the grid set-up; while the latter offers a better stress redistribution that causes a crack spreading and a less brittle failure.

3) Less stiff FRP material appeared to be more effective both in increasing ultimate strength and stiffness of the panels due to the fact that stiffer materials are more vulnerable to de-bonding, especially when the number of plies increases.

4) Low increases in shear strength are attributable to peeling occurring in the portions next to the applied compressive loads (where high stress causes premature cracks) and to the lower tensile strength of the brick.

2.2.2 Belarbi *et al.* (2003)

The main objective of this research was to evaluate the effectiveness of different types of retrofitting schemes using GFRP rods on upgrading the load-carrying capacity and ductility of URM walls. The second objective was to develop analytical models to predict the response of URM walls under in-plane loading. Six full-scale walls were tested under monotonic in-plane load, without axial load.

Test wall 1A was constructed without retrofit scheme and was used as the control wall. Test wall 1B was strengthened using 4 near surface mounted GFRP rods (Ø9.5mm) placed vertically in grooves in the middle of the masonry blocks. Test wall 1C was strengthened using 10 GFRP rods (Ø 6.4mm) placed in grooves at every bed joint. The primary goal of the retrofit schemes of test wall 1B and 1C was to increase the load capacity of the walls. Test wall 2A was strengthened using 2 GFRP rods (Ø 6.4mm) placed in grooves at the outside head joints. Test wall 2B was strengthened using 4 GFRP rods (Ø 6.4mm) placed horizontally in the middle 4 bed joints. The strengthening scheme of Test wall 2C was a combination of Test wall 2A and 2B. The retrofit schemes of Test wall 2A, 2B and 2B were selected with the primary goal of increasing the displacement capacity of the walls without much gain in the load carrying capacity. In all the test walls, the strengthening was applied to only one side of the wall.

Test observations and conclusions are summarized as follows:

1) Test wall 2A twisted significantly in the direction of the strengthened face and reached its ultimate state when the concrete block in the compression zone failed by local crushing.

2) Strengthening of walls using structural repointing with GFRP rods leads to a significant increase in the initial stiffness, and ultimate displacement of walls.

3) Using vertical GFRP rods in certain retrofit applications may help to stabilize URM walls against out-of-plane failure without incurring significant increase in the in-plane load capacity.

4) When fewer vertical GFRP rods are used to strengthen walls, the contribution of dowel action to resist the shear force along the head joints is confines.

5) The analytical model that predicts the shear capacity in terms of $V_{M,V}+V_{F,H}$ ($V_{M,V}$ is the shear capacity of the wall without GFRP when the wall failed along the head joints, $V_{F,H}$ is the horizontal GFRP reinforcement contribution) matches well with the test results. This indicates that the assumptions made during development of the analytical models are reasonable. The assumption is that the effective stress developed in the horizontal FRP rods equals half of the ultimate tensile strength.

2.2.3 Zhao *et al.* (2003)

This work studied the effectiveness of strengthening cracked concrete block masonry walls using continuous CFRP. Three specimens were tested and all of them were 190mm in thickness, 1400mm in width and 1000mm in height. Wall-1 was control specimen; wall-2 and wall-3 were strengthened with 200mm width of CFRP in diagonal arrangement before cracked and after cracked, respectively. Each specimen was subjected to a number of in-plane loading cycles while maintaining constant axial load.

Test results and some conclusion are summarized as follows:

1) All the specimens failed in shear failure or shear-sliding failure mode.

2) CFRP can increase the ultimate loads. Compared with Wall-1, the ultimate loads of wall-2 and wall-3 are increased by 54.2% and 193.3%, respectively.

3) CFRP can also increase the stiffness of the strengthened concrete block walls in the later stage of loading due to the action of CFRP system that defers the appearance of diagonal cracks and restricts their development.

4) CFRP can improve the lateral deformation of the walls. The ultimate displacement of wall-2 and wall-3 are increased by 116.1% and 29.0% compared with wall-1 respectively.

5) Furthermore, the increase in ultimate load, stiffness and ultimate displacement of the concrete block wall strengthened with CFRP after cracking is less than that of the wall strengthened before cracking.

2.2.4 Hiotakis *et al.* (2003)

The study reported an experimental research program to investigate the effectiveness of using external bonded carbon fibre sheets as a retrofit and repair method for reinforced concrete shear walls. The experimental testing program included two phases. In the first phase of the study, CFRP Sheets had an elastic tensile modulus of 230GPa, a tensile strength of 3480MPa and an ultimate strain of 1.5%. In phase two, similar CFRP Sheets were used except that the tensile strength was 4800MPa and the ultimate strain was 1.7%. An improved anchor system was used in the second phase of the study to transfer the load from the CFRP Sheets to the support of the specimen more effectively.

The four shear wall specimens of the first phase study included a control wall, a repair wall and two strengthened walls (wall 1 and wall 2). The repair wall test results were obtained from testing of the damaged control wall that was repaired by applying one-layer of CFRP sheets. Wall-1 was strengthened with one vertical ply of carbon fibre sheets and wall 2 was strengthened with two vertical plies and one horizontally. These walls were tested to fail in the in-plane direction subjected to a predetermined increasing quasi-static cyclic load pattern. The results from the first phase of study showed a slippage occurred in the anchoring system and this slippage resulted in reduction of the ultimate load capacity. During the first phase, the specimens exhibited significant out-of-

plane torsion deformation due to the lack of sufficient lateral restraint of the shear wall specimens. To alleviate these problems, a new test set-up was used for the new series of tests in phase two of the study. The new test set-up included a lateral restraint mechanism to prevent out-of-plane deformations of the wall and an improved anchoring system was also used in phase two. In the second phase of the study, there were five specimens. Control wall, repair wall and wall1 had the same characteristics as in phase one. Wall 2 in phase two had two vertical layers of CFRP sheets instead of one in phase 1 on each side of the wall. Strengthened wall 3 had 3 vertical layers of CFRP sheets and one horizontal layer on each side of the wall.

Test results and some conclusion are summarized as follows:

1) Most failure modes were ductile flexural modes, except wall 2 for which the failure mode was ductile up to the point where sudden debonding of the CFRP sheets from the concrete surface occurred, followed by rupturing of the CFRP sheet in phase 2. The failure mode was ductile up to the point where rupture of CFRP sheets occurred in phase 1.

2) The repair by the CFRP sheets recovered about 90% of the original elastic stiffness and increased the yield load and ultimate lateral load.

3) Before the cracking of concrete and yielding of the vertical steel reinforcement the contribution of the CFRP sheets in the flexural resistance of the wall was relatively small, while the flexural resistance from CFRP sheets greatly increased after the yielding and subsequent fracture of the vertical steel reinforcement and crushing of concrete.

4) CFRP sheets increase the pre-cracked stiffness, the secant stiffness at yield, the cracking load, the yield load and the ultimate flexural capacity of undamaged walls.

5) The anchoring system for the vertical carbon fibre sheets is an important element of the carbon fibre strengthening system.

2.2.5 Other Studies

Beside the above review described in detail, there are other previous research studies about the use of FRP in strengthening shear walls subjected to in-plane load. The study of Triantafillou (1998) focused on the presentation of analytical models for the contribution of FRP to the shear capacity of strengthened element within the framework of ultimate limit state. At the same time, he also illustrated another research work in which he aimed at establishing a systematic analysis procedure for the short term strength of FRP – strengthened masonry walls under monotonic out-of-plane bending, in-plane bending and in-plane shear, all combined with axial load through analytical derivation of moment, axial and shear capacity and of their associated interactions. An experimental testing of standard masonry wall specimens under various loading conditions confirmed his analysis.

Ehsani *et al.* (1997) carried out an experimental study that involved construction and testing of 37 clay brick specimens with FRP overlays to investigate the effectiveness of using FRP overlays bonded to the surface of solid clay brick in enhancing the shear strength of these elements. The test results proved that FRP overlays could be very effective in strengthening bed joints of URM walls. He also observed that the strength and stiffness of the specimens were highly influenced by the fibre orientation. Changing the fibre orientation from 90^{o} to 45^{o} led to a slight increase in the ultimate load.

Cosenza *et al.* (2002) discussed the use of FRP reinforcement for shear and torsion strength, mainly with respect to a practical calculation model. They concluded that a shear failure can be prevented and a flexural failure is obtained if sufficient FRP is provided and the shear and torsion strength of concrete members can be increased considerably by means of externally bonded FRP reinforcement.

A series of in situ tests performed on panels were carried out by Corradi *et al.* (2002) to characterize the behaviour of the masonry typical of the areas struck by the seismic events of 1997-1998 and to study the effectiveness of the seismic-upgrading both on

undamaged and damaged walls. Again this work showed that the use of FRP on masonry structures increased both in terms of shear strength and stiffness. Public works and Government Services Canada, through research and development, has demonstrated the successful and cost effective application of this kind of advanced composite material in a few buildings. This conclusion was summarized by Foo *et al.* (2003).

2.3 Conclusion

From the above review of the literature, it is evident that the use of FRP as a mean of strengthening existing shear walls is effective. However, the studies only concentrated on solid shear walls, no research work on strengthening perforated masonry shear wall using FRP has been conducted or published. Therefore, research on the behaviour of masonry shear walls with openings strengthened by FRP is required. This thesis presents a beginning of a data pool for information regarding this subject.

3. EXPERIMENTAL PROGRAM

3.1 Introduction

The experimental phase of this research consisted of testing of four full-scale reinforced concrete masonry shear walls with central openings and related material tests. The wall specimens included one control wall and three strengthened walls with externally epoxy bonded Carbon Fibre Reinforced Polymers (CFRP) Sheets. The details of each specimen will be discussed in detail in Sec. 3.3. Each wall was loaded vertically by constant loads and horizontally by varying in-plane loads. The major parameters investigated were amount and layout of the CFRP Sheets. This chapter presents the material properties, the test specimen design and the test set-up.

3.2 Materials

Masonry is a multi-component structural material. In order to have better understanding of the structural behaviour of the primary specimens, ancillary tests were conducted on individual masonry units, mortar cubes, grouts and masonry prisms. For the reinforcement consisting of steel rebars and the CFRP Sheets, a number of tension coupon tests were performed.

3.2.1 Individual Masonry Unit

Standard 200x200x400mm Hollow Concrete Masonry Units with specified strength of 15MPa were used in this experimental program. Six units were tested in accordance with CSA standard A165.1 and A165. 2-94 to obtain the compressive strengths. The six selected unit specimens were capped with gypsum cement at the top and bottom surfaces to obtain a flat surface and were subjected to increasing compressive load in a testing machine (MTS 6000) until failure took place. Photo 3-1 shows the individual unit specimens. The compressive strength was obtained by dividing the failure load by the effective cross-sectional area, which was 39600mm^2. Table 3-1 summarized the results of

the tests. The mean value of the compressive strength of the units was 18.6MPa and the standard deviation was 1.50MPa.

3.2.2 Mortar

Type S mortar was used to build specimens in this test program. A total of twelve standard 50mm mortar cubes were tested in accordance with CSA standard A179-94. Two groups of samples for testing were taken from different mortar batches. MTS 1000 testing machine, which conforms to the appropriate requirement given in CSA standard, was used to obtain the compressive strength of mortar. Table 3-2 summarizes the results of the tests. Mortars in Group 1 had a mean compressive strength of 14.4MPa, while Mortars in Group 2 had a mean compressive strength of 16.9MPa. The results show that the compressive strength of the mortar in Group 1 was almost 18% lower than that in Group 2. This is because most of the mortar cubes in Group 1 had more rough surfaces.

3.2.3 Grout

Twelve grout prisms of 75x75x150mm were tested to obtain the in-situ grout compressive strength. The specimens were divided into two groups and each group was taken from different batches. The specimens were prepared to simulate the absorption of moisture in the actual masonry using a mould made from masonry units. A paper towel liner was used to prevent bonding of the grout to the masonry units. Photo 3-2 shows the preparation of grout test specimen. The top and bottom surfaces of the specimens were capped with plaster to provide flat loading surfaces. The MTS1000 test machine was used to obtain the compressive loads. Table 3-3 shows the result of the tests. Grout of Group 1 had a mean strength of 16.4MPa, while grout of Group 2 had a mean strength of 20.5MPa. The results show the compressive strength of the grout in Group 2 was 25% greater than Group 1, possibly because of a higher water/cement ratio in Group 1.

3.2.4 Masonry Prisms

Two sets of prisms were tested at an age of 131 days to evaluate the compressive unreinforced strength of the masonry walls. Five grouted and five ungrouted prisms were

constructed using the same materials as those in walls during constructing the structural masonry wall specimens. All prisms were tested in accordance with procedures prescribed in CSA standard CAN/CSA – A369-1-M90. Each prism was one and a half blocks wide (0.6m) and five courses high. Uneven surfaces with curvature from grout shrinkage were filled with fine sand for all grouted prisms. Each specimen was capped at the top and bottom with a 11mm thick piece of fibre board to obtain a uniform load transfer between the testing machine platens and the prism. The load data were recorded manually from the MTS 6000 display module. For each prism, two LVDTs were used to obtain the prism longitudinal displacement. Photo 3-3 shows the details of the prisms and instrumentations.

The compressive stress of each prism was obtained by dividing the failure load by the effective cross sectional area. Table 3-4 shows the strength results of the tests. As expected, the compressive strength of the ungrouted prisms was greater than that of the grouted prisms. The mean compressive strength of grouted prisms was 9.3MPa with a standard deviation of 0.87MPa, while the ungrouted prisms had an average compressive strength of 11.4MPa with a standard deviation of 1.26MPa. Accordingly, the compressive strength of wall specimens can be taken as 10.56MPa assuming 40% grouting.

The modulus of elasticity, E_m, was calculated from a regression line based on the strain-stress curve at the lowest R^2 of 0.9881 for ungrouted prisms and 0.9777 for fully grouted prisms. The values of the modulus of elasticity are shown in Table 3-4. Compared with grouted prism that had a mean modulus of elasticity of 7725MPa, ungrouted prism had a 90.5% higher mean value of E_m, which is 14717MPa. Consequently, the modulus of elasticity of wall specimens can be taken as 10522MPa assuming 40% grouting.

The failure mode observed was as expected based on the basic concept summarized by Hendry (1991). The ungrouted prisms failed by vertical splitting in their own plane. The final failure also involves some crushing of mortar as the two halves of masonry buckle out. For grouted prisms under compressive loading, the face-shells of the masonry typically split always from the grout cores. This failure mechanism is caused by a

wedging action of the grout, the wedge shape developing because of the taper of cores of the hollow units. Photos 3-4 and Photo 3-5 show the typical failure modes for fully grouted and ungrouted prisms.

3.2.5 Steel Reinforcement

There were two types of steel reinforcement bars used in the structural wall specimens; W15M and B15M. Two coupon tension tests were performed for each type of steel rebars in accordance with the requirements of ASTM A370. The MTS1000 testing machine was used for the coupon tests and the data were recorded by a data acquisition system. Each coupon was 355mm long with 85mm griping length at each end. An extensometer with an initial gauge length of 50mm was attached to each specimen to attain the elongation. For the first coupon specimen, W15M, two strain gauges were also mounted on the specimen to examine the accuracy of the extensometer and the results proved that extensometer was accurate enough to provide the data of elongation. Table 3-5 shows the results of test for the following material properties: yield strength (σ_y), ultimate tensile strength (σ_u), and the modulus of elasticity (E).

3.2.6 Carbon Fiber Reinforced Polymer (CFRP) Sheets

Carbon Fibre Reinforced Polymer (CFRP) Sheets used as reinforcement in the experimental study were Wabo® MBRACE CF130 with viscous epoxy. The CF130 is a unidirectional high strength carbon fibre fabric supplied in 625mm wide roll where the individual fibres are uniaxial in the longitudinal direction and perpendicular cross weaves are used to hold the longitudinal fibres in plane. Six tension coupons of the fibre reinforcement were constructed during the application of the fibres to the last wall specimen, Wall 4, and were tested in accordance with ASTM D3039/D 3039M-00. A plastic channel mould with a length of 500mm and a width of 25mm was made to construct the coupon specimens, which were 25mm wide and 325mm long. Each coupon was six-layer thick in the gauge region and eight-layer thick in the grip region. Emery cloth was used as friction tab to introduce the load into the specimen successfully and prevent premature failure because of the significant discontinuity. MTS1000 testing

machine was used to apply the tensile load. Three 5mm strain gauges were mounted on each coupon in the longitudinal, lateral and 45° directions. The load and strain data were recorded by a data acquisition system.

The stress-strain behaviour of the carbon sheet coupons in tension shown in Figure 3-1 is characteristically linear and elastic in a wide range of stress level. The failure modes of all the coupons belong to explosive gage middle failure. Table 3-6 reports the major material properties obtained from tests and the theoretical modulus of elasticity, which is obtained using Equation 3.1 provided by Hollaway (1993). That theoretical modulus of elasticity (E_c) is only approximate 3% higher than the experimental modulus of elasticity (E_t) shows that the strain in the matrix equals the strain in the fibre and the bond between the two components is perfect since the theoretical equation of E_c is based on the assumption that strain in the matrix equals the strain in the fibre and the bond between the two components is perfect.

$$E_c = Em'Vm' + E_f V_f' \tag{3.1}$$

where,

E_c = the modulus of elasticity along the fibre direction, (MPa),

E_m' = the modulus of elasticity of the matrix (epoxy), the specified value is 3034MPa,

E_f = the modulus of elasticity of the fibre, the specified value is 227000MPa,

V_m' = the volume fraction of the matrix, the values are shown in Table 3-6, and

V_f' = the volume fraction of the fibre, the value are shown in Table 3-6.

3.3 Test Specimens

3.3.1 Specimen Design

The design strength of masonry shear walls is often governed by flexure, but low walls with a low aspect ratio (H/L, where H stands for the height of the wall and L the length of

the wall) may be dominated by shear. The main objective of this experimental program is to study the shear behaviour of load bearing masonry shear walls with large openings reinforced with CFRP Sheets. A low aspect ratio, H/L = 0.95, was chosen. To ensure that the tested walls fail in shear rather than in flexure, it is necessary to counteract the bending moment or create a situation where the bending moment capacity exceed the shear capacity so that the test wall fail in shear. The objective was achieved using an external hold-down method detailed in Sec 3.4. Ghanem *et al.* (1992) demonstrated that walls with evenly distributed reinforcement have a later onset of severe cracking than the walls with reinforcement only on the periphery. The wall specimens were designed with evenly distributed reinforcement. This arrangement of vertical reinforcement is more effective in dowel action for shear resistance. No horizontal shear reinforcement was used in the wall specimens.

Large openings in shear walls cause significant decrease in strength and stiffness of the walls and precipitate a change in failure mode due to the stress concentrations around the opening and the reduced effective shear area. Current engineering practice requires that reinforcement should be laid in the bed joints above and around the openings to distribute the overstressing or undesirable stress concentration in the surrounding masonry and improve the wall integrity simultaneously. The reinforcement around openings in the shear wall specimens with large openings in this experimental program was provided in the form of externally bonded CFRP Sheets. To highlight the effects of CFRP Sheets, no additional reinforcement around the openings was used inside the wall. For the comparative study, Wall 1 was designed as reference wall without CFRP Sheets. For the parametric study, Wall 2, Wall 3 and Wall 4 were strengthened with CFRP Sheets. Variables in the strengthened walls with CFRP were the amount and layout of CFRP Sheets.

3.3.2 Specimen Details

Four full-scale concrete masonry wall specimens with openings at the centre of the walls were designed considering the available testing resources at University of Alberta. All

wall specimens had the same geometric properties and were constructed by professional masons. Each specimen was built on a steel base plate attached to a W 310X74 steel base beam using 16mm diameter (A325) steel bolts on each side of the dowel. Photo 3-6 shows the wall specimen base preparation. Except for Wall 1 which was constructed in the testing frame, the other three walls were transferred to the testing frame using 10 Ton lifting device. Each wall specimen was 3990mm long, 3800mm high (19 courses), and 190mm thick. A central opening of 1210mmx1210mm was constructed on the top of the 6^{th} course. Standard 15MPa masonry block and factory mix type S mortar were used. The blocks were laid in running bond and only the cores with steel reinforcement were grouted. Horizontal joint reinforcement consisted of #9 gauge ladder type located at every second course. The vertical reinforcement consisted of 15M steel bars spaced every third core. Vertical reinforcement was spliced to dowels with a lap length of 40d. Dowels consisted of 15M steel bars and were point welded on the steel base plate. A 75mmx75mmx6mm steel plate was welded to the top of each vertical reinforcement bar to provide enough development length at the top of the wall. A two-course high lintel beam with 2-15M flexural reinforcement and 10M stirrup at the spacing of 150mm was designed. A bond beam two-course high with 3-15M flexural reinforcement was also constructed. Construction of the wall specimens was completed within two weeks. All the specimens were cured under ambient conditions in the laboratory for a minimum of 28 days. Figure 3-2 and Figure 3-3 show a series of schematics of the typical test specimen.

The study was concentrated on the effects of CFRP Sheets in enhancing the shear strength for masonry wall with an opening. So the major difference between the wall specimens was the amount and arrangement of CFRP Sheets as mentioned before. Wall 1 was designed as the control wall without externally bonded CFRP Sheets. Wall 2, Wall 3 and Wall 4 were strengthened using externally bonded CFRP Sheets. Wall 2 and Wall 3 had the same layout of CFRP Sheets around the opening. The variable was that the CFRP strips in Wall 2 had a width of 156mm while the CFRP strips in Wall 3 were 78mm wide. In Wall 4, additional four CFRP strips with a width of 78mm were mounted in the middle of each pier on two sides of wall in addition to the same CFRP strips as those in Wall 3. Figure 3-4 to Figure 3-6 show the layout of the CFRP Sheets.

3.4 Application of CFRP Sheets

Prior to initiating surface preparation procedures, the Carbon Fibre Sheets were cut into the strips required for the testing. Before installation of the CFRP strips the surfaces of the wall specimens had to be prepared. First the location of CFRP strips was marked, and then a hand grinder was used to remove projections. Next the fine dust was removed from the surfaces by a compressed air. To prevent excess epoxy, masking tapes were bonded around the edge of the CFRP strips region.

The process of application of CFRP Sheets involved the following steps. First a primer coat was applied on the surface of masonry to provide a high bond base coat for this composite strengthening system and a roller was used as application equipment for primer. After twenty four hours to cure primer the putty which functions as the second component of the epoxy system was applied to the primed substrate using a spring steel trowel to level small surface defects and fill the joints, and to provide a smooth surface. Another Twenty four hours later, the base coat of saturant was applied using a roller to begin saturation of the fibre reinforcement sheets. Then the strips of fibre were laid out on the first layer of wet saturant and pressed into place by hand. Next the second coat of saturant was applied to the top of the fibre strips using a roller to ensure full penetration of the saturant throughout the fibre strips. Last a steel roller was used to press and smooth the surface of the composite strengthening system to remove any air bubbles. All components of the epoxy system have the same Part A to Part B mix ratio of 3:1 by volume. The fibre reinforcement was allowed to cure for at least one week before instrumentations were applied. Photo 3-8 shows the application of CFRP Sheets.

3.5 Test Set-Up

Figure 3-7 and Figure 3-8 show the test set-up that consisted of four elements: lateral loading assembly and its reaction system, gravity loading system, out-of-plane bracing system and subsidiary hold-down system.

3.5.1 Lateral Loading Assembly

Figure 3-9 shows the schematic of the lateral loading assembly. The lateral load was provided by a 450kN hydraulic jack connected to a hydraulic pump. The jack was mounted to the reaction frame by four bolts and was bearing on plate D, a 47mm thick steel plate. The lateral load was transmitted from plate D to a 49mm thick steel plate, plate B which transmitted the load to plate A, a 19mm thick steel plate bolted to plate B on one side and welded to two steel channels on the other side. These channels will be referred as side loading channels. The lateral load was then transmitted from the side loading channels to specimens through six 25mm ϕ thread rods which bolted channels to specimens. A set of rollers and a sphere between plate D and plate B were used to release the lateral degree of freedom to ensure no undesirable restraint and obtain the lateral load perpendicular to specimens. This loading assembly prevents the local crush on specimens that would be caused by small bearing area if the jack was bearing directly on the wall face. To ensure no local crushing at the first 25mm ϕ bolt location, four plies of fibre boards were placed between plate A and the specimen to provide enough bearing area. Photo 3-7 shows the lateral loading system in detail.

3.5.2 Lateral Loading Reaction System

The lateral loading reaction system is a self-equilibrating system consisting of a reaction frame and a stop assembly. The reaction frame was available in the structural laboratory and was designed by Mobeen (2002). It consisted of four steel columns and a set of braces. Four W-section columns formed the corners of the square. Diagonal braces in vertical and horizontal planes were provided to control the lateral movement of the frame. Horizontal braces only at the level of the lateral load were introduced to transfer the lateral forces to the columns by truss action and minimize the local deflection of beam at the place where the jacks were mounted. Cross braces positioned at two levels in two side bays parallel to the direction of lateral loads were provided to control and minimize the lateral drift of the reaction frame that in turn helped in saving the stroke of lateral jacks. The reaction frame was designed for a lateral load of 1000kN, which is much higher than

the capacity of wall specimen in this test program. The reaction frame had adequate stiffness under lateral load to ensure that the lateral deflection of the frame could be neglected without causing any significant error in the test. Figure 3-7 and Figure 3-8 show the detailed schematic diagrams and Photo 3-9 shows a view of the frame.

A stop assembly attached to the bottom of lateral loading reaction frame was introduced to avoid slippage of the wall specimens under high lateral load. The stop assembly consisted of a series of steel plates and beams bolted to each other shown in Photo 3-10. One end of stop assembly was bolted to the base beam and other end bore directly on the frame columns of the lateral loading reaction frame and thus equilibrated the lateral force introduced by jacks mounted on the reaction frame. Two sets of floor anchor system at each end of the steel base beam were introduced to minimize the vertical motion and rotation of the steel base beam. Figure 3-10 shows a scheme of the floor anchor system.

3.5.3 Gravity Loading System

A constant vertical load, which simulates the gravity load, was applied by four jacks connected to a single hydraulic pump through a W460X74 (G 40.21 350W) distributing beam located at the top of wall specimens. Four hydraulic jacks were mounted against the underside of the strong floor and attached to four threaded steel tie rods (diameter 20mm). Steel rods were positioned symmetrically near the middle of each pier beside the opening and matched the structural holes in the strong floor. The load distributing steel beam was 460mm high in attempt to evenly distribute load on the top of specimen from two point concentrated loads. A piece of fibre board was used between the load distribution beam and the top of specimen to allow for uniform bearing at the top of the wall. Although a constant vertical force of 100kN was desired for each specimen, variations in applied vertical load occurred because of the difficulty in proportioning all four rods to proper tension under the action of the lateral loads. Figure 3-7 and Figure 3-8 show schematic diagrams of the gravity loading system. Photo 3-12 shows a view of this gravity loading system.

3.5.4 Out-Of-Plane Bracing System

To avoid out-of-plane movement of the wall caused by an accidental eccentricity of the lateral load, an out-of-plane bracing system was introduced at the level of the lateral load. It consisted of two large steel plates (1500mmx400mmx21mm) and a steel cylinder 50mm Ø, 300mm long that formed a rectangular steel frame. Two small steel plates (350mmx190mmx6mm) were welded to the rectangular steel frame between two large steel plates to enhance the stiffness. Four out-of- plane braces were used, two of which provided on each end of the wall. Each brace was attached to the lateral load reaction frame beams at one end through eight bolts, while the steel cylinder roller at the other end of the brace bore on the side loading channels bolted to the wall. Figure 3-8 and Photo 3-11 show the details of this out-of-plane bracing system.

3.5.5 Subsidiary Hold-down System

The main purpose of this research was to study the shear behaviour of the masonry wall. To ensure that the test wall fail in shear rather than in flexure, an external hold-down system was provided to create a situation where the bending moment capacity exceeded the shear capacity so that the test wall failed in shear. Figure 3-7 shows the schematic diagrams of the subsidiary hold-down system. It consisted of two steel tie rods positioned between the bottom of the base beam and the top of the vertical load distribution beam at the heel of the wall. When uplift occurred at the heel of the shear walls under high lateral loads, the tie rods were tensioned automatically and produced a compressive force sufficient to restrain the uplift, thus avoiding flexural failure due to bending moment whose maximum value occurred at the heel of the wall. Clearly the external hold-down system may have a considerable effect on the local shear stresses and strains at the heel of wall. This zone, however, was far from the test region around the opening. Although an internal hold-down system may overcome the above problem, it requires incorporating large amounts of peripheral vertical reinforcement to ensure a shear failure. The external hold-down system was also simple to construct and easy to monitor.

3.6 Instrumentations

Four different types of instrumentation were used to monitor the following aspects of specimen behaviour: 1) applied loads and reaction loads; 2) overall lateral displacement; 3) slippage of wall relative to the base steel beam and 4) masonry and CFRP Sheets strains. All experimental data about load, reaction and displacement were recorded through an electronic data acquisition system. A Demec gauge was used to measure strains.

3.6.1 Measurement of Applied and Reaction Loads

A calibrated measurement system was used in lateral applied load from the jack connected to a hydraulic pump. The values of lateral loads were obtained according to the oil pressure of the hydraulic pump through a calibrated measurement system. Two load cells were used in reaction system. One was placed at the top of the end of the steel base beam to measure the uplifting forces caused by lateral loads. The other load cell located at the top of the vertical distribution beam was used to monitor the hold-down forces. A 20,000 lb load cell was used in Wall 2, Wall 3 and Wall 4 to monitor the hold-down forces. During the Wall 4 testing this small load cell reached its capacity, and a 50,000 lb load cell was used to replace the small load cell. Four calibrated strain gauges were attached to each tension tie rod of gravity loading system to measure the vertical load applied through each rod individually.

3.6.2 Measurement of Displacement and Slippage

The displacement of the wall was measured using seven Linear Variable Displacement Transducers (LVDT) in each wall specimen. Figure 3-11 to Figure 3-14 show the layout of the LVDTs. In all wall specimens the overall lateral displacements were measured using LVDT at the bottom, ½ high level, ¾ high level and the top of the wall. Four LVDT instruments were attached to the lateral load reaction frame at one end and to the specimen at the other end. The lateral load reaction frame was considered as a rigid frame because of its much higher stiffness compared to the specimens. The LVDT at the bottom

of specimen was also used to estimate the slippage of the wall relative to steel base beam. For the first tested control wall, Wall 1, a LVDT mounted at the top of the steel base beam and the middle of the first bottom layer of block was used to measure the vertical displacement at the heel of the wall specimen from the uplifting. However, it was observed that the big horizontal cracks occurred at the higher joints during the first specimen testing, so one end of the LVDT used to measure the vertical displacement was changed to the middle of the block right under the wall opening, while the other end was attached to the top of the steel base beam.

Lourenco and Rots (1997) discussed the failure mechanism as several panels forming a masonry wall with openings. Based on this theory, the other two LVDTs were mounted in the expected tension regions to investigate the maximum displacement of the wall. Since two major diagonal cracks were observed in the piers of the Wall 1 beside the opening, two LVDTs across the direction of the diagonal cracks were introduced in the Wall 2, Wall 3 and Wall 4 specimens.

3.6.3 Measurement of the Strains

A 100mm Demec gauge was used to measure the strains of the masonry wall and CFRP Sheets. One division on the gauge equals 0.002mm. All Demecs were glued to the specimen and the layout of the Demecs varied from test to test. Generally the Demecs were place at the corners of openings. In Wall 4, two additional lines of Demecs were mounted on the CFRP strips in the middle of piers to investigate the strains of these CFRP strip. Figure 3-11 to Figure 3-14 show the position of the Demecs in detail.

A Fluke ^{TM} electronic data acquisition system was used to collect the experimental data. A Hewlett packar ^{TM} X-Y plotter recorded the lateral load vs. lateral displacement curve, so it was easy to discover the anomalies during the testing.

3.7 Test Procedure

3.7.1 Position of Walls

Each wall was constructed on a steel base beam. The control wall, Wall 1 was constructed in the testing frame, while the other three walls were lifted into the test frame using an overhead crane. Three pieces of 750mmx200mmx25mm steel plates plastered at the top and the bottom were placed under the steel base beam to level the steel base beam and function as support plates. These plastered steel plates were connected through the strong floor using 35mm ϕ bolts. A steel buckle was bolted to each side of the steel base beam to connect a large turnbuckle whose other end was connected to high strength strands connected to a shackle which was attached to the crane. After centering all the components the specimen was positioned over the support plates.

3.7.2 Test Preparation

After the specimen was properly aligned the vertical load distribution beam was placed at the top of the wall. Then the stop assembly was bolted to the end of the steel base beam and two sets of floor anchor system were also bolted through strong floor at each end of the steel base beam. Next the lateral loading assembly was introduced at the top of wall specimen. This assembly was bolted to the lateral load reaction frame and specimens through two side loading channels. Following the arrangement of the lateral loading assembly four tie rods went through the strong floor to introduce the gravity load. Then the out-of-plane bracing system was placed between the specimen and the lateral loading reaction frame beam. Finally all instrumentations including jacks, LVDT and Demec were mounted to the wall specimens. The detail about instrumentation was discussed in Sec.3.6. Before testing a scaffold was constructed for measuring the Demec data and marking the cracks during testing.

3.7.3 Loading Procedure

After positioning of the wall specimen the initial Demec data reading were taken and then a vertical load was applied through four tie rods to simulate the real loading condition on a shear wall. The vertical load was slowly increased to its maximum value of 100kN and then maintained approximately at this value during the entire test. Following the application of gravity load the shear wall specimens were tested under in-plane load using a computer controlled data acquisition system which was used to record all electronic readings. All the electronic instrument measurements were recorded at around 5kN lateral load intervals. Demec data readings were recorded at regular intervals up to 40kN lateral load. During the test wall specimens were visually inspected and the cracks were marked and the mode of failure was recorded.

The subsidiary hold-down system was applied during the testing and the test was continued until catastrophic failure occurred. The loading procedure for each specimen is described in detail in chapter 4.

Table 3-1 Individual Masonry Unit Compressive Strengths

Specimen Number	Max.Load (kN)	Strength (MPa)
Unit 1	779.0	19.7
Unit 2	651.9	16.5
Unit 3	803.4	20.3
Unit 4	780.0	19.7
Unit 5	704.7	17.8
Unit 6	701.8	17.7
	Mean	18.6
	Std.dev.	1.50
	C.O.V	0.08

Table 3-2 Mortar Cube Compressive Strengths

	Group 1		Group 2	
Specimen Number	Max.Load (kN)	Strength (MPa)	Max.Load (kN)	Strength (MPa)
1	31.4	12.6	38.6	15.4
2	31.1	12.4	43.4	17.4
3	34.1	13.6	45.3	18.1
4	41.4	16.6	42.9	17.2
5	38.4	15.4	43.5	17.4
6	39.8	15.9	39.5	15.8
Mean		14.41		16.88
Std.dev		1.77		1.04
C.O.V.		0.12		0.06

Table 3-3 Grout Prism Compressive Strengths

	Group 1			Group 2		
Specimen Number	Max.Load (kN)	Cross Sectional Area (mm^2)	Strength (MPa)	Max.Load (kN)	Cross Sectional Area (mm^2)	Strength (MPa)
1	79.5	6006.0	13.2	135.0	5814	23.2
2	98.3	6121.5	16.1	121.4	6437	18.9
3	100.5	5852.0	17.2	114.7	6080	18.9
4	91.5	5851.3	15.6	113.2	5852	19.3
5	102.1	5700.0	17.9	137.9	5929	23.3
6	109.1	5885.5	18.5	119.2	6162	19.3
Mean			16.4			20.5
Std.dev			1.91			2.15
C.O.V.			0.12			0.10

Table 3-4 Masonry Prism Test Results

	Grouted			Ungrouted		
Specimen Number	Max. Load (kN)	Strength (MPa)	E_m (MPa)	Max. Load (kN)	Strength (MPa)	E_m (MPa)
1	1170	10.4	7700	739.9	12.5	11200
2	950.1	8.5	7400	637.3	10.7	15550
3	1072.7	9.6	8000	735	12.4	17400
4	994	8.9	7800	588.4	9.9	N/A
5	929.5	8.3	10100	535.6	9.0	N/A
Mean		9.3	7725		11.4	14717
Std.dev		0.87	250		1.26	3183
C.O.V.		0.09	0.03	.	0.11	0.22

Table 3-5 Steel Reinforcement Tension Coupon Test Results

Specimen	Yield Stress (MPa)	Ultimate Stress (MPa)	Modulus of Elasticity (MPa)
W15M	459.5	633.75	219400
B15M	478.5	799.25	214450

Table 3-6 Carbon Fiber Reinforced Polymer Coupon Test Results

Specimen Number	V_f	V_m	Max.Stress (MPa)	Max.Strain ($x10^{-6}$)	E_c (MPa)	E_t (MPa)
1	0.300	0.700	1148	16502	70224	70900
2	0.298	0.702	1121	17113	69776	66200
3	0.317	0.683	1227	17056	74031	72600
4	0.296	0.704	1133	17093	69328	67800
5	0.305	0.695	1100	17000	71344	65400
6						Discard
Mean	0.30	0.70	1146	16953	70941	68580
Std.dev.	0.01	0.01	48.64	256	1883	3079
C.O.V.	0.03	0.01	0.04	0.02	0.03	0.04

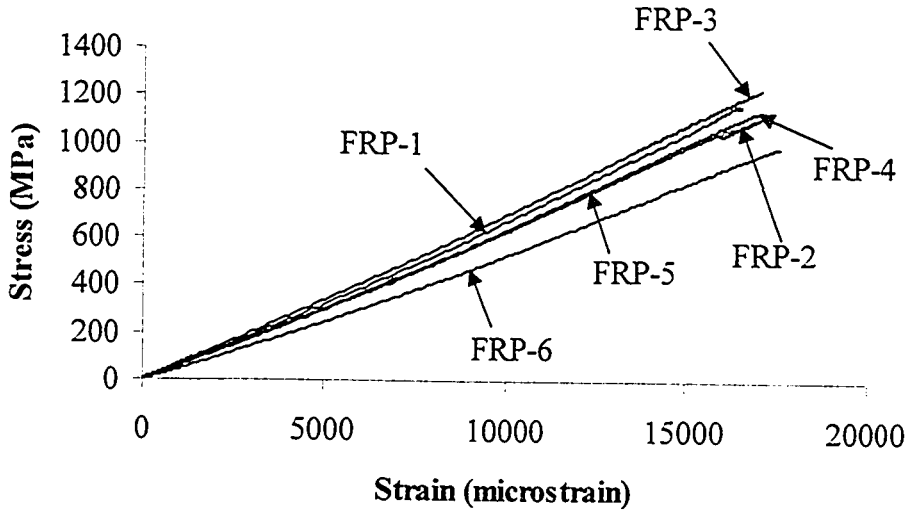

Figure 3-1 CFRP Coupon Tension Test Behavior

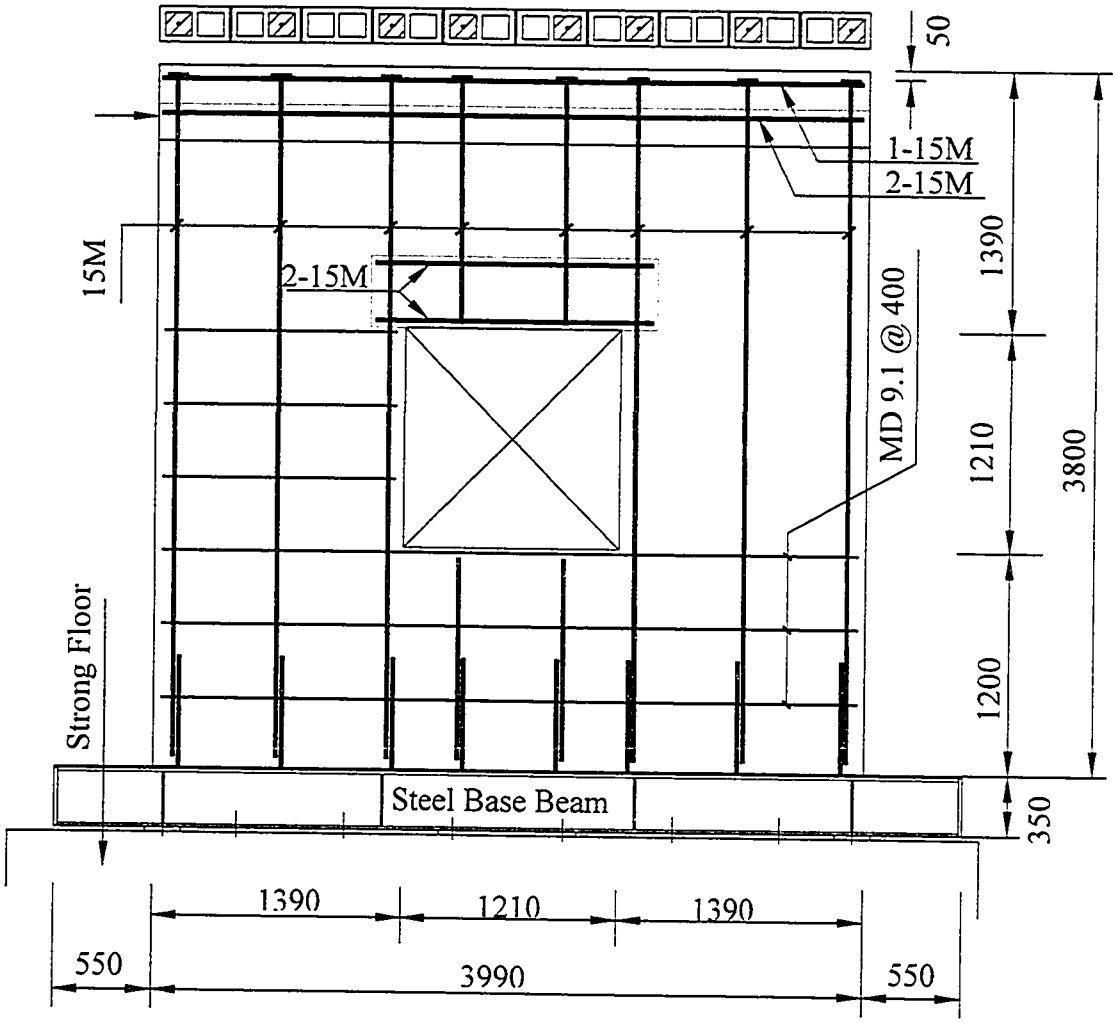

Figure 3-2 Steel Reinforcement Arrangement

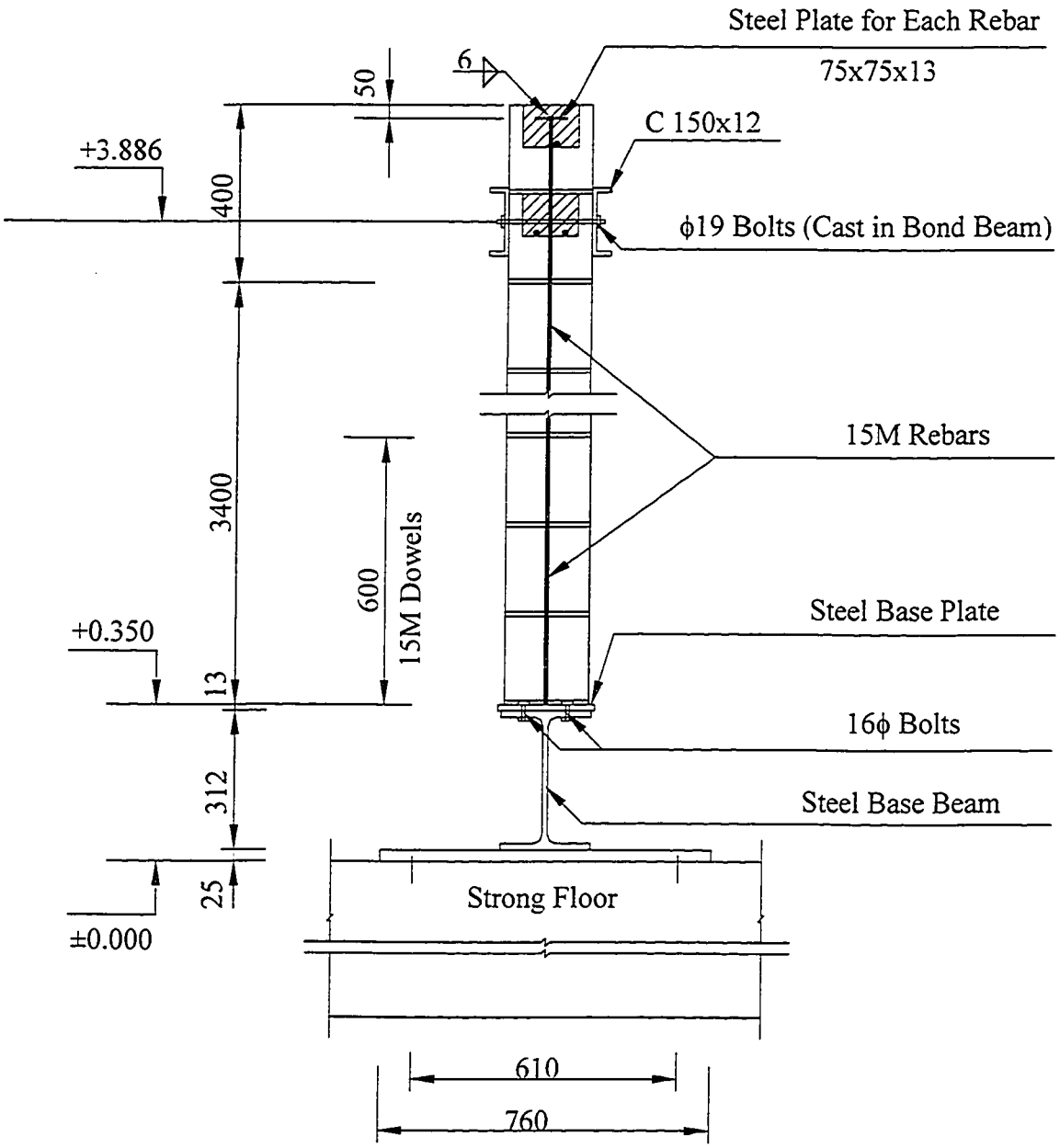

Figure 3-3 Specimen Cross-Section

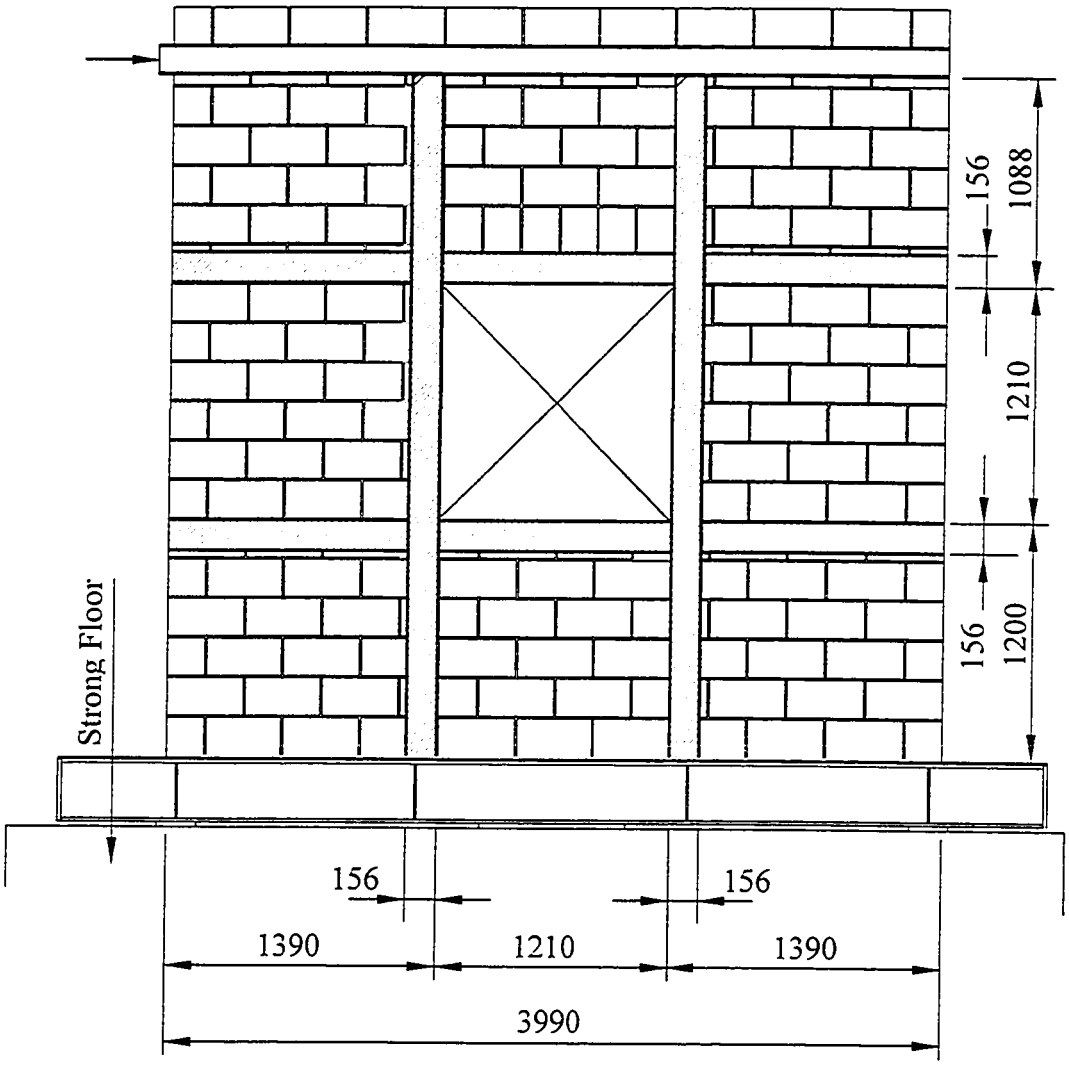

Figure 3-4 CFRP Layout for Wall 2

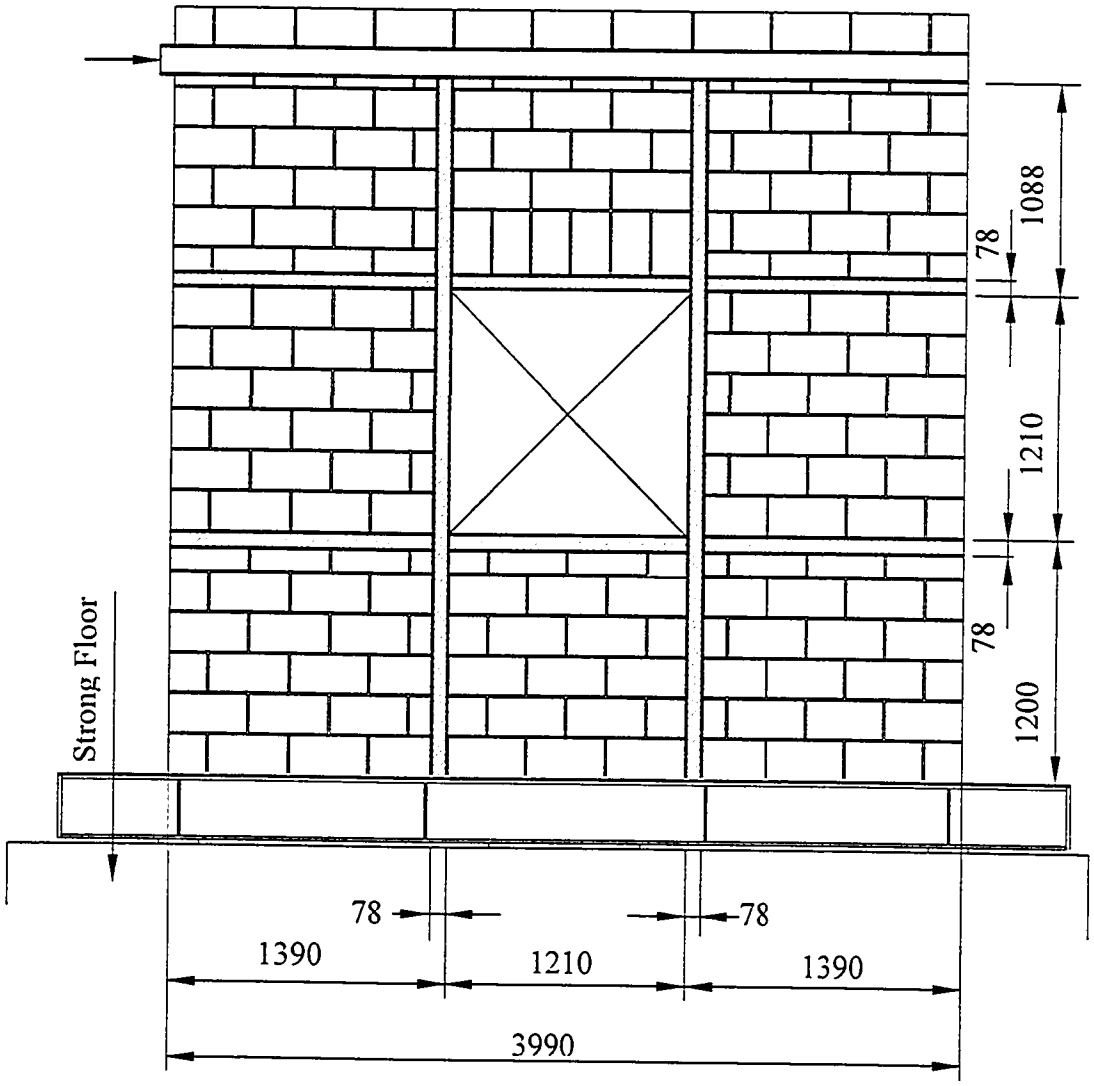

Figure 3-5 CFRP Layout for Wall 3

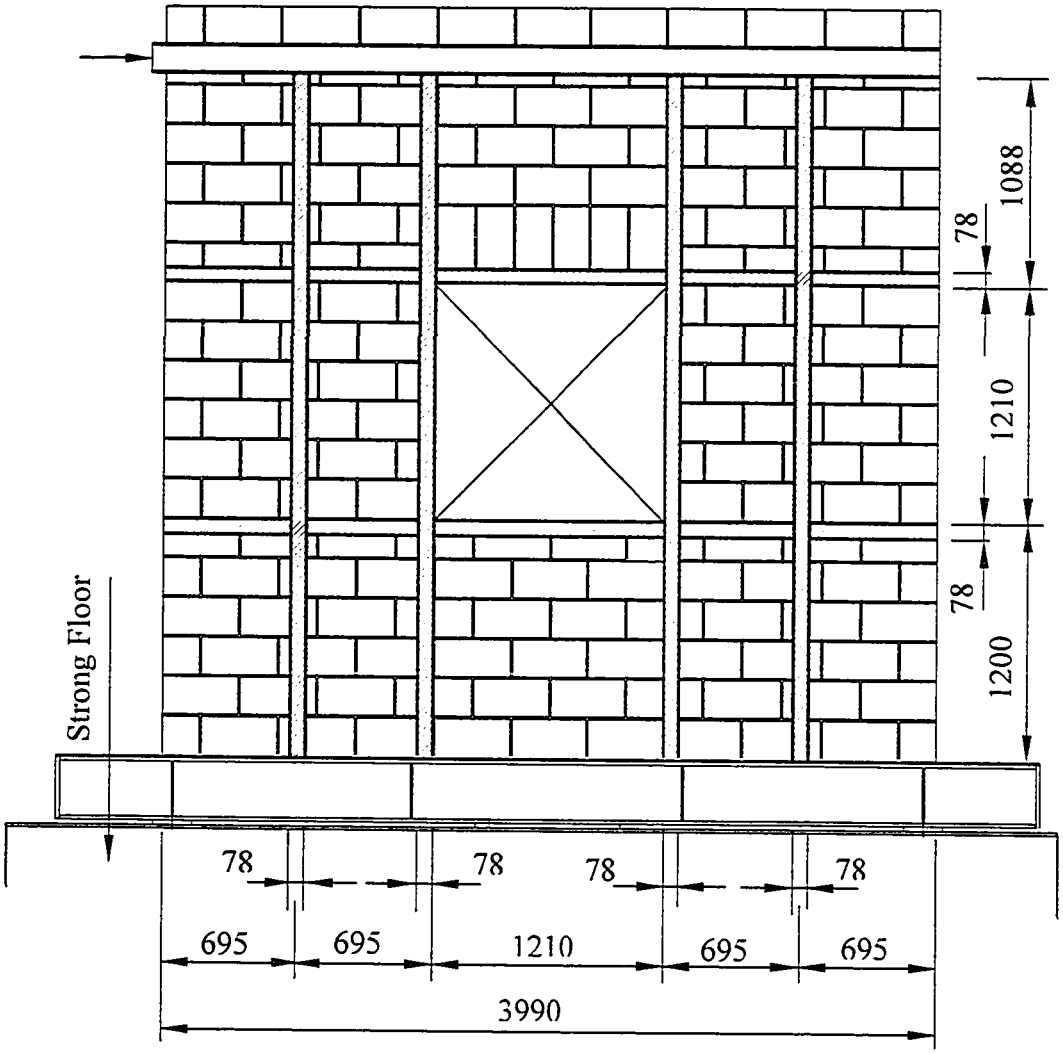

Figure 3-6 CFRP Layout for Wall 4

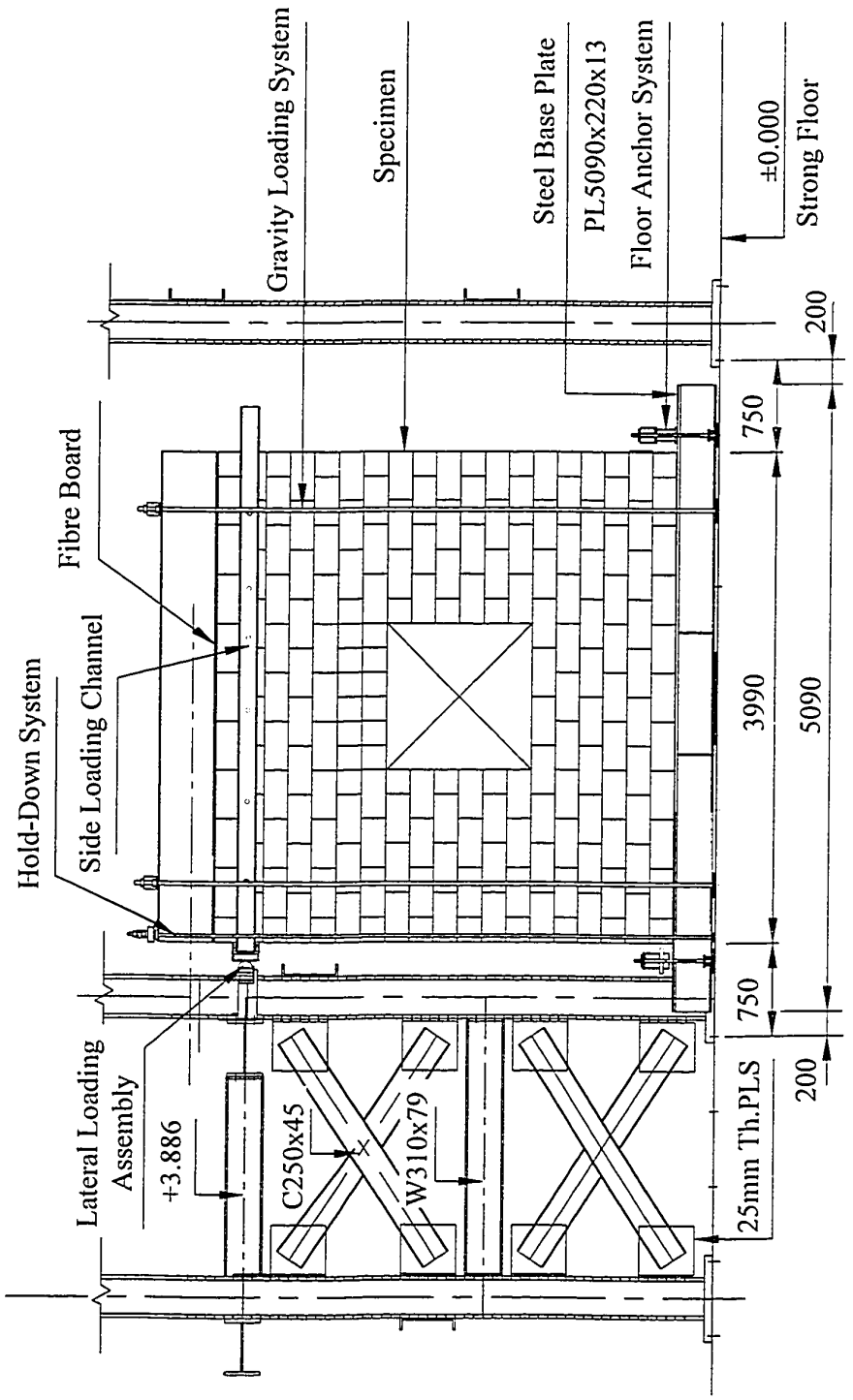

Figure 3-7 Test Set-up

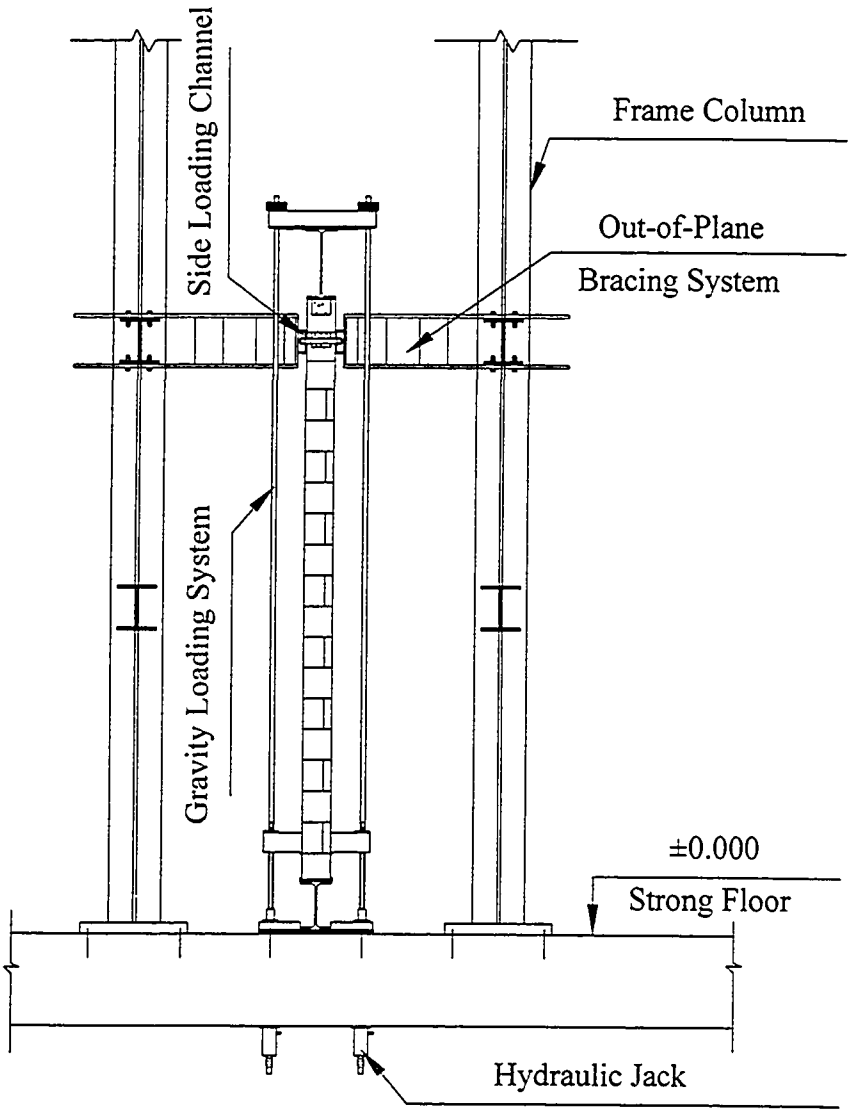

Figure 3-8 Set-up Cross-Section

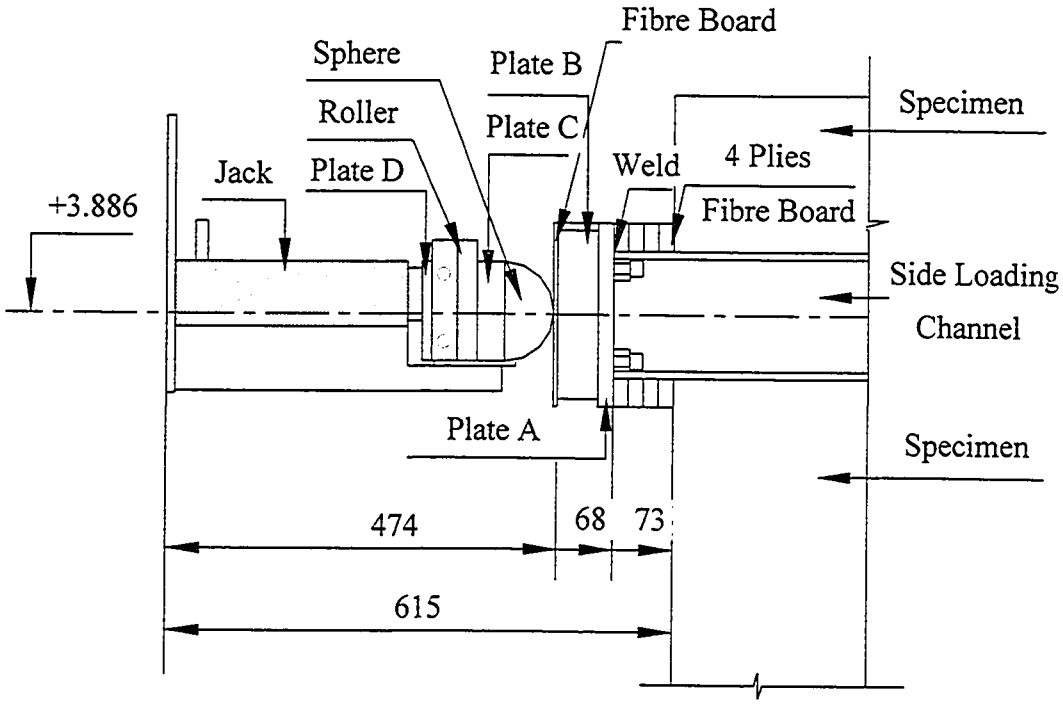

Figure 3-9 Lateral Loading Assembly

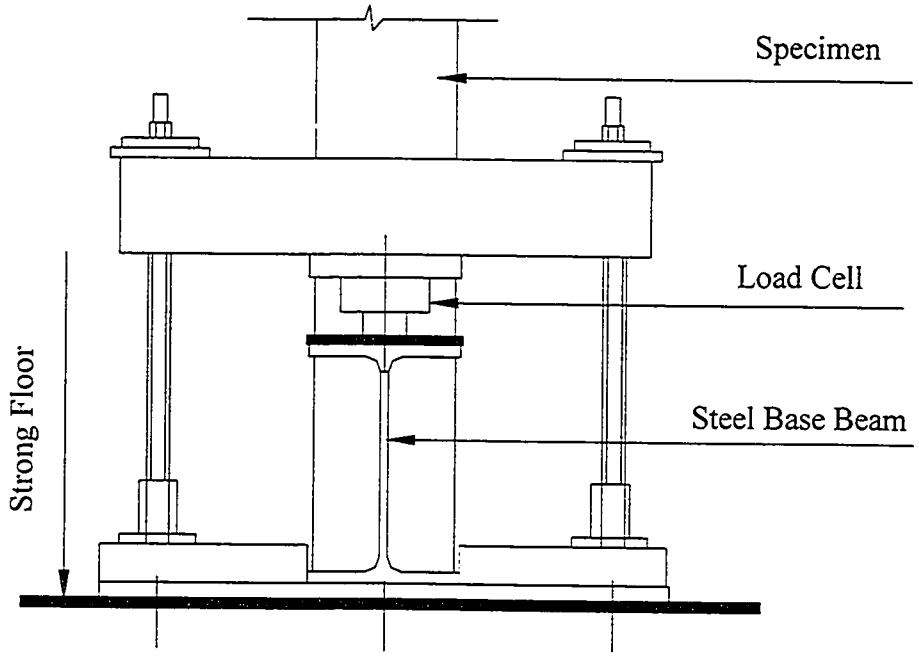

Figure 3-10 Floor Anchor Systems

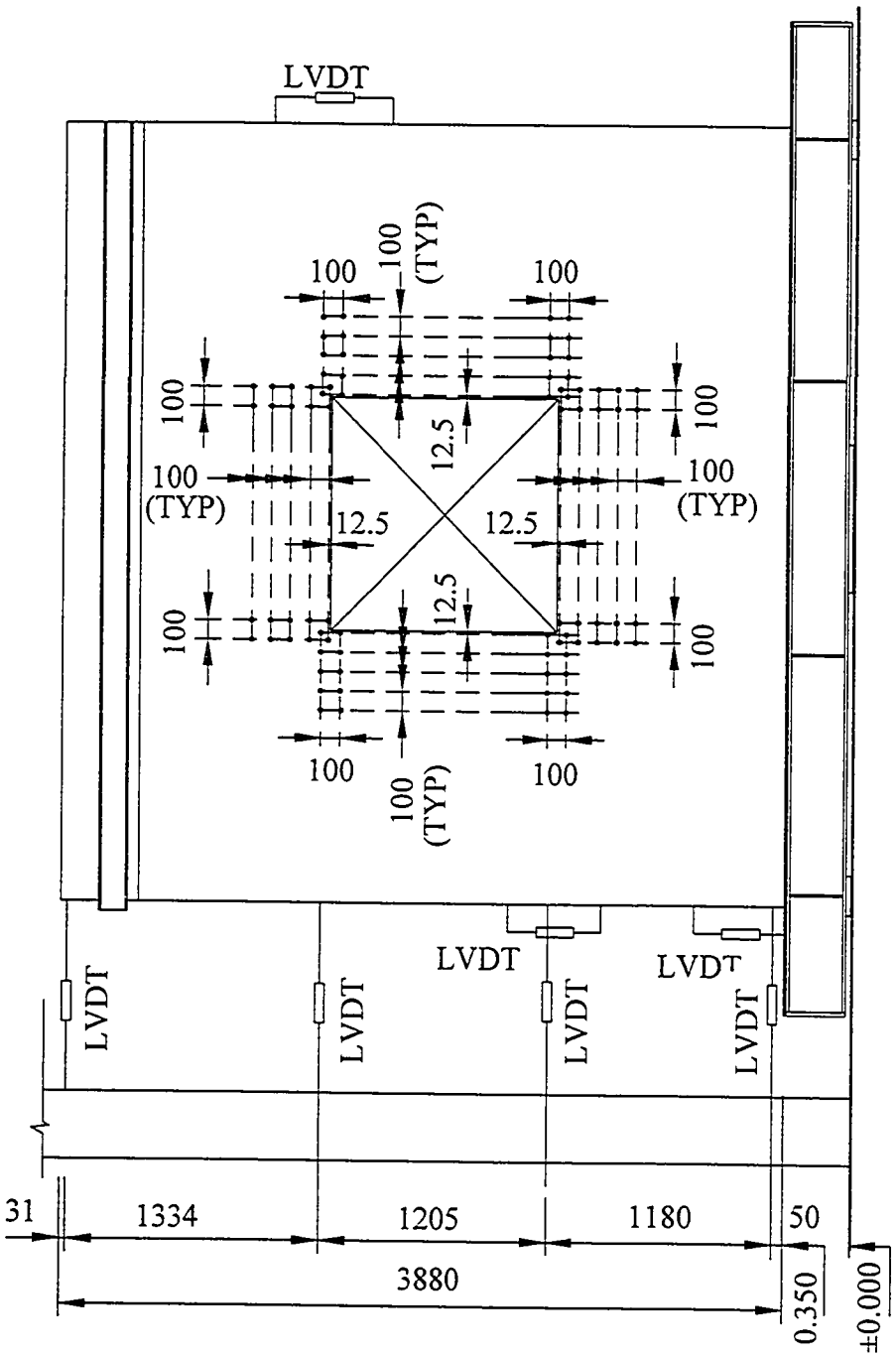

Figure 3-11 Instrumentation Layout for Wall 1

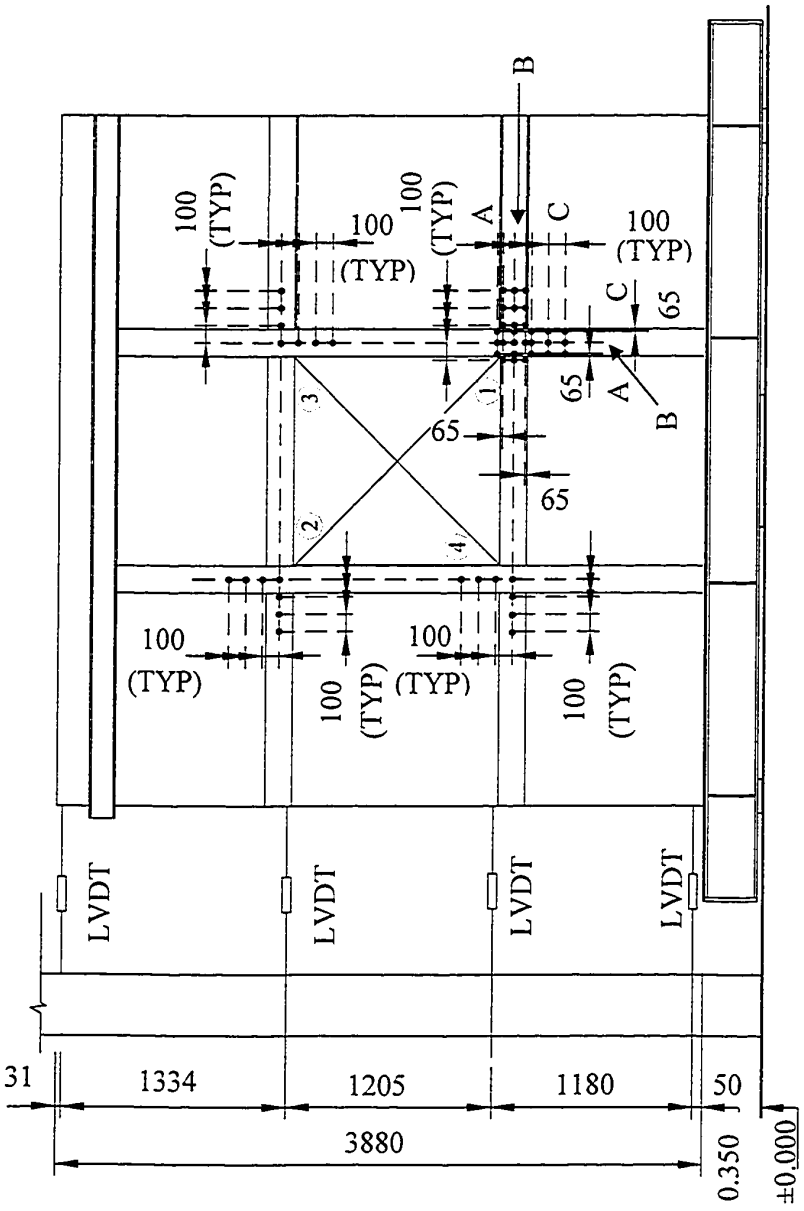

Figure 3-12 Instrumentation Layout for Wall 2

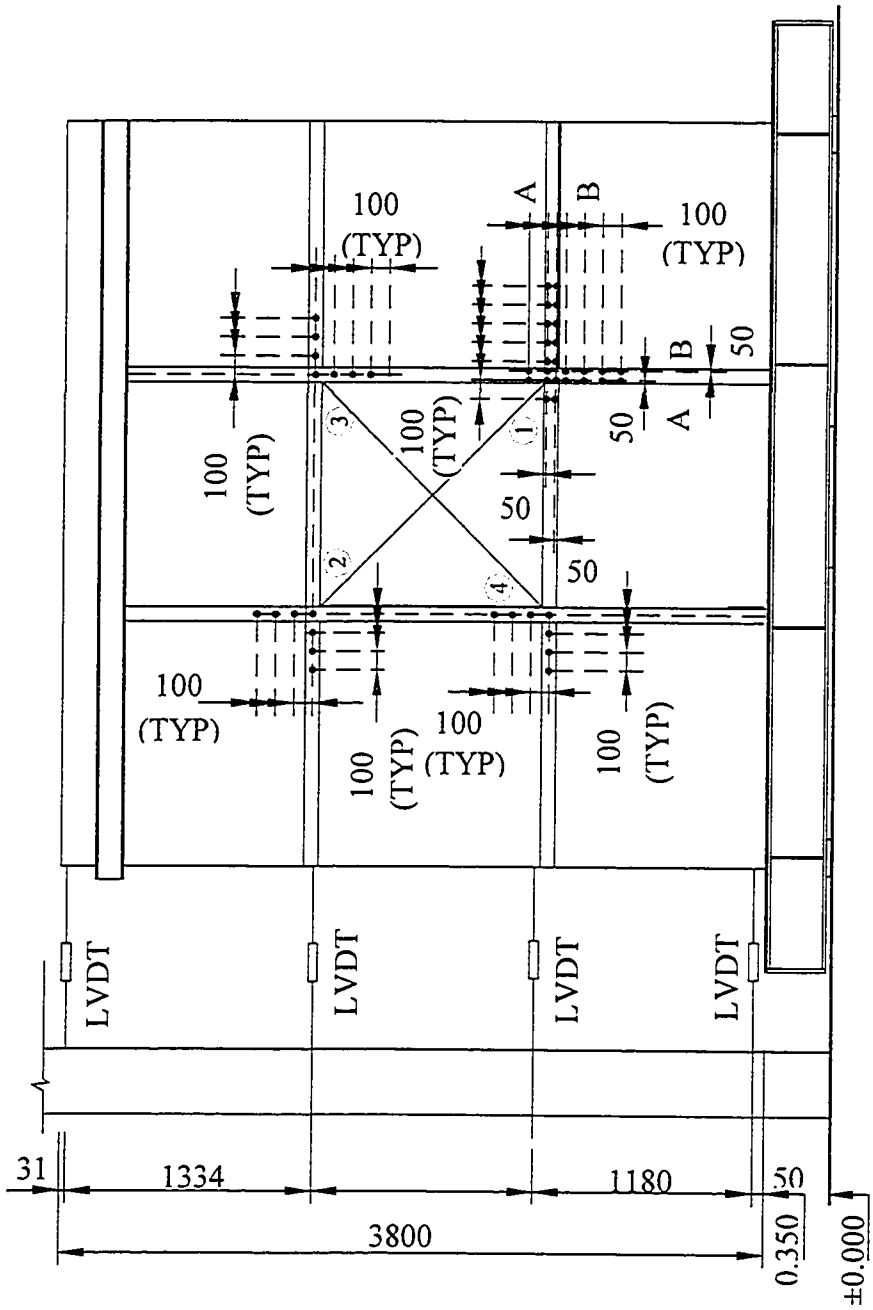

Figure 3-13 Instrumentation Layout for Wall 3

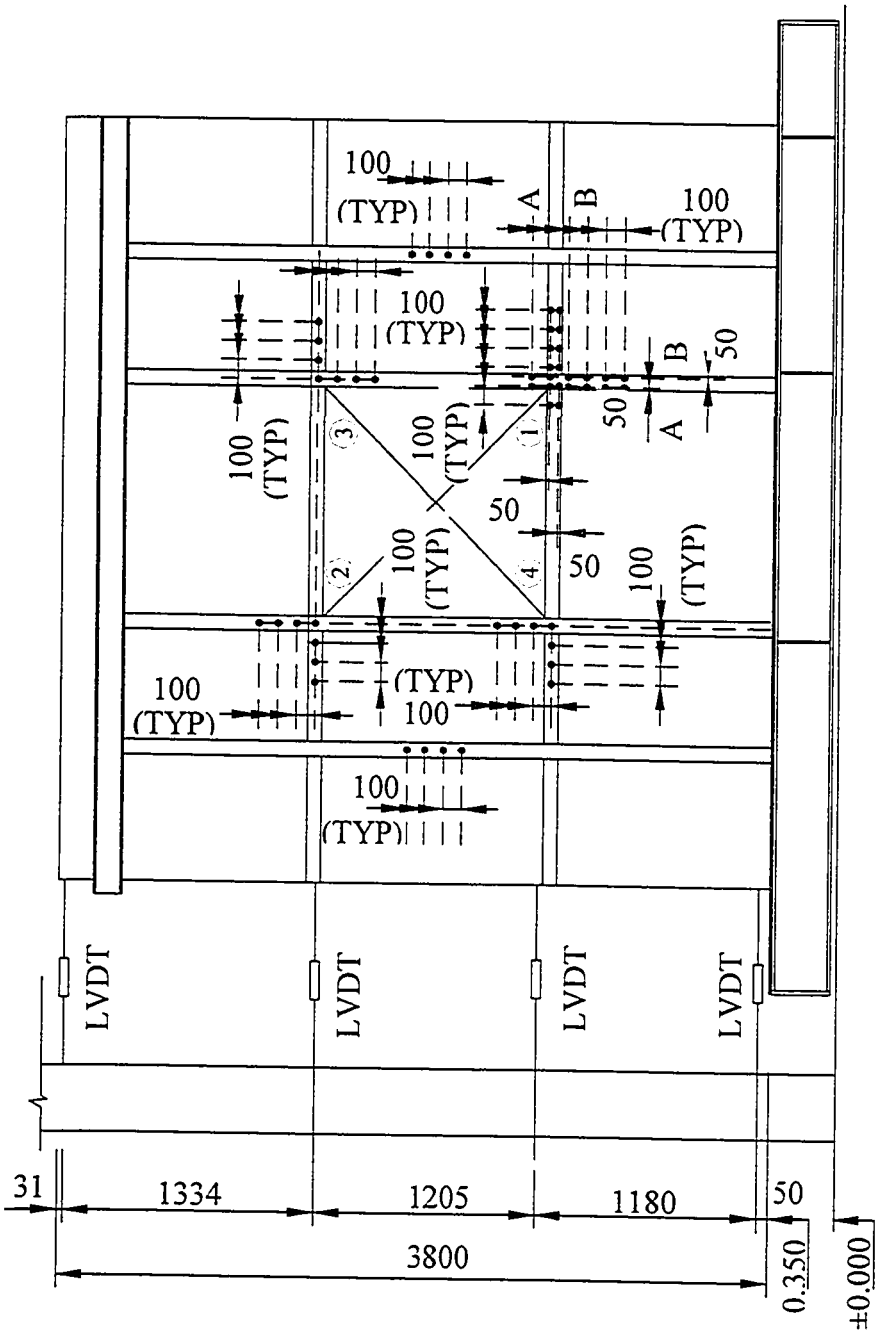

Figure 3-14 Instrumentation Layout for Wall 4

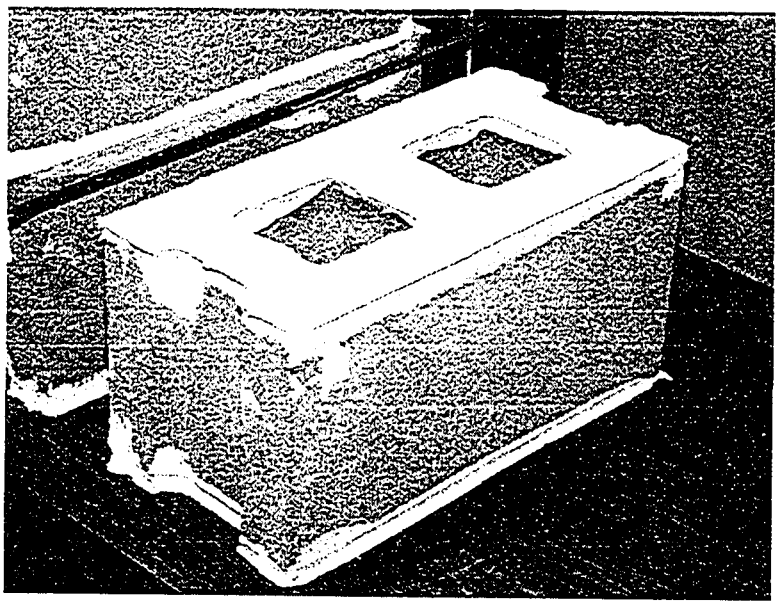

Photo 3-1 Individual Unit Specimen

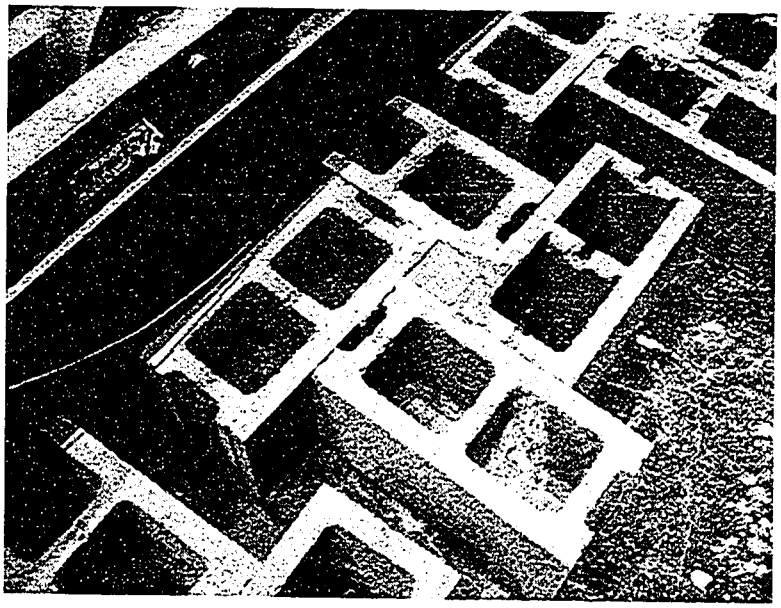

Photo 3-2 Preparation of Grout Specimen

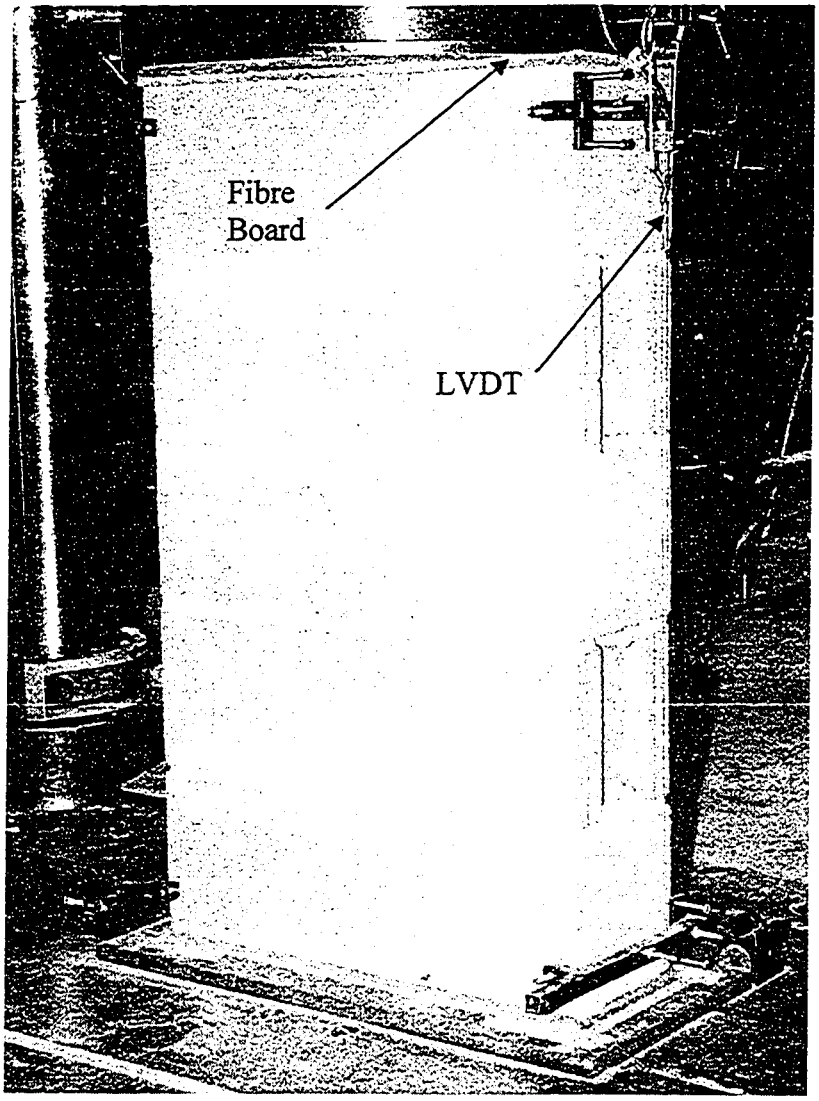

Photo 3-3 Typical Prism Specimen and Instrumentations

Photo 3-4 Typical Failure Modes for Ungrouted Prisms

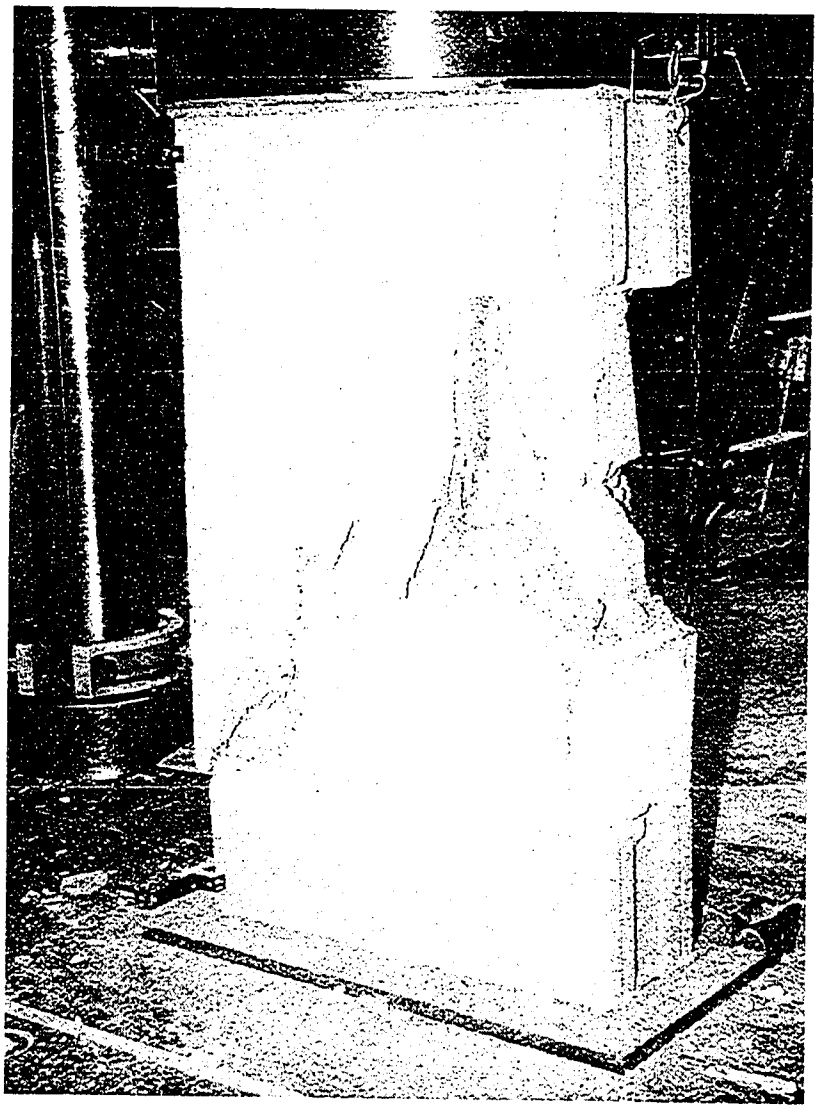

Photo 3-5 Typical Failure Modes for Fully Grouted Prisms

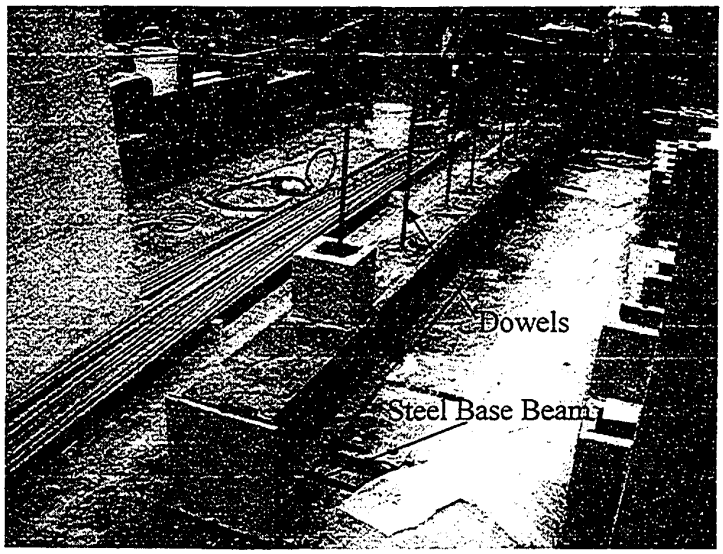

Photo 3-6 Wall Specimen Base Preparation

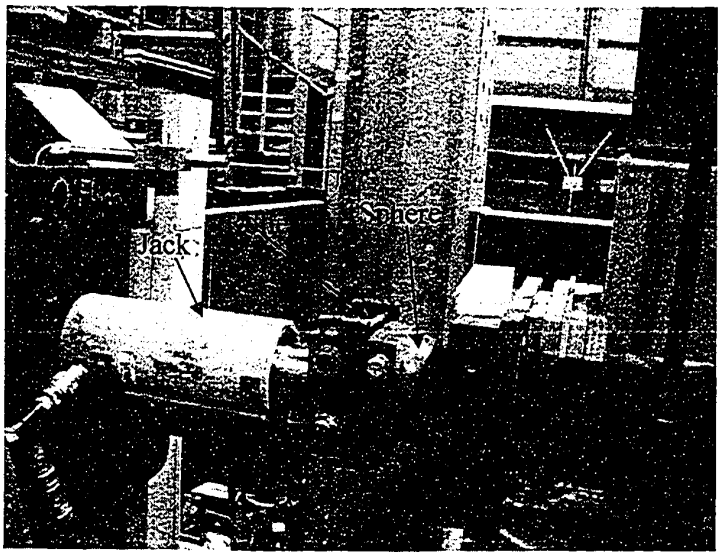

Photo 3-7 Lateral Loading Assembly

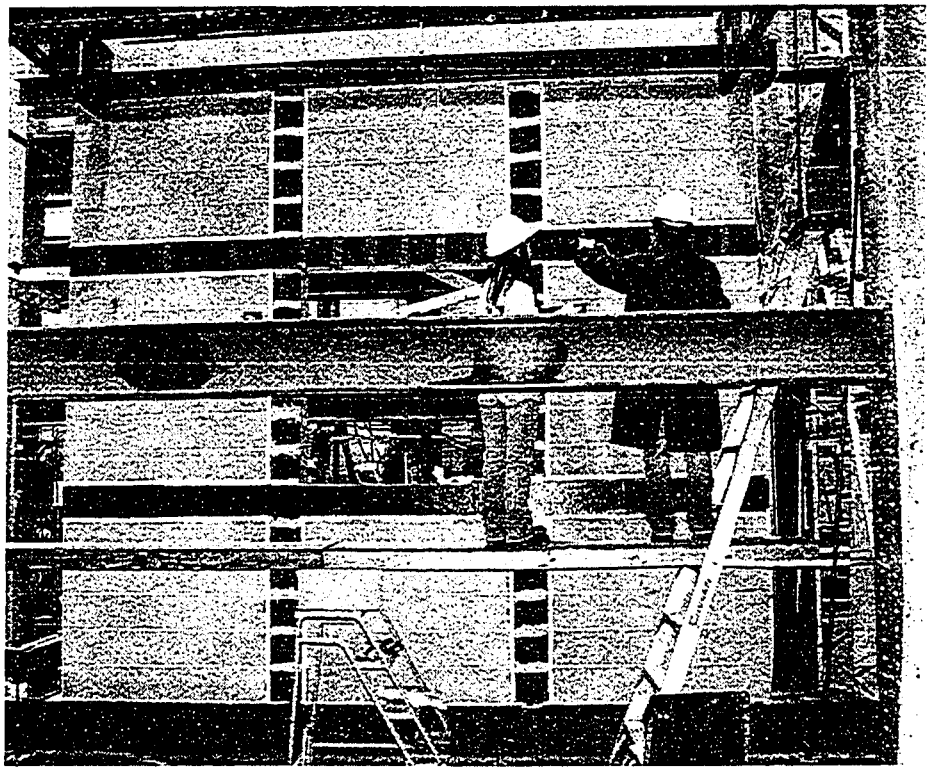

Photo 3-8 Application of CFRP Strips

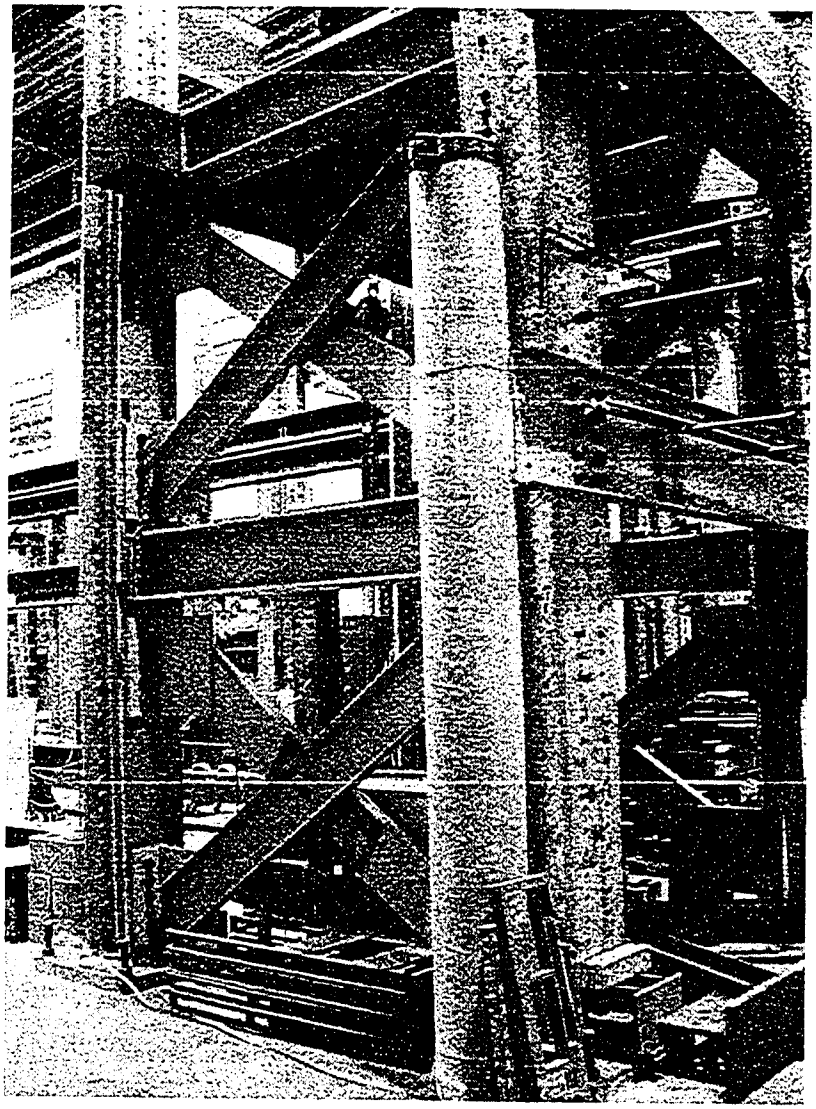

Photo 3-9 Lateral Loading Reaction Frame

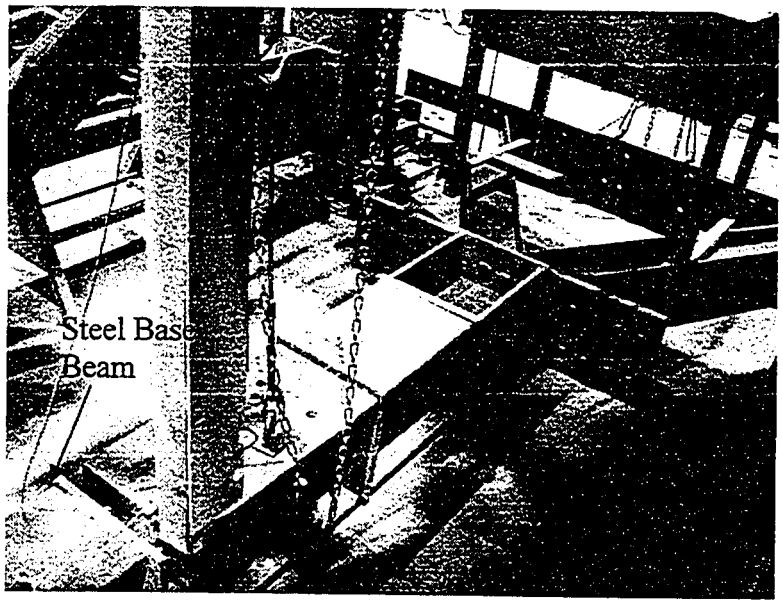

Photo 3-10 Stop Assembly

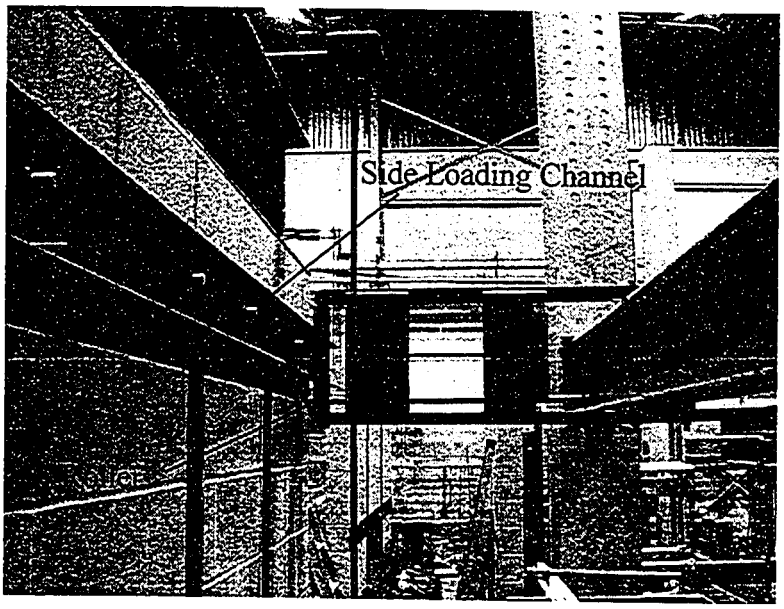

Photo 3-11 Out-of-Plane Bracing System

Photo 3-12 Gravity Loading System

4. RESULTS AND OBSERVATION

4.1 Introduction

The major test results of the experiment are presented in this chapter. The primary areas of interests are lateral load versus wall top displacement relationship and the strains of CFRP Sheets and masonry. In addition, observed crack patterns and the failure characteristics are also discussed.

4.2 Lateral Load-Displacement Behaviors

The lateral load versus top displacement behaviour for each wall under monotonic In-Plane loading is shown in Figure 4-1 through Figure 4-4 individually. In these figures the displacement is the measured horizontal top displacement subtracting the base wall slippage. The section also describes the lateral loading procedure for each wall in detail.

4.2.1 Wall 1 (Control Wall)

Specimen Wall 1 was designed as reference wall without externally epoxy-bonded CFRP Sheets. After application of a gravity load that was kept constant at 100kN with a variation of 5% throughout the test, the lateral load was applied under force control using the hydraulic jack. Figure 4-1 illustrates the lateral load versus top displacement behaviour of the control wall. Three lateral load cycles were applied at a lateral load level of 25kN to obtain the elastic stiffness of this wall specimen. It can be observed that three linear segments from the cyclic loads almost coincide with each other. Thus the elastic stiffness can be calculated as 40877N/mm by dividing lateral load under 25kN by the displacement at this load level. Last a monotonic in-plane push lateral load was applied at different load level control.

The Load versus Displacement curve in Figure 4-1 shows six regions. The first stage of loading ended at point B in Figure 4-1 with a lateral load of 75kN and 3.0mm top displacement. The control wall was in the elastic stage before this point. At this point, first cracks were observed and these cracks caused a slight degradation in stiffness

resulting in slight change in slope of the response curve. From point B to C the effective stiffness was almost constant and only some small cracks appeared at the bottom corner of the opening during this period. At point C, the second degradation in stiffness occurred because a large number of cracks appeared in the two piers beside the opening at this time. This stiffness was kept constant from point C to D. The loop between point D and E was due to an unloading process started at the point D. As the increase of lateral load, tensile stress developed at the heel of the wall due to up-lifting. When the lateral load level reached 220kN, corresponding to point D in Figure 4-1, a wide tension crack appeared in the heel of the wall and wall failed in flexure. To continue the test and obtain a shear failure mode, an external hold-down system was introduced at the heel of the wall. During the application of this hold-down system, the wall was unloaded for safety purpose and then the wall specimen was loaded to shear failure at Point E. It's evident that another degradation in stiffness occurred at point D as a result of the tension failure at the heel of the wall. Point E defines the lateral load capacity of 226kN with 26.8 mm top displacement. The load decreased dramatically after point E, and the top displacement continued to increase to 29.7 mm at the point F with the lateral load of 132kN. The test was then terminated. All loads corresponding to major cracking occurrences will be shown in Sec 4.4. The roughness of the curve was due to small creep during the halt of loading to take Demec reading or mark cracks during test.

4.2.2 Wall 2 (Strengthened with 8 CFRP Strips of 156mm Wide)

Before application of the lateral load, Wall 2 followed the same test procedure as Wall 1. Lateral load versus top displacement response of Wall 2 is shown in Figure 4-2. Three cycles of lateral loads at 25kN were first applied to the wall and an initial stiffness of 22063N/mm was obtained from three coincident lines. And then the lateral load was applied at the top of the wall by pushing. There are several points to distinguish the changing behaviour of Wall 2 during the different lateral load levels. From point A, the origin of the curve, to point A', which corresponds to a lateral load of 110kN and a top displacement of 7.0mm, the wall behaved elastically. At Point A', the first cracks appeared under the bottom corner of the opening, and there was a very slight degradation in stiffness at this time. Thus, point A' can be neglected and the slope of the curve can be

considered the same from point A to B. An external hold-down system was introduced at point A`. Until point B with a lateral load of 160kN and 10.5mm top displacement, there is no change in slope of the response curve. Large diagonal cracks occurred at the piers beside the opening at the point B, resulting in a degradation in stiffness. Two more stiffness degradations and evident drop in load occurred at points C and D. Point C with a 274kN lateral load and 23.8mm top displacement corresponds to large tension cracks at the heel of the wall, while point D at the lateral load of 340KN with a top displacement of 40.9mm represents some crushing and spalling of masonry. It should be noticed that there was a rapid increase in top displacement due to the spread of the large cracks during this loading stage. Point E defines the ultimate lateral failure force of 359kN with a top displacement of 53mm. Similar to Wall 1, a sudden large drop in load occurred at point E, while the displacement continued to increase until point F, which has a lateral load of 170kN and a maximum top displacement of 57mm. Finally Wall 2 was unloaded to point G to end this specimen test.

4.2.3 Wall 3 (Strengthened with 8 CFRP Strips of 78mm Wide)

Wall 3 was tested under the constant gravity load of 100kN with a variation of 5%. The lateral loading procedure and the lateral load versus top displacement were almost the same as those of Wall 2. Figure 4-3 shows the lateral load versus top displacement relationship of Wall 3. The wall behaviour is described in six different regions divided by seven points in Figure 4-3. Before application of the monotonic in-plane lateral load, three cyclic loads at 25kN were again applied in order to obtain the initial stiffness that had a value of 35585kN/mm in this wall. There are four evident degradations in stiffness throughout this specimen testing. Point B, which represents the lateral load of 160kN and a top displacement 9.3mm, marks the first degradation in stiffness corresponding to a large amount of cracks appearing at this time. When the lateral load reached 280kN with a 23.0 mm top displacement at point C, a second reduction in stiffness occurred resulting from the rapid propagation of a major diagonal crack. Between point C and D, the lower stiffness is attributed to the rapid spread of major diagonal cracks and some spalling of the masonry. From point D to E, the stiffness is higher than that from point C to D but a little lower than that from point B to C. This can be caused by a higher loading rate

during this loading region compared with the loading region from Point C to D. Point E points out an ultimate lateral force of 330kN with a 41.4 mm top displacement and point F corresponds to the maximum top displacement of 49.4mm with a load of 172kN. From point F to G Wall 3 was unloaded to complete this wall specimen testing.

4.2.4 Wall 4 (Strengthened with 12 CFRP Strips of 78mm Wide)

Wall 4 was tested under the constant gravity load with a variation of 5% following the same loading procedure as Wall 2 and Wall 3. Figure 4-4 illustrates the lateral load versus top displacement behaviour of Wall 4. The initial stiffness of 29968kN/mm of Wall 4 was obtained on the basis of the lateral cyclic loads at 25kN. Eleven points in Figure 4-4 were used to describe the behaviour of this specimen. There was no degradation in stiffness at point A', which corresponds to the appearance of the first cracks at 135KN lateral load and 6.5mm top displacement. The first degradation in stiffness again occurred at point B that caused a large amount of diagonal cracks under a lateral load of 160kN with 10.2 mm top displacement. When a big tension crack appeared at point C representing the situation under 300kN lateral load and 28mm top displacement, another degradation in stiffness occurred. Followed Point C, a slight drop in lateral load occurred at point C'. This load drop was caused by those cracks spreading suddenly and fast at the heel of the wall. A loop between point D and E represents an unloading process for changing a load cell whose capacity was exceeded at point D. It can be seen that some slight jumps in the curve occurred between point D' to E. These jumps describe some cracks which spread to cross the wall thickness. The maximum lateral force of 351kN with a 49.5mm top displacement defines point E. It is apparent that no dramatic drop in lateral load occurred at maximum force unlike the other three walls. At point E, there was only slight drop in load and this behaviour shows that Wall 4 is more ductile than the other walls. Until point E' with a 328kN lateral load and a 56.9mm top displacement, the lateral load had an abrupt drop and the maximum top displacement of 63.5mm was reached at point F corresponding to a load of 220kN. Finally the wall test was completed to point G by an unloading process.

4.3 Strain Behaviors

The strains were obtained based on the Demec data. The location of Demec was discussed in chapter 3. Since the four corners around opening in walls were considered as the critical regions, strains will be investigated in these four regions for each wall. Wall 1 measured the strains of masonry and other three walls studied the strains of CFRP Sheets.

4.3.1 Wall 1

Lourenco and Rots (1997) described the failure model of walls with openings as follows: "Initially the wall acted as a single rigid, rectangular panel; at the end of the test, the wall acted as several rigid, approximately rectangular sub panels." Based on these results, Wall 1 was expected to act as eight sub panels. To study interface behaviour between eight panels, a set of strains between every two adjacent panels were measured in both vertical and horizontal directions. Figure 3-11 shows the details of the measured regions while the strain behaviour is shown in Figure 4-5. In Region 1 and Region 2, almost all values of strain are positive, indicating these two regions are in tension. Strains in region 1 and region 2 are much higher than those in region 3 and region 4 that are mainly in compression. Figure 4-5 shows that strains developed relatively even before a load level of 180kN after which no more Demec data was measured for safety reasons.

Compared with the horizontal strain behaviour of region 3 and 4, it can be seen that the compression and tension regions in these two regions are anti-symmetric. The slightly higher value of vertical strain in region 4 was caused by some diagonal cracks that went through this region at a lateral load of 140kN. A jump in vertical strain at 140kN in region 1 corresponds to a crack occurring in this location at this load level, and two sets of higher horizontal strains in region 1 correspond to the joint strains where the weak bond between the mortar and the block showed larger strains.

4.3.2 Wall 2, Wall 3 and Wall 4

Strains of CFRP Sheets for Wall 2, Wall 3 and Wall 4 were recorded. Figure 3-12 through Figure 3-14 show the measured location of CFRP Sheet strains in detail. The strains in the CFRP Sheets were measured in the same four regions as those in the control wall but in different direction. Many more Demecs were mounted on the CFRP Sheets in the region 1 since this region is critical from the strain behaviour analysis and crack pattern observations of the control wall testing. For Wall 2 strengthened with 156mm wide CFRP strips, three lines for strain study were measured in each vertical and horizontal direction in region 1 shown in Figure 3-12. While only two investigated lines were measured in each vertical and horizontal direction in region 1 for Wall 3 and Wall 4 because these CFRP strips were only 78mm wide shown in Figure 3-13 and 3-14. Only one line for strain investigation was measured in other regions for Wall 2, Wall 3 and Wall 4.

The strain behaviour of CFRP reinforcement was shown in Figure 4-6 to Figure 4-8. Strains of CFRP Sheets will be discussed in four regions around opening. Evidently, Wall 3 and Wall 4 had an average higher strain than strains of Wall 2 in tension region 1. This can be attributed to the wider CFRP strips that provided more effective restraint of the development of cracks. It can be seen that strains in line A were higher than strains in line B, indicating that strains of CFRP Sheets that are closer to the opening were greater than those of CFRP Sheets further to the opening. In region 2, Wall 3 and Wall 4 had similar strain behaviour, but strains of Wall 4 were higher than Wall 3. Again, Wall 2 had lower strains in tension region 2 than that in Wall 3 and Wall 4, that's maybe because strains measured in Wall 2 were further away from the opening compared with Wall 3 and Wall 4 for region 2. Compared with the strain behaviour of region 3, it is apparent that the extra CFRP strips in the middle of piers in Wall 4 changed the strain behaviour of region 3. After application of extra CFRP strips, strains in region 3 showed a larger compression and no tension in vertical direction. The same effect of extra CFRP strips occurred in region 4 of Wall 4 based on the observation of horizontal strain behaviour. It should be

noted that horizontal strains of region 4 in Wall 2 are almost positive indicating this region were in tension, while negative horizontal strains of region 4 for Wall 3 and Wall 4 show that CFRP reinforcement was in compression at this location. Comparison of strain behaviours of CFRP Sheets between region 5 and region 6 in Wall 4 demonstrates that the panels in region 5 and region 6 acted anti- symmetrically.

4.4 Failure Modes

Shear walls subjected to horizontal loads may fail in one of three ways. The first one is sliding failure, which is resisted by dowel action of vertical reinforcement and by friction on the mortar bed. The other two failure modes are flexural failure and shear failure. Two distinct modes of failure were observed in these wall specimens: flexural failure and shear failure. Firstly the flexural mode of failure for specimen Wall 1 (control wall) occurred with a distinctly dominant flexural crack at the horizontal mortar bed in the second lowest course of the heel of the wall. In order to force a shear failure, an external hold-down system was applied and Wall 1 continued to carry the increasing lateral load until it failed in shear indicated by a dominant diagonal tensile cracking. The other three walls strengthened with CFRP Sheets failed in shear. In all strengthened walls a hold-down system was applied at the heel of walls before the flexural failure occurred. Photo 4-1 through Photo 4-4 illustrates the failure modes through the crack patterns of walls after failure.

4.5 Crack Patterns

Figure 4-9 to Figure 4-12 show scheme crack patterns that were mainly observed from one side of wall and formed at the various levels of lateral load. On these patterns heavy lines indicate the major or wide cracks and hatched areas present crushing or spalling at the masonry. It is evident that walls behaved mainly in a shear mode where the diagonal shear cracks progressed with increasing lateral loads and those diagonal cracks at the critical sections started to widen up until walls finally failed by diagonal splitting of masonry wall and debonding of the CFRP strips from the concrete masonry surfaces which the major diagonal shear cracks went through.

4.5.1 Wall 1

Figure 4-9 illustrates the cracks that formed at different lateral load levels in Wall 1. The first crack was observed at a lateral load of 75kN. It was a diagonal crack that formed at the bottom corner of the opening and then progressed through the bed and head joints in a stair-stepped pattern because of the lower block/mortar interface bond strength comparing with the tensile strength of units. At a lateral load of 140kN extensive stair-stepped cracks appeared at the bottom corner of the opening and on the pier in the toe of the wall. This load level also caused some horizontal flexural cracks at the heel of the wall. At the lateral load of 160kN some diagonal cracks occurred at the other two opening corners. It was noticed that the first sign of cracks through the block was exhibited at this load level. After this load level, some fine dust fell down from the masonry and a light noise was heard. Also some diagonal cracks started to progress with increasing lateral loads. A major diagonal crack formed at 180kN lateral load and it was inclined at approximately 45° diagonally from the right top corner of opening to the second lowest course in the toe of the wall. This diagonal crack propagated fast and became predominant. Several diagonal cracks also appeared in the same region and the other regions.

Until 200kN lateral load only two new 45° diagonal cracks were observed parallel to the major cracks in the right pier, while the sound from the wall became louder and louder indicating a quick spread of a horizontal flexural crack at the second lowest bed joint in the heel of the wall. And then a loud noise was recorded that was caused by separation of these two blocks between the first and second lowest courses and a sudden split in the second lowest course in heel of the wall. The behaviour of this wall was governed by local flexural failure in the heel of the wall because of the bending of the vertical reinforcement.

In order to force the wall to fail in shear, an external hold-down system was applied and the wall continued to carry increasing lateral loads until another loud cracking sound was recorded at a maximum lateral load of 226kN. This loud noise was caused by a diagonal

splitting along that major 45° diagonal crack in right pier and crushing of the masonry at the toe of the wall. At this point a new big crack appeared inclined up at 45° diagonally from the toe of the wall where a crush occurred. Clearly this wall failed in a shear mode because of the low resistance by dowel action of the vertical rebar and this control wall had no shear reinforcement to resist the lateral load. There was an abrupt loss of load carrying capacity of 42%. Photo 4-1 shows the view of the crack patterns for Wall 1 after failure.

4.5.2 Wall 2

As expected this wall specimen failed in a shear mode. Figure 4-10 represents the cracks that formed in Wall 2. Four 156mm wide CFRP strips and a central opening divided the wall into eight regions shown using numbers from 1 to 8 in Figure 4-10.

The first cracks mainly occurred in region 2, 4, 6 and 8 at110kN lateral loads. All these cracks are in a stepped pattern and appeared under the steel channel at the top of the wall in region 2 or beside or under the CFRP strips in regions 4, 6, and 8. More extensive first cracks in Wall 2 compared with that in Wall 1 illustrate that the shear forces were transferred to a larger area of masonry panel because of the application of CFRP strips.

Few new cracks were observed before a lateral load of 160kN. At 160kN lateral load some new stair-stepped cracks formed in regions 4, 7 and 8, while the first sign of cracks through the block was observed in region 8 at this load level. At a lateral load of 200kN more extensive stair-stepped cracks appeared in all regions. It's important to mention that several diagonal cracks inclined at about 45° occurred at the top corner of the opening and beside the CFRP strips to the edge of the wall and the top of the CFRP strips in region 5 and at the bottom of the strips at the toe of the wall in region 8. After this point some new diagonal cracks occurred with the approximate diagonal angle of 45° in seven regions with exception of region 3. As the lateral load increased, some diagonal cracks in regions 5 developed and extended under the horizontal CFRP strips.

At 276kN lateral load, there was a loud sound caused by the flexural horizontal cracks that formed in the middle of the lowest block at the heel of the wall. A small sudden drop in lateral load was observed at this point, while the wall could still carry the increasing load until another loud noise occurred at a lateral load of 330kN. This noise was caused by spalling of masonry between two major cracks in region 5 and a big tension crack at the second lowest head joint in the heel of the wall. Although there was another light drop in lateral load at this load level, the wall still had the capacity to carry increasing load until a series of loud noises were recorded at the maximum lateral load of 359kN. These noises were firstly caused by several dominant diagonal cracks splitting through the wall thickness and some spalling of masonry, and then a sudden debonding of horizontal CFRP strips from the masonry surfaces which the dominant diagonal went through was recorded

At failure some new diagonal cracks were observed in regions 5 and 8 and a long vertical splitting was formed from the bottom of the dominant cracks in region 5 to the toe wall in region 8. Rupture of the vertical CFRP strips were observed at the left bottom corner of opening in region 4 and at the right top corner of opening where the dominant diagonal cracks went through in region 5. There was an abrupt loss of load carrying capacity of approximate 53%. Photo 4-2 shows the view of the crack patterns for Wall 2 after failure.

4.5.3 Wall 3

The cracking pattern observed for Wall 3 was similar to the patterns observed for Wall 2. Figure 4-11 illustrates cracks formed at the various lateral load levels. Similarly there are eight regions divided by four 78mm wide CFRP strips shown in Figure 4-11 to describe cracks. The first cracks appeared again at an 110kN lateral load. These stair-stepped cracks mainly formed in region 2, 6, 7 and 8 and they propagated along the bed joints and across the head joints. A horizontal tension crack was also observed at the second lowest bed joint in the heel of the wall. At a lateral load of 160kN extensive stair-stepped cracks occurred in almost all regions with exception of region 3. The first sign of cracks through the block was also observed at this load level, similar to Wall1 and Wall 2.

Before 280kN lateral load, extensive diagonal cracks formed in seven regions with exception of region 3 at the approximate equal load intervals. Some of these diagonal cracks had a rapid progress and became dominant cracks as the load increased. At 280kN lateral load level there was a loud noise because of a sudden splitting of the first head joint from the heel of the wall. This splitting only caused a very small drop in loads; however it caused an evident degradation in stiffness. At this point two major diagonal cracks inclined at about 45° from the corner of the opening in region 5 had developed and became dominant cracks. Simultaneously, some flaking of surface of the masonry was also apparent in this region.

As the load increased some 45° diagonal cracks in regions 5 and 8 propagated fast and some low sounds were heard until two loud noises were recorded at the ultimate lateral load. The first loud noise was from the 45° diagonal cracks which went through the whole wall thickness. Following this sound another loud noise was recorded from the sudden delaminating (debonding) of the end of horizontal CFRP strips under the opening. Simultaneously a sudden vertical splitting of masonry from the toe of the wall up to dominant diagonal crack was recorded.

After failure some new diagonal cracks were also observed in regions 1, 4, and 5. There were also two ruptures of CFRP strips. One of them is the same as that in the Wall 2 and it appeared on the vertical CFRP strip at the top right corner of the opening into which the dominant diagonal cracks extent. The other one appeared on the horizontal CFRP strip beside the vertical CFRP strip at the left top corner of opening. There was an abrupt loss of load carrying capacity of approximate 48%. Photo 4-3 shows the view of the crack patterns for Wall 3 after failure.

4.5.4 Wall 4

Wall 4 behaved in a more ductile manner than the other three walls. Figure 4-12 illustrates cracks that formed in Wall 4. The first crack load was 135kN and some stair-stepped cracks in region 2, 7 and the left part of 6 indicated as L/6 in Figure 4-12 were

observed at this point. At a160kN lateral load extensive diagonal cracks appeared in almost all regions and the first sign of cracks through blocks in regions R/1 and R/8 were again observed. This situation matched the degradation in stiffness. Several new diagonal cracks appeared evenly in almost all regions except for region 3 after this load and some of these cracks had a rapid progress as the load increased.

The initial diagonal cracks with an angle of 45° in region 5 at a lateral load of 220kN and in region 8 at 180kN lateral load progressed so fast that they become dominant. There was a loud sound from the interface separation between the heel of the wall and the steel base beam because of broken dowels. It can be explained that no-weldable steel rebars were used as dowel welded on the steel base beam in this wall specimen and the high tension stress from the welding caused the rupture of the rebars in this wall. This was proved by the investigation that two dowels at the heel of the wall were broken at the welding location. There was a slight drop in lateral load; however the wall still carried the increasing load until the maximum lateral load of 351kN. Started from a lateral load level of 300kN the 45° major diagonal cracks in regions 5 and 8 widened up fast and at the same loading region the re were a series of small sounds. S everal loud noises were recorded before the debonding of the end of horizontal CFRP strips at the right bottom of opening.

Following the debonding of CFRP strips, the major 45° diagonal cracks at the top of deboned CFRP in region L/5 went through the masonry wall thickness and extent into those major cracks at the bottom of debonded CFRP in region R/8. Spalling of the masonry between major 45° diagonal cracks was apparent at this time. In addition to the rupture of CFRP strips at the right top corner of opening where the major diagonal cracks crossed the wall thickness in region L/5, there were other two evident failures of CFRP strips. One of them is bending deformation, it appeared on the vertical CFRP strip crossed by debonded horizontal CFRP strip in the middle of the pier because this vertical CFRP strip restrained the development of debonding of the horizontal CFRP strips at this location. The other CFRP rupture was observed at the left bottom corner of opening in region R/4 where a large 45° diagonal crack developed through this vertical CFRP strip.

Unlike Wall 2 Wall 3, no vertical splitting of masonry was observed from the toe of the wall. Photo 4-4 shows the view of the crack patterns for Wall 4 after failure.

It's important to mention that there was not an abrupt drop in maximum lateral load at failure in Wall 4. The maximum lateral load decreased slowly to 93% of this load capacity and then there was a sudden loss of load carrying capacity of about 33%. During this period the wall gave an enough damage warning. Apparently Wall 4 demonstrated more ductile than other three walls.

After testing the failed wall investigation was carried out and it showed that all the vertical reinforcement rebars in the middle of right pier bent where the major diagonal tension shear cracks crossed and this behaviour illustrated the effective dowel action of vertical reinforcement under In-Plane lateral load.

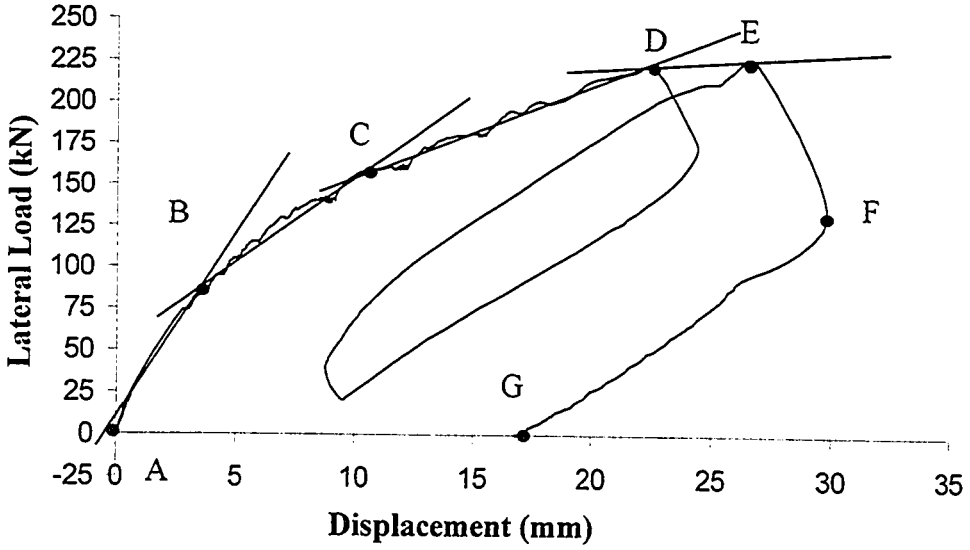

Figure 4-1 Lateral Load Vs. Top Displacement of Wall 1

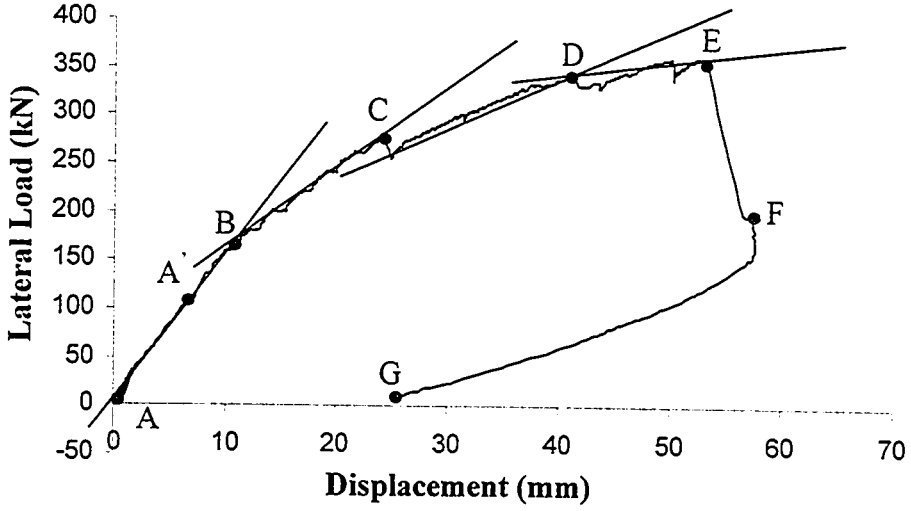

Figure 4-2 Lateral Load Vs. Top Displacement of Wall 2

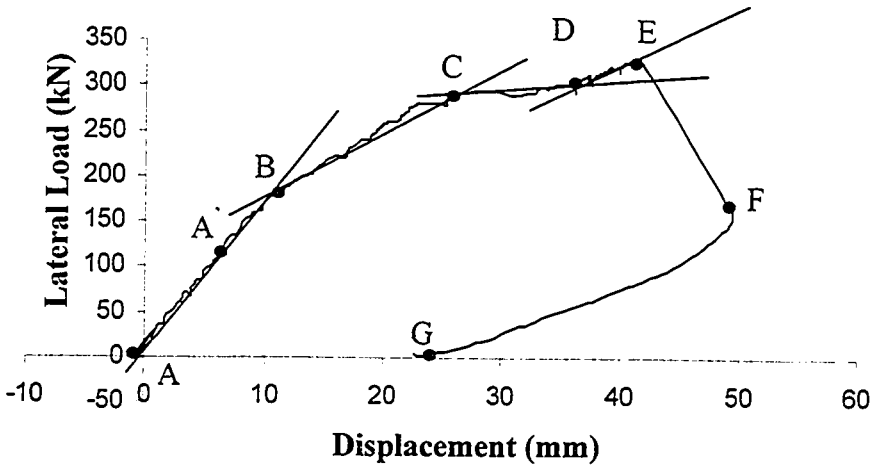

Figure 4-3 Lateral Load Vs. Top Displacement of Wall 3

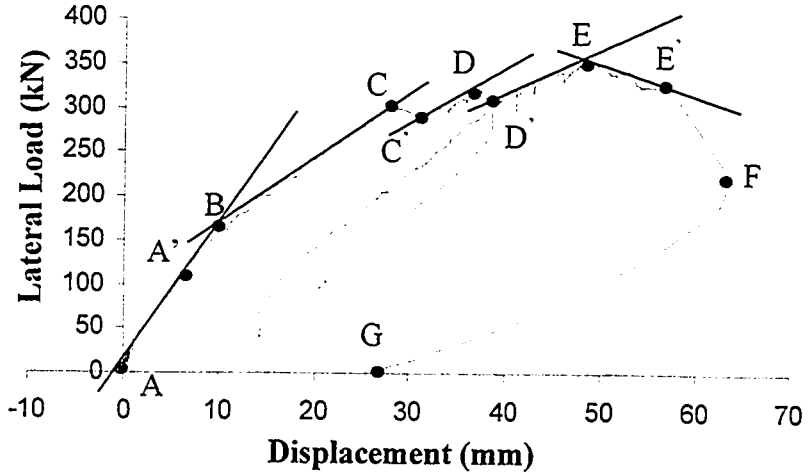

Figure 4-4 Lateral Load Vs. Top Displacement of Wall 4

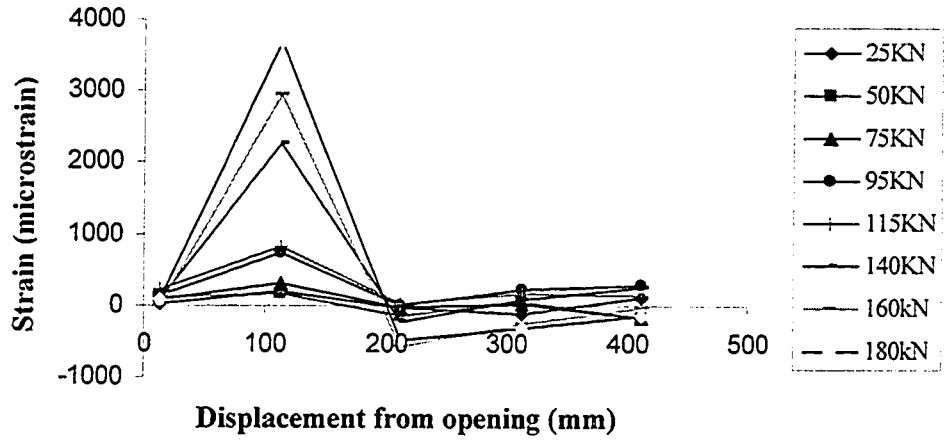

Vertical Strain Behaviour of Region 1 (Wall 1)

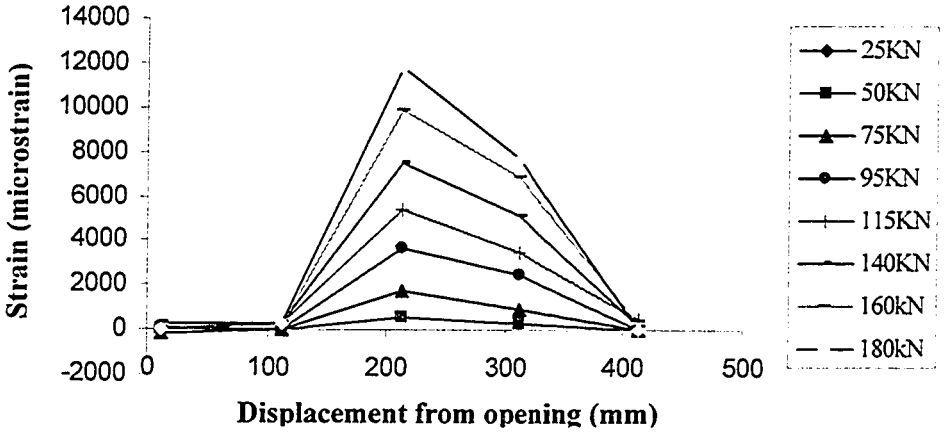

Horizontal Strain Behaviour of Region 1 (Wall 1)

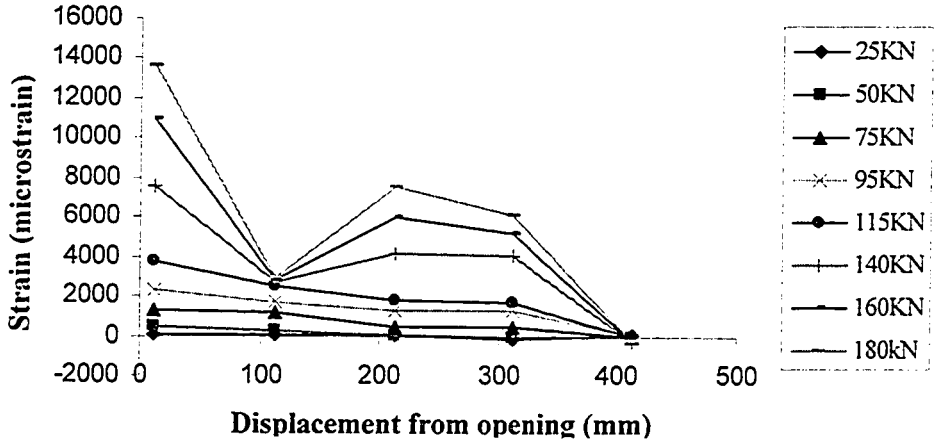

Vertical Strain Behaviour of Region 2 (Wall 1)

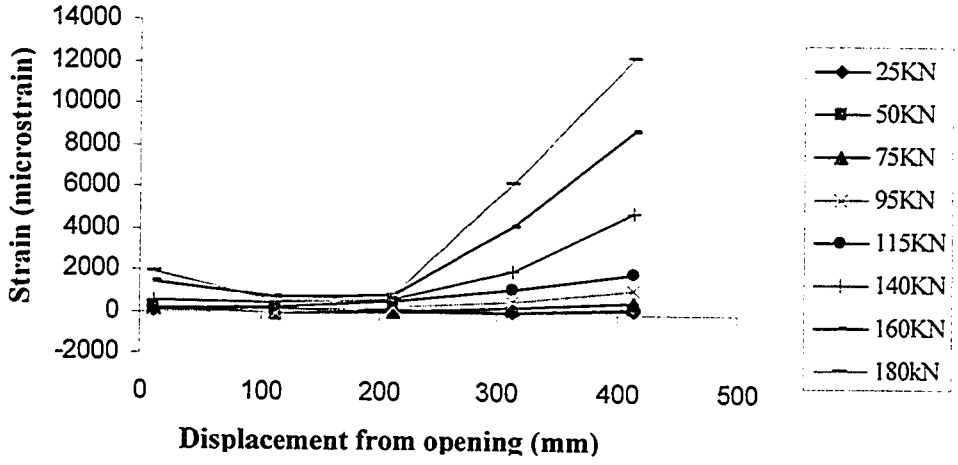

Horizontal Strain Behaviour of Region 2 (Wall 1)

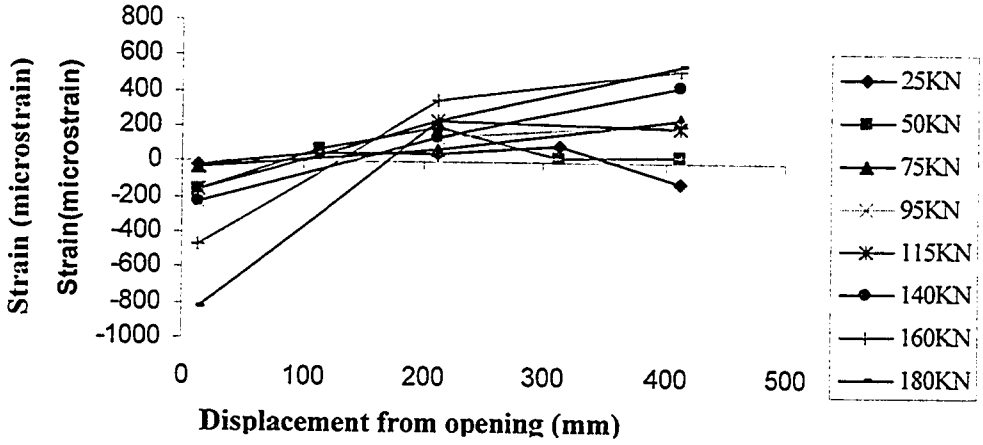

Vertical Strain Behaviour of Region 3 (Wall 1)

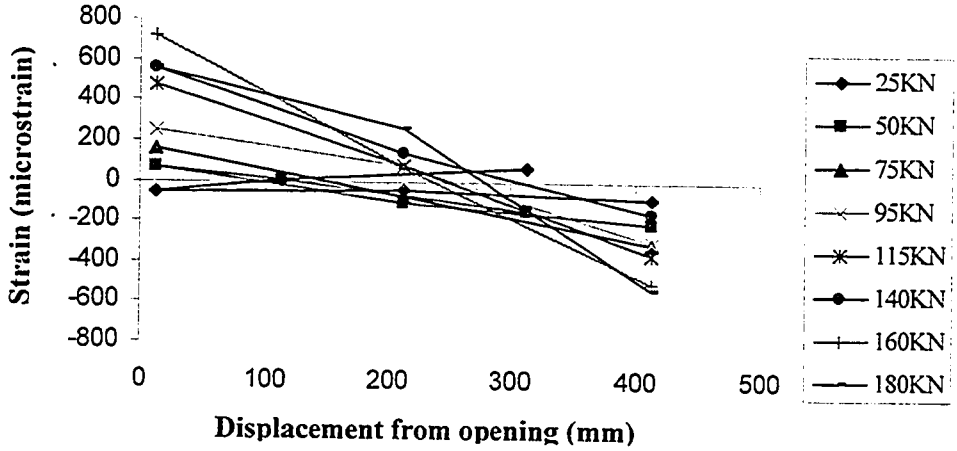

Horizontal Strain Behaviour of Region 3 (Wall 1)

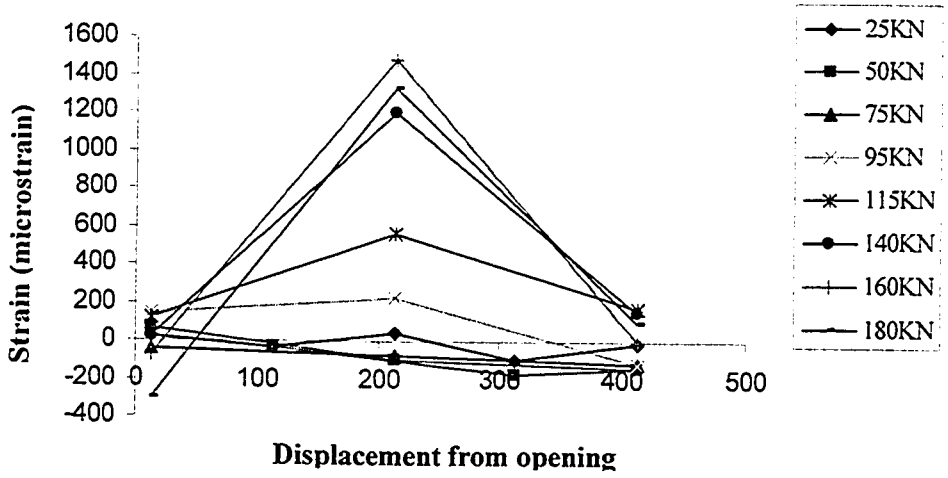

Vertical Strain Behaviour of Region 4 (Wall 1)

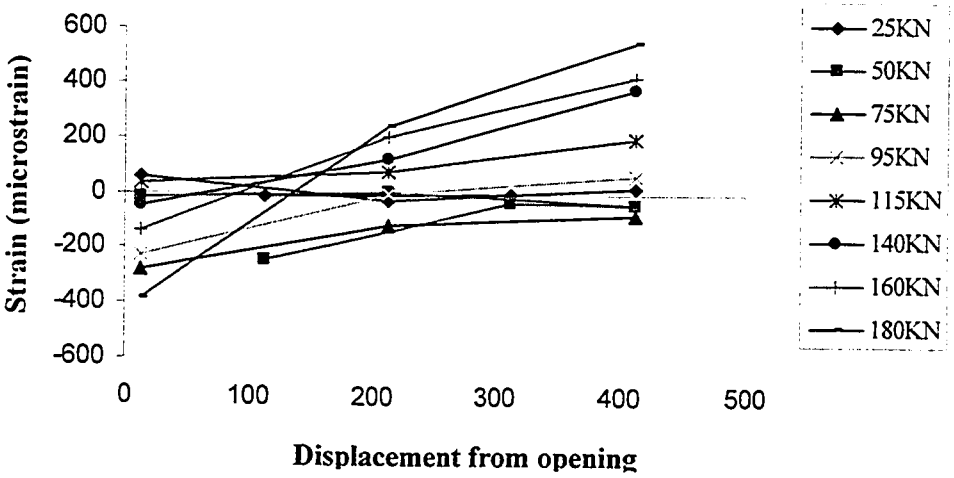

Horizontal Strain Behaviour of Region 4 (Wall 1)

Figure 4-5 Strain Behaviors of Wall 1

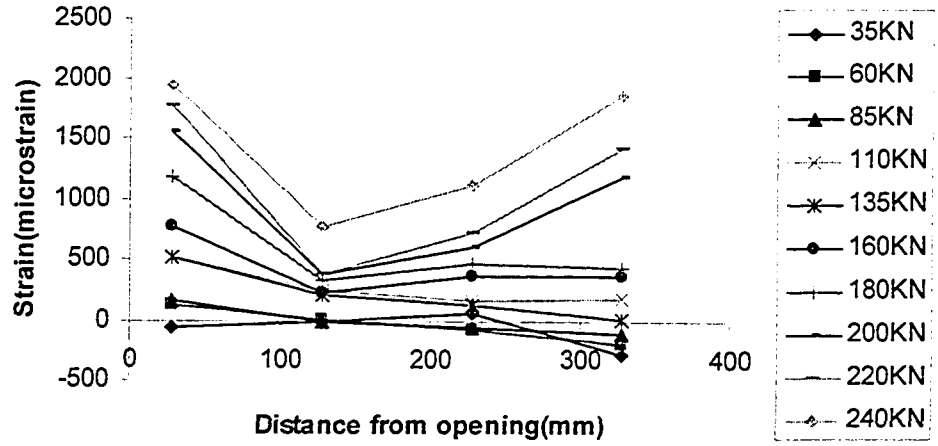

Vertical Strain behaviour of Region 1 (Line A) (Wall 2)

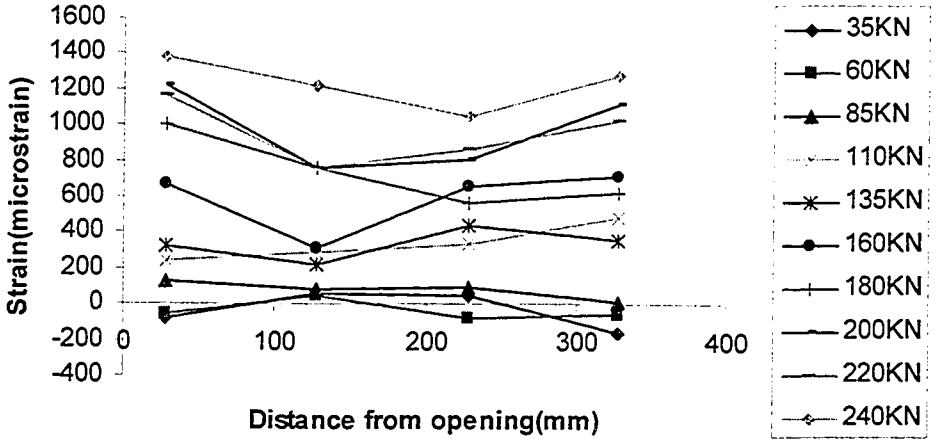

Vertical Strain behaviour of Region 1 (Line B) (Wall 2)

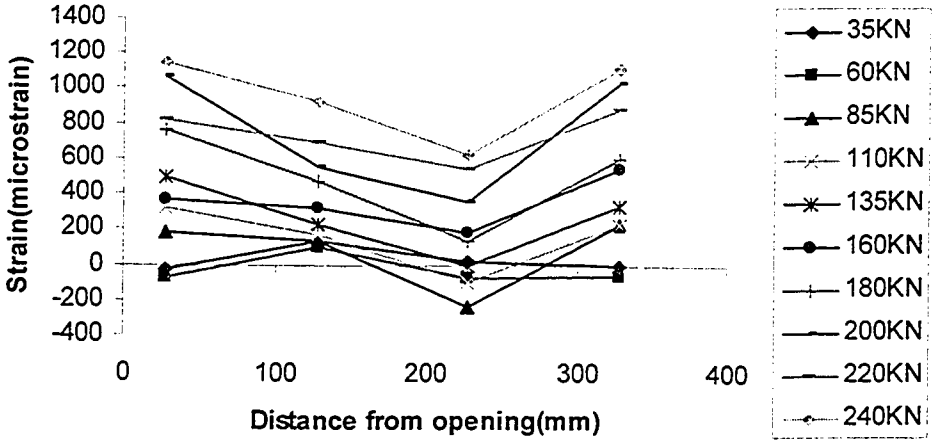

Vertical Strain behaviour of Region 1 (Line C) (Wall 2)

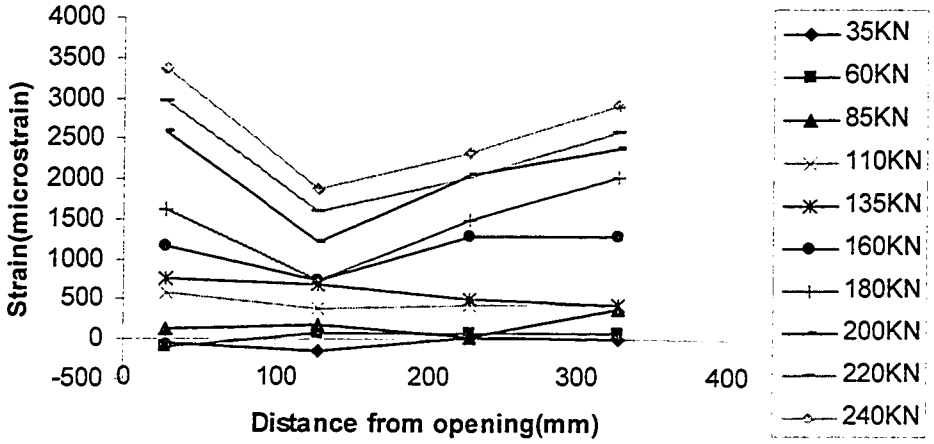

Horizontal Strain behaviour of Region 1 (Line A) (wall 2)

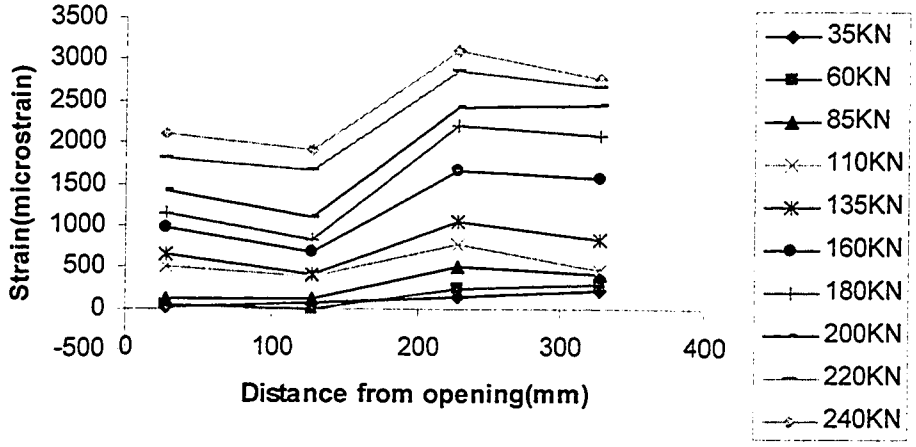

Horizontal Strain behaviour of Region 1 (Line B) (Wall 2)

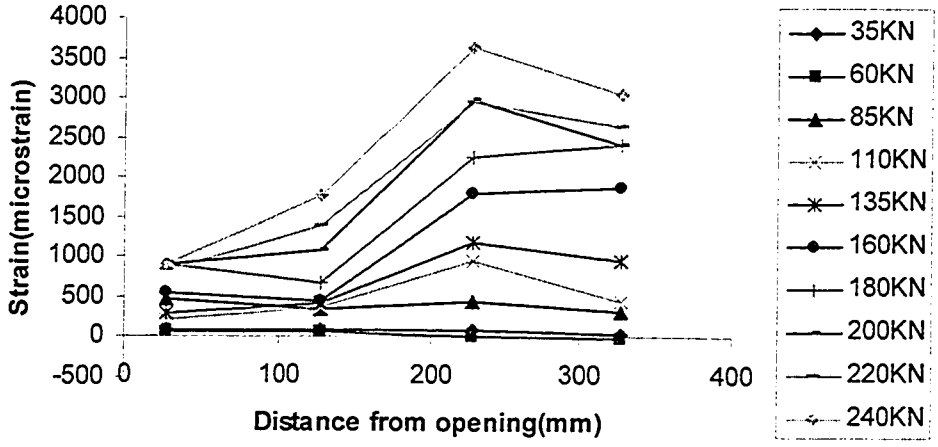

Horizontal Strain behaviour of Region 1 (Line C) (Wall 2)

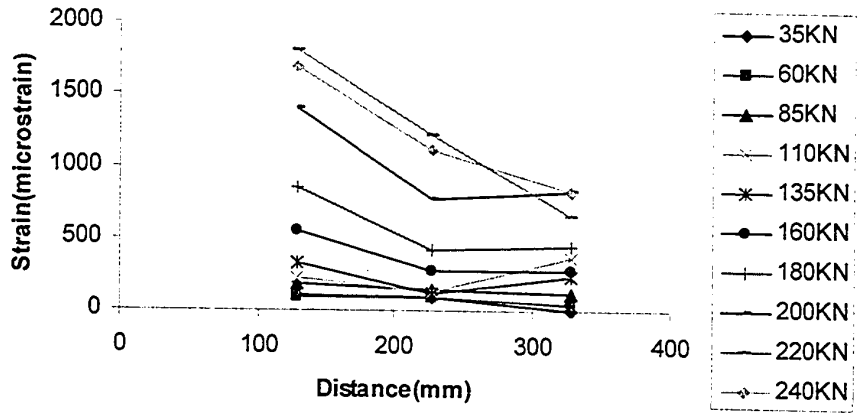

Vertical Strain behaviour of Region 2 (Wall 2)

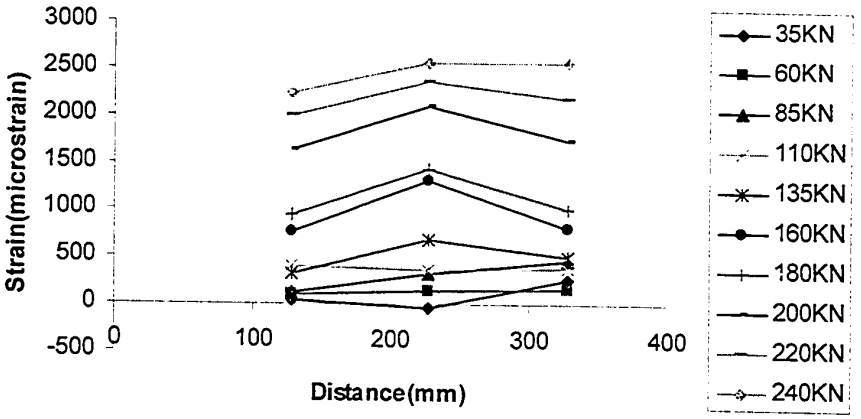

Horizontal Strain behaviour of Region 2 (Wall 2)

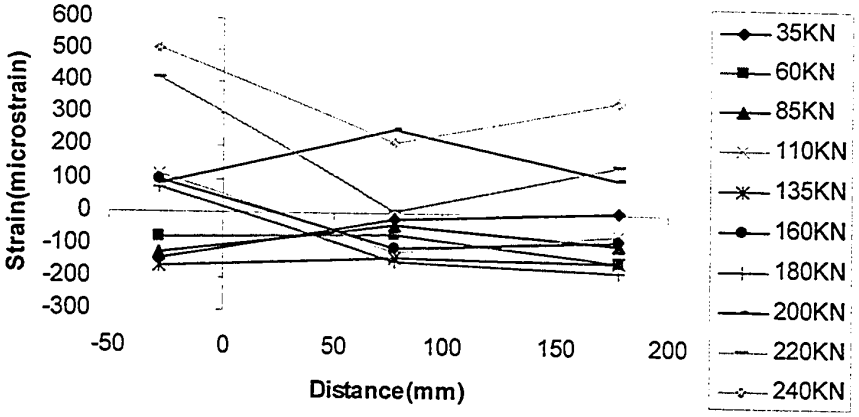

Vertical Strain behaviour of Region 3 (Wall 2)

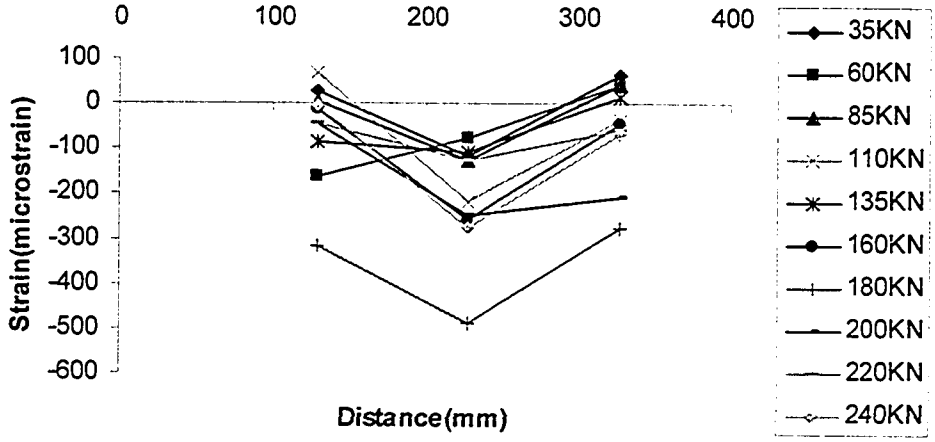

Horizontal Strain behaviour of Region 3 (Wall 2)

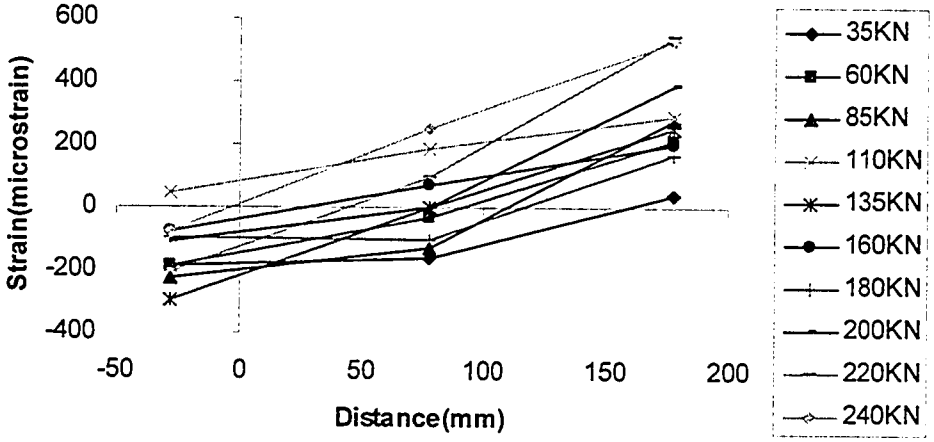

Vertical Strain Behaviour of Region 4 (Wall 2)

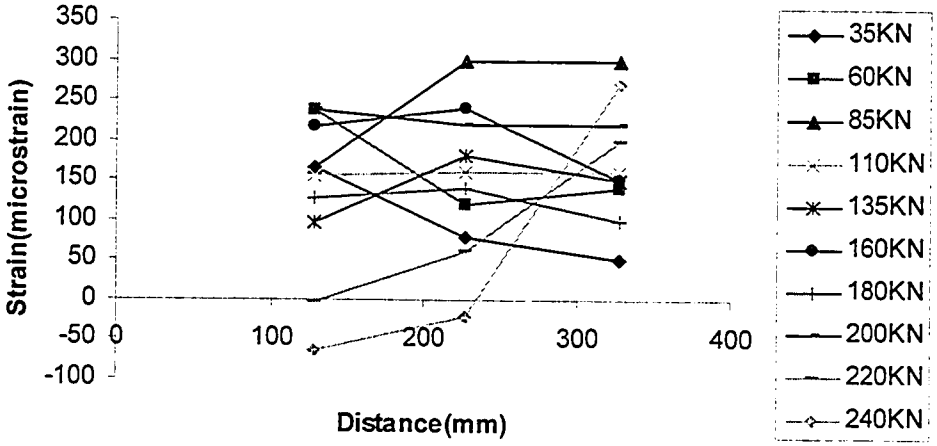

Horizontal Strain Behaviour of Region 4 (Wall 2)

Figure 4-6 Strain Behaviors of Wall 2

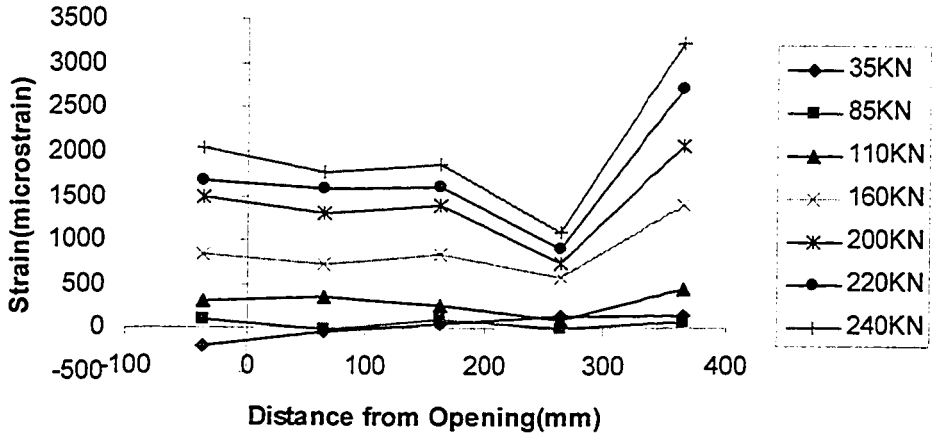

Vertical Strain Behaviour of Region 1 (Line A) (Wall 3)

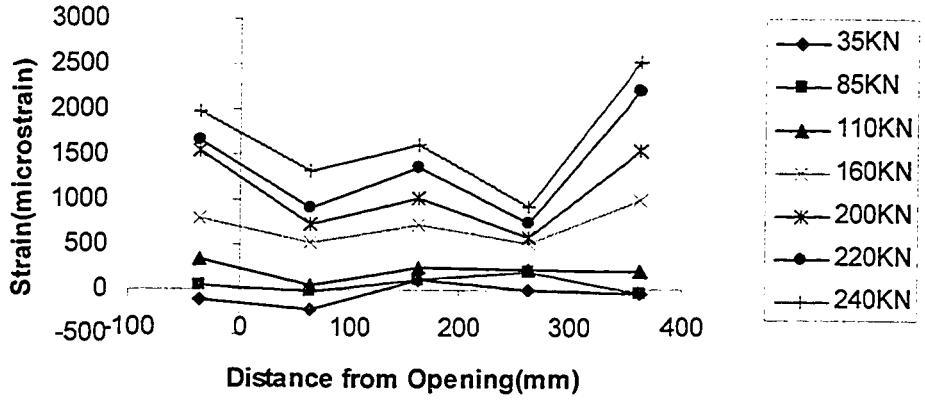

Vertical Strain Behaviour of Region 1 (Line B) (Wall 3)

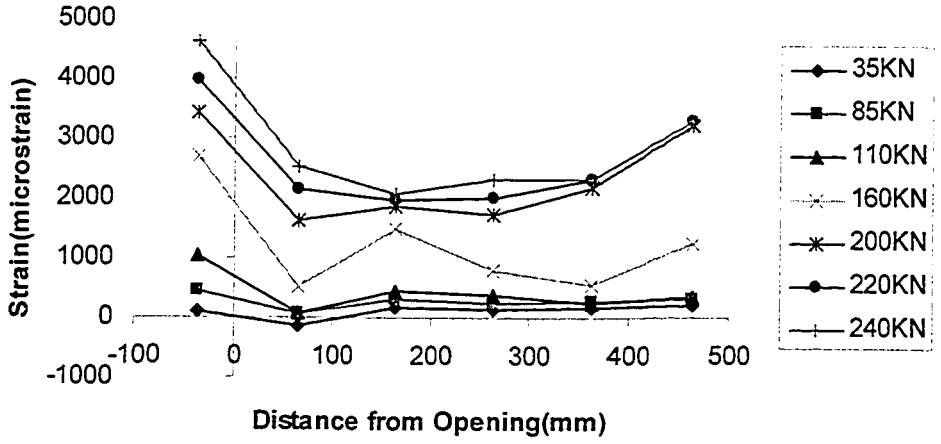

Horizontal Strain Behaviour of Region 1 (Line A) (Wall 3)

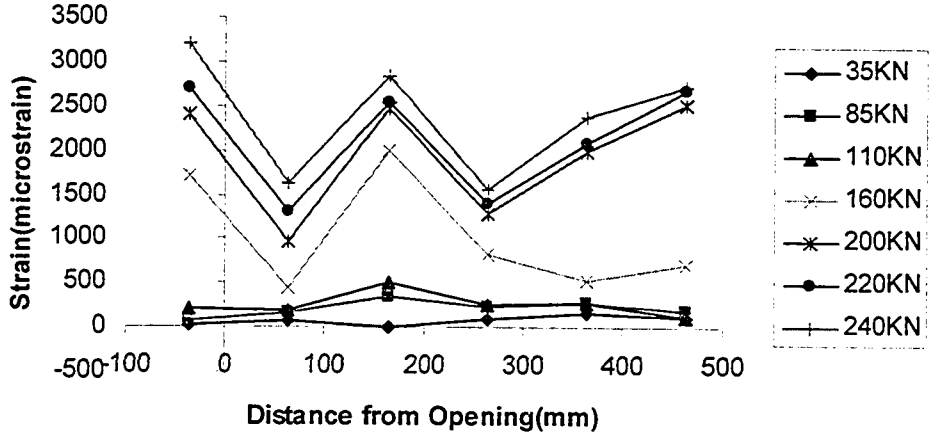

Horizontal Strain Behaviour of Region 1 (Line B) (Wall 3)

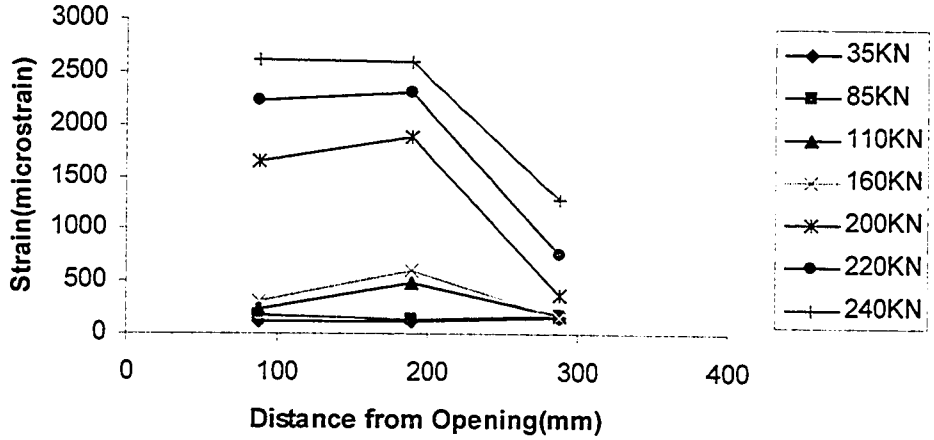

Vertical Strain Behaviour of Region 2 (Wall 3)

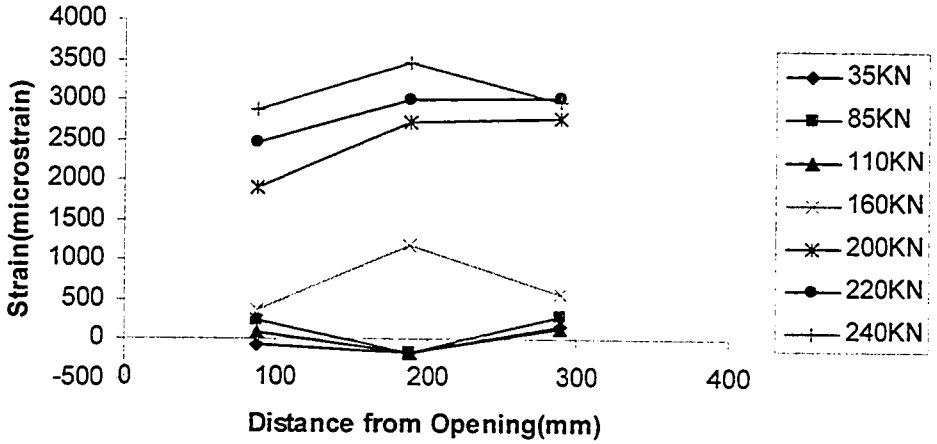

Horizontal Strain Behaviour of Region 2 (Wall 3)

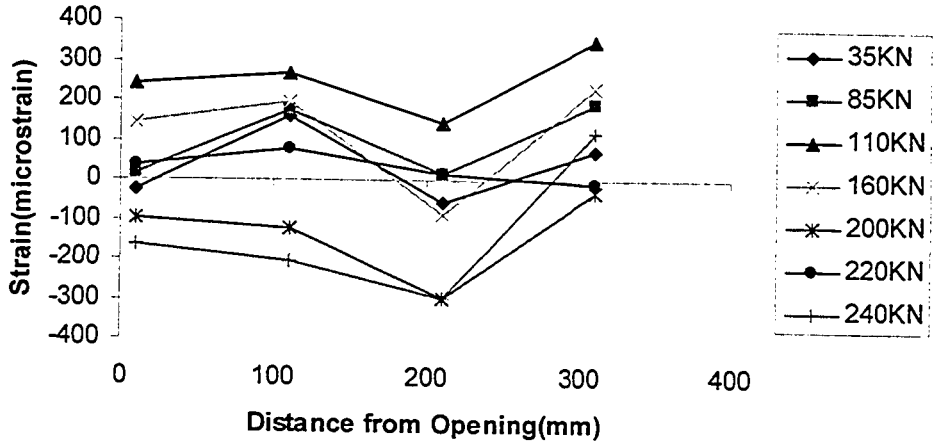

Vertical Strain Behaviour of Region 3 (Wall 3)

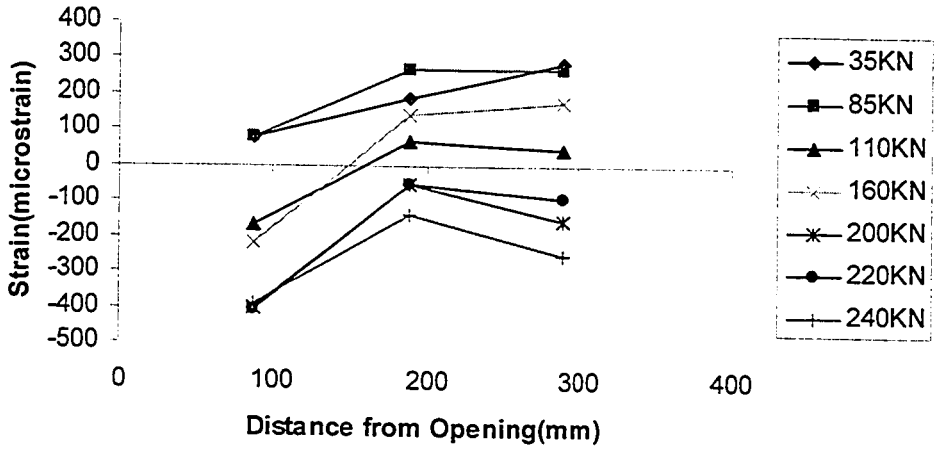

Horizontal Strain Behaviour of Region 3 (Wall 3)

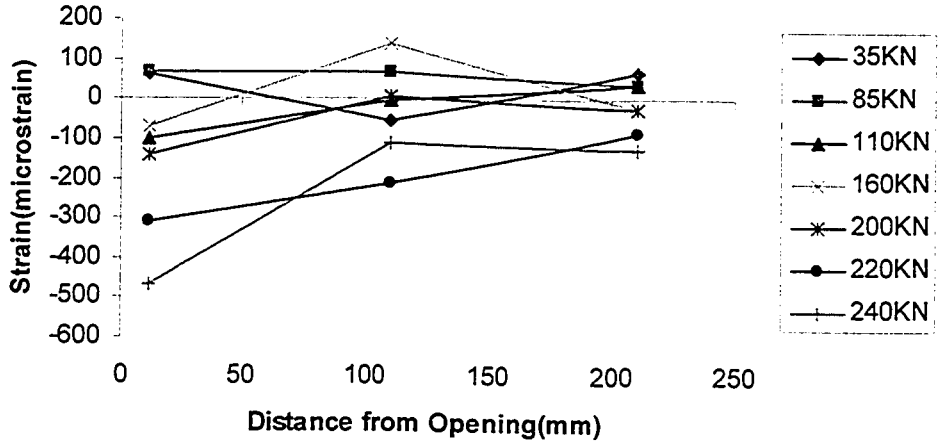

Vertical Strain Behaviour of Region 4 (wall 3)

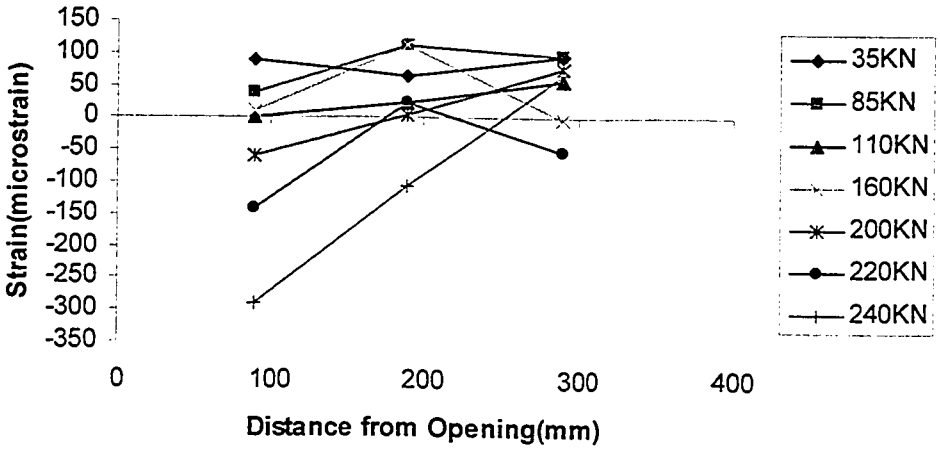

Horizontal Strain Behaviour of Region 4 (Wall 3)

Figure 4-7 Strain Behaviors of Wall 3

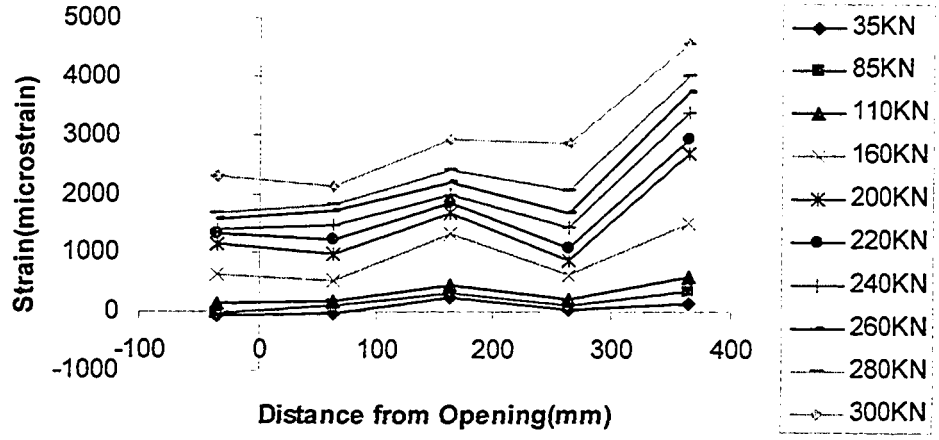

Vertical Strain Behaviour of Region 1 (Line A) (Wall 4)

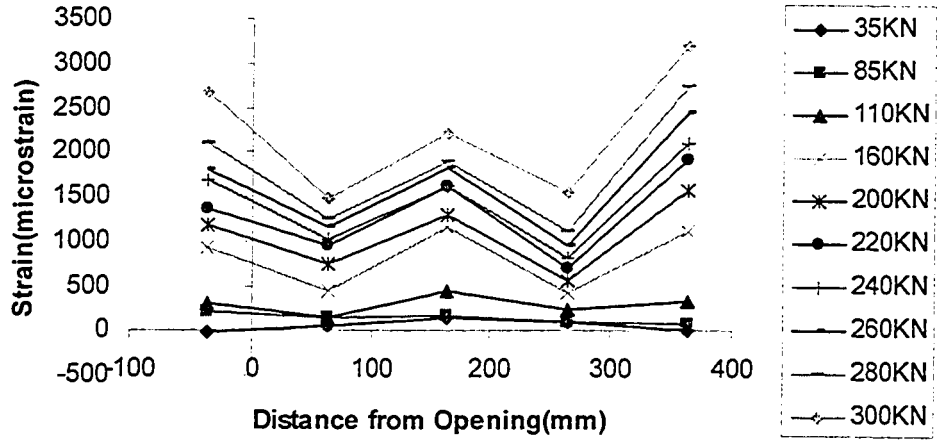

Vertical Strain Behaviour of Region 1 (Line B) (Wall 4)

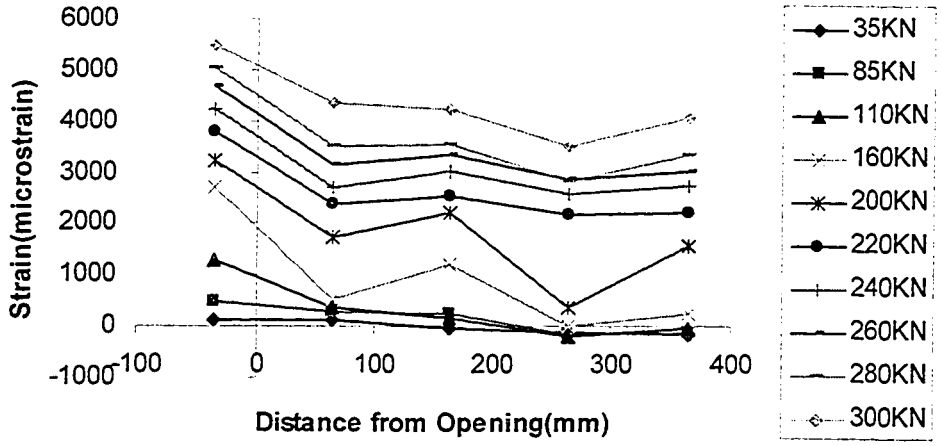

Horizontal Strain Behaviour of Region 1 (Line A) (Wall 4)

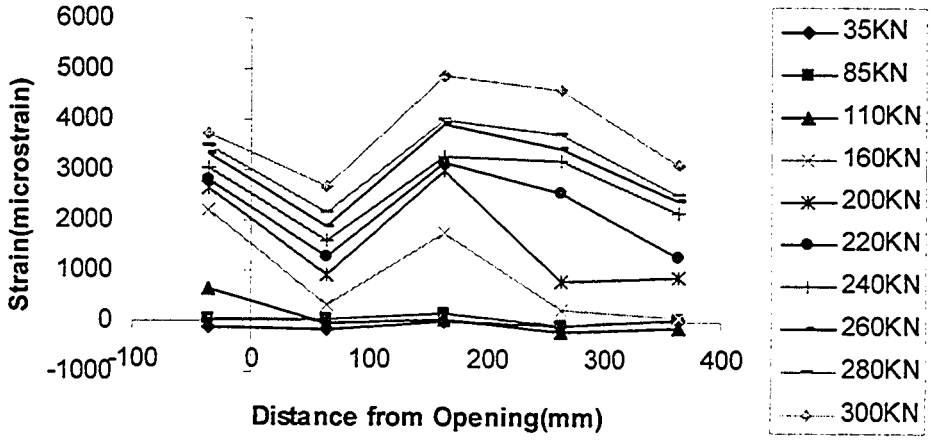

Horizontal Strain Behaviour of Region 1 (Line B) (Wall 4)

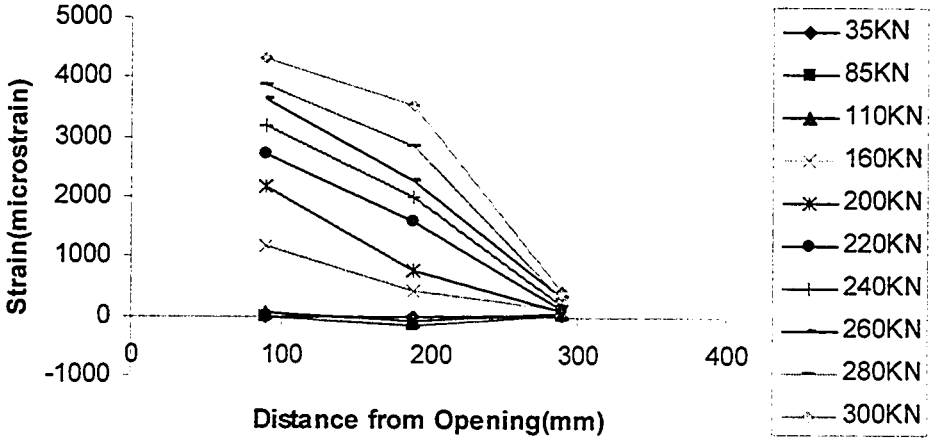

Vertical Strain Behaviour of Region 2 (Wall 4)

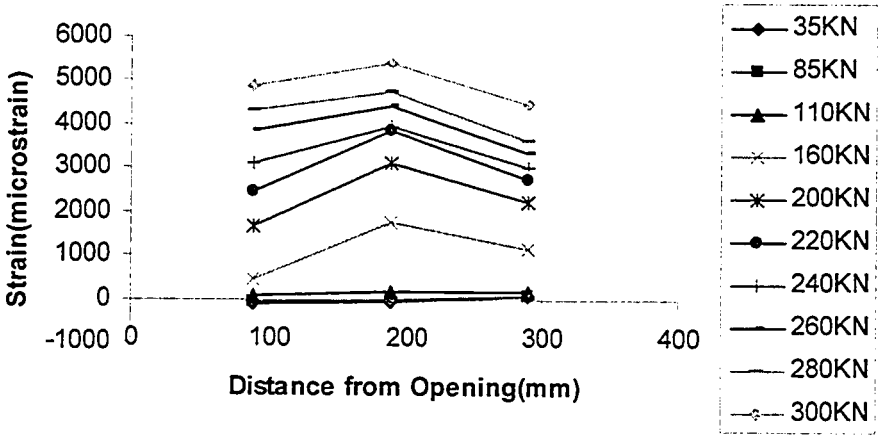

Horizontal Strain Behaviour of Region 2 (Wall 4)

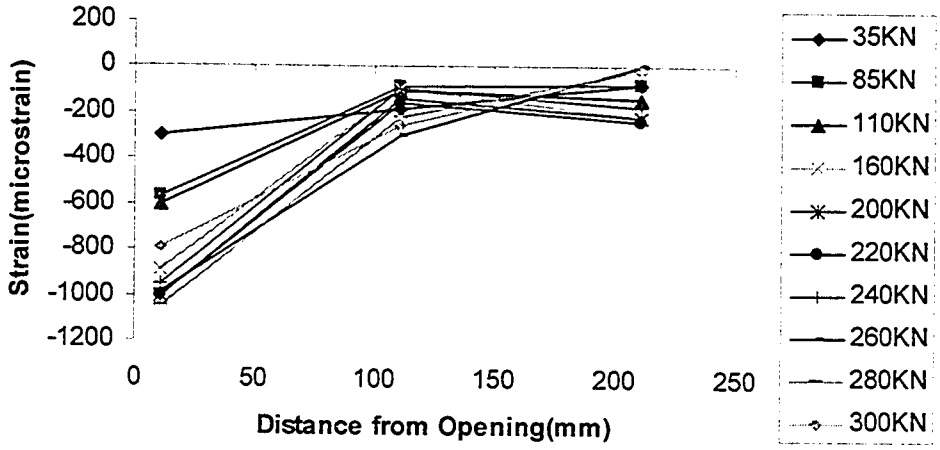

Vertical Strain Behaviour of Region 3 (Wall 4)

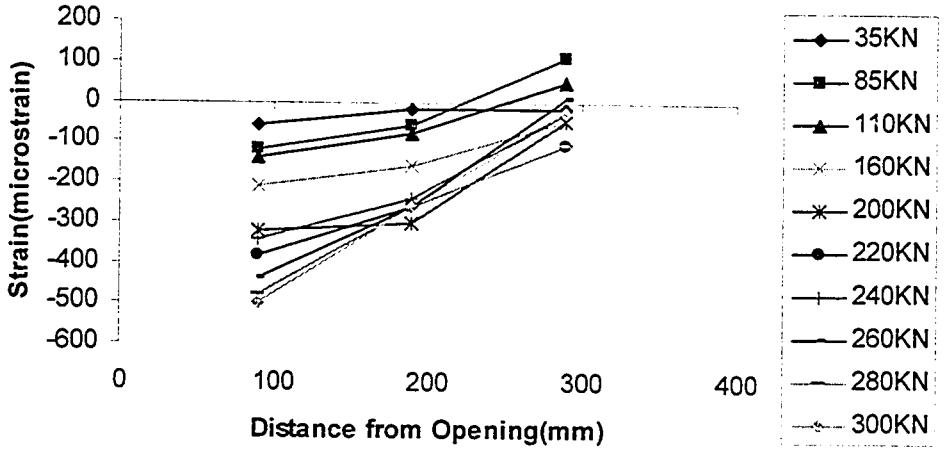

Horizontal Strain Behaviour of Region 3 (wall 4)

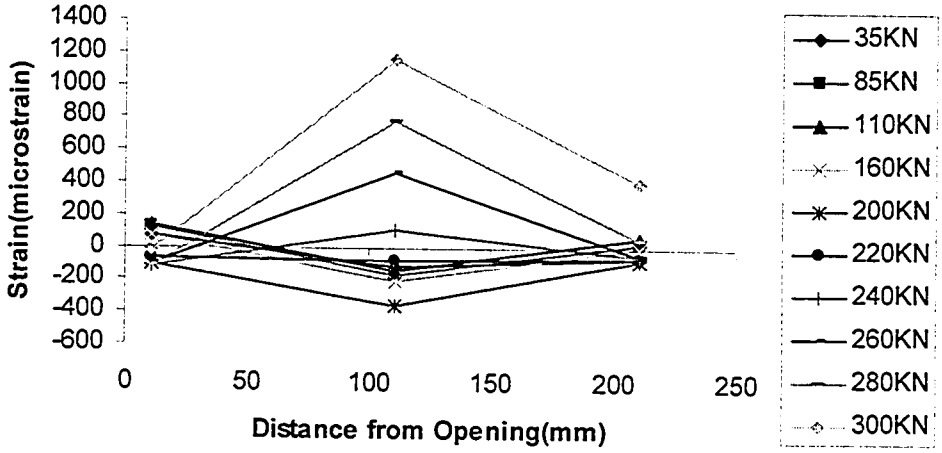

Vertical Strain Behaviour of Region 4 (Wall 4)

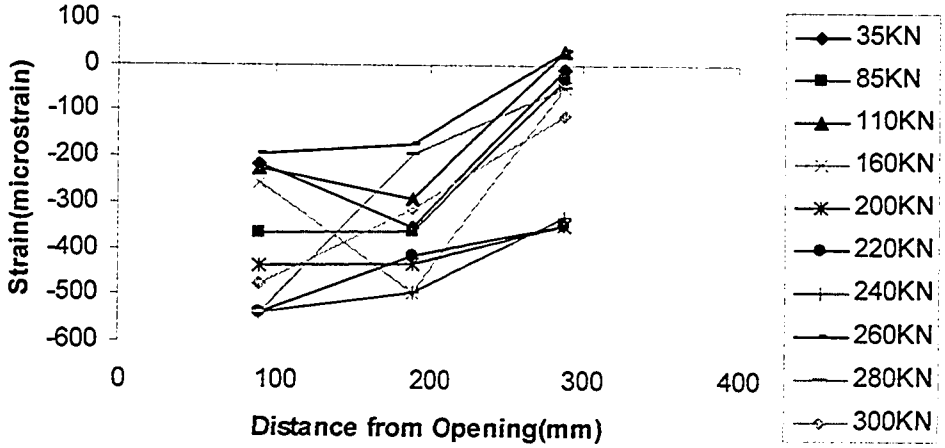

Horizontal Strain Behaviour of Region 4 (Wall 4)

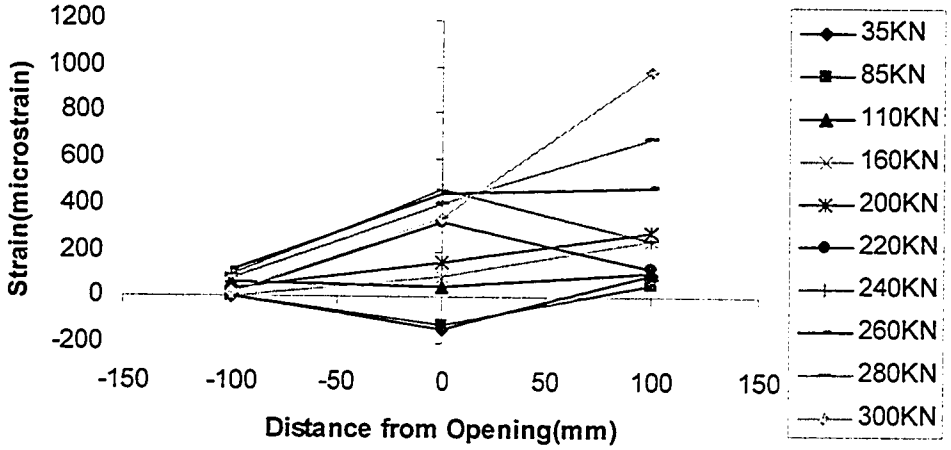

Vertical Strain Behaviour of Region 5 (Wall 4)

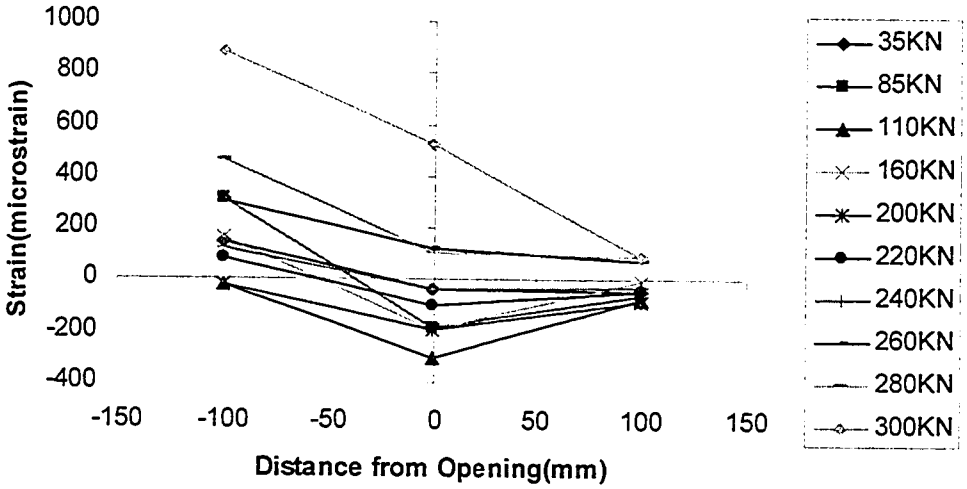

Vertical Strain Behaviour of Region 6 (Wall 4)

Figure 4-8 Strain Behaviors of Wall 4

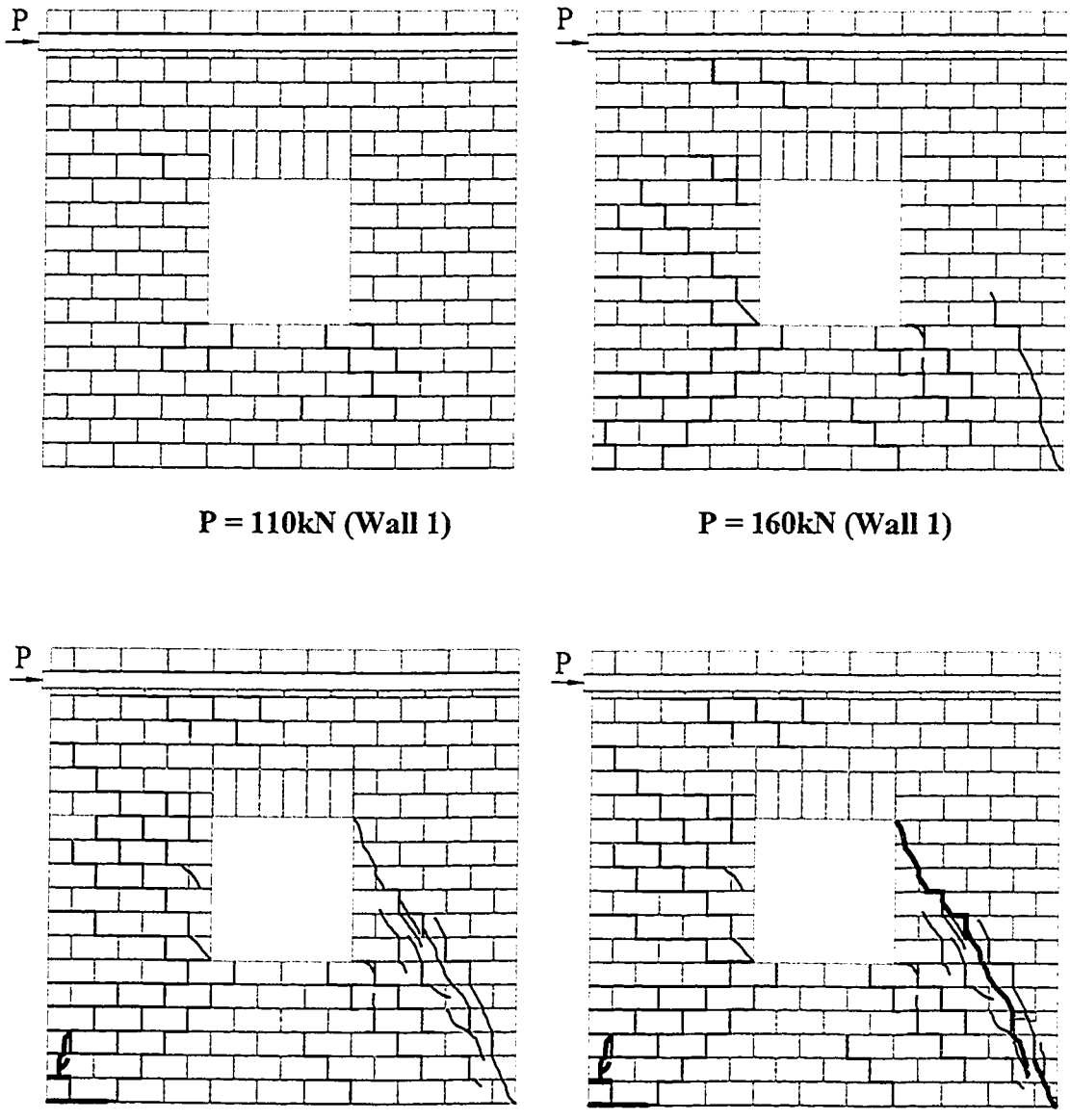

Figure 4-9 Crack Patterns of Wall 1

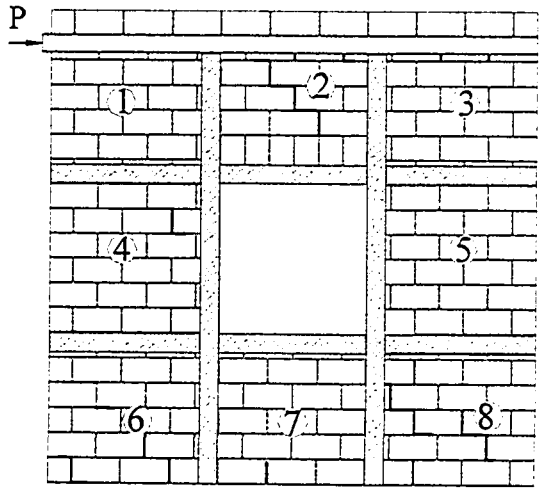

P = 110kN (Wall 2)

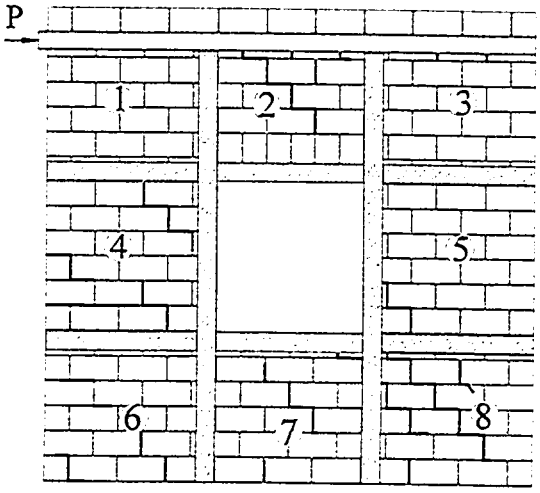

P = 160kN (Wall 2)

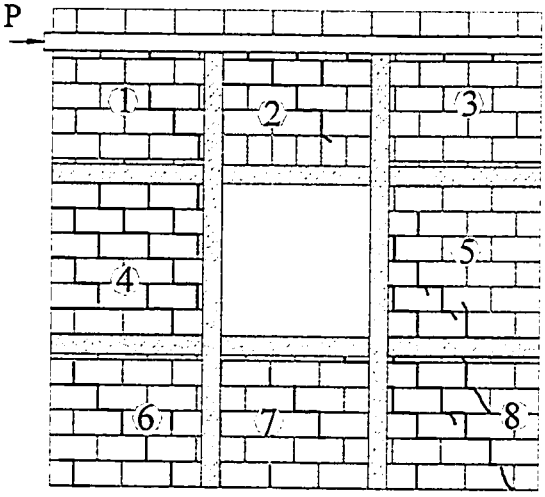

P = 200kN (Wall 2)

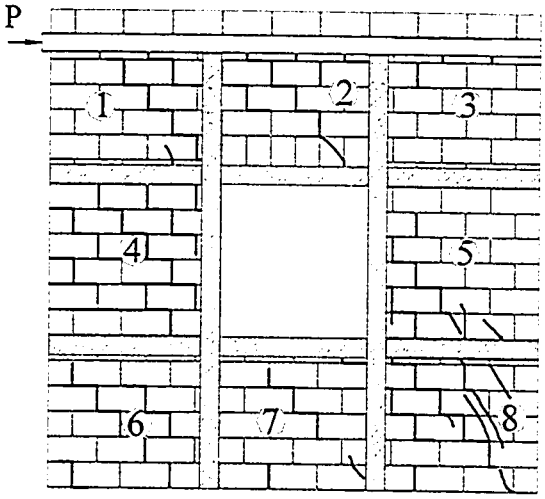

P = 240kN (Wall 2)

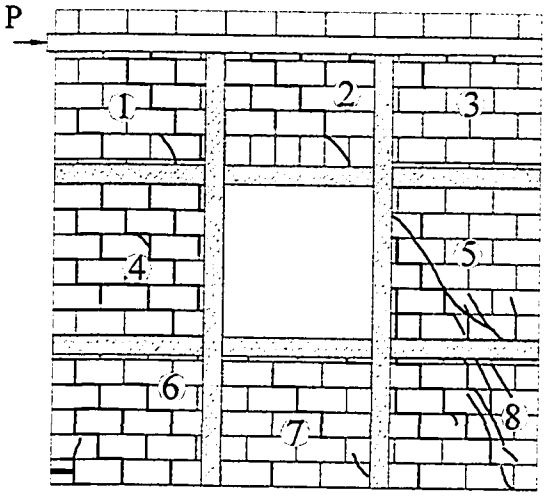

P = 280kN (Wall 2)

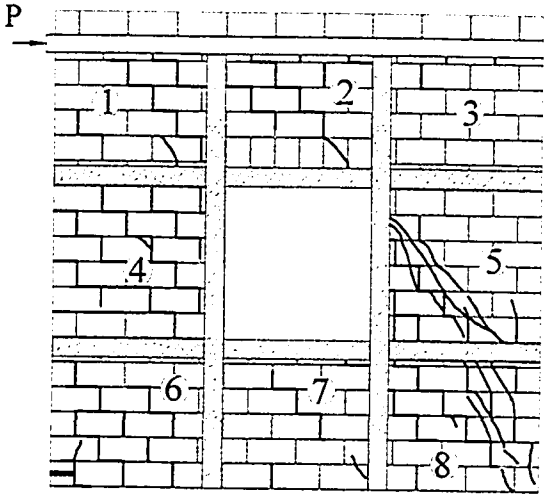

P = 330kN (Wall 2)

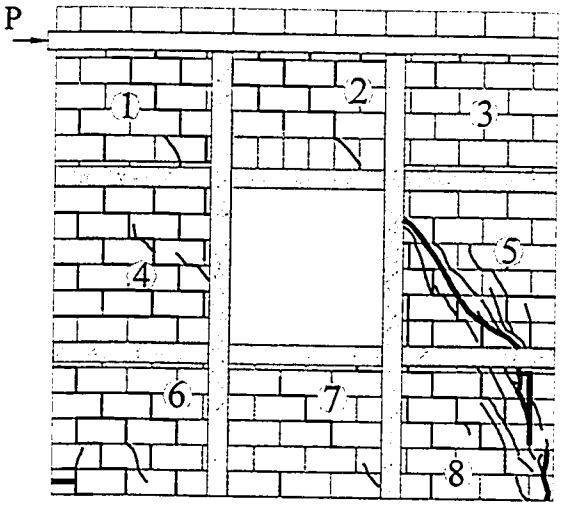

P = 359kN (failure load) (Wall 2)

Figure 4-10 Crack Patterns of Wall 2

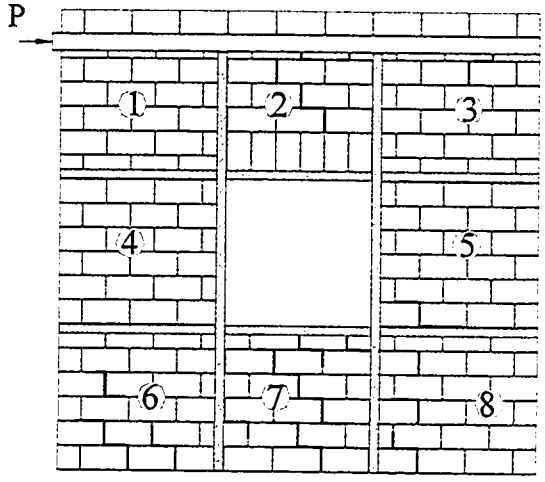

P = 110kN (Wall 3)

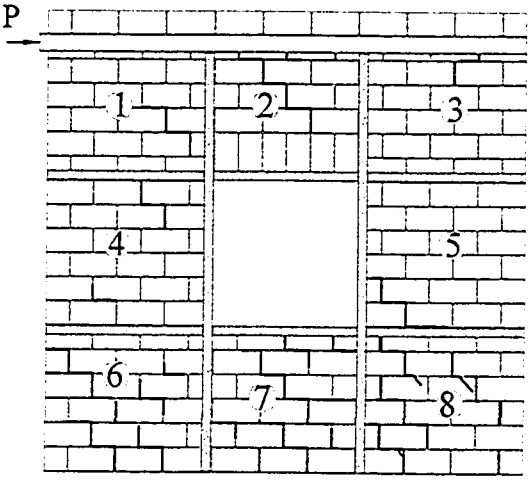

P = 160kN (Wall 3)

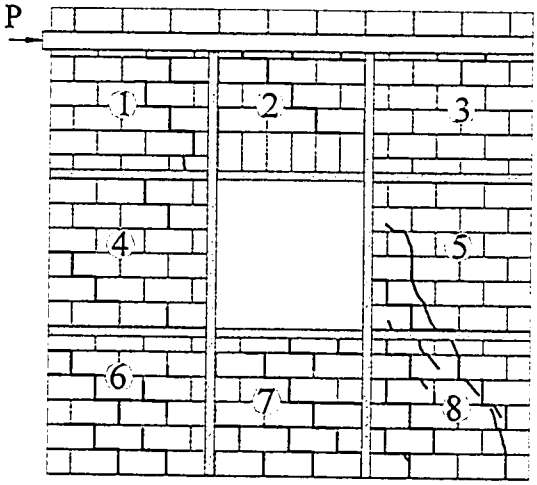

P = 200kN (Wall 3)

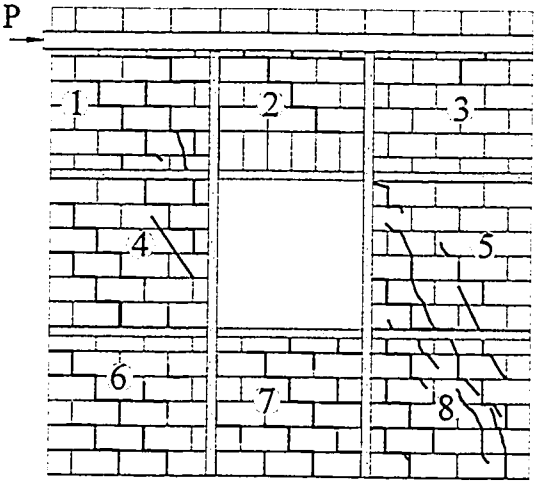

P = 240kN (Wall 3)

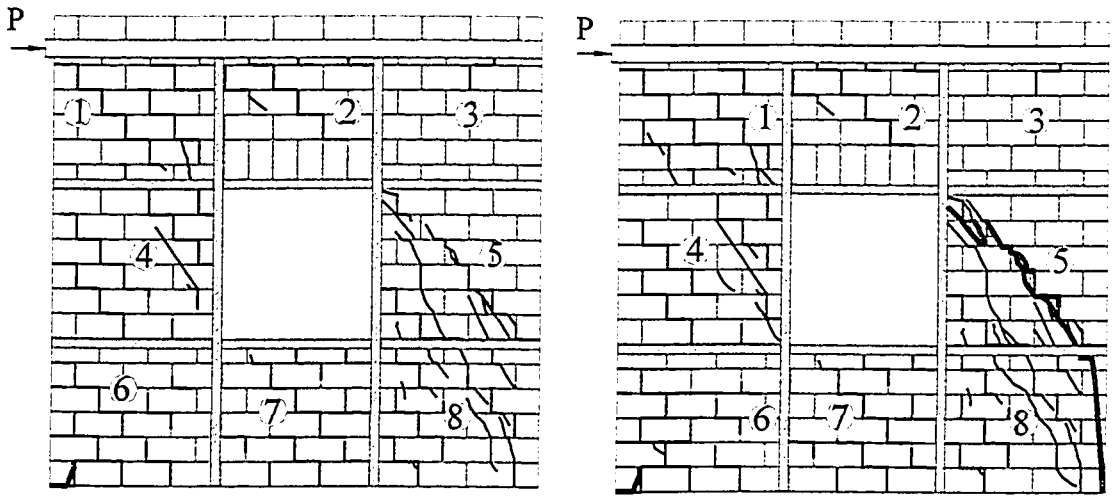

P = 280kN (Wall 3) **P = 330kN (failure load) (Wall 3)**

Figure 4-11 Crack Patterns of Wall 3

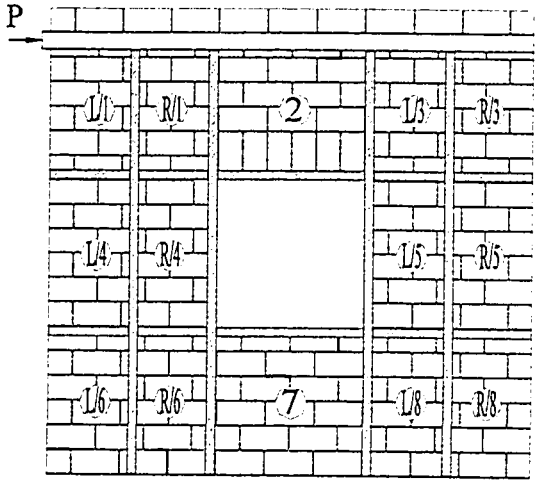

P = 110kN (Wall 4)

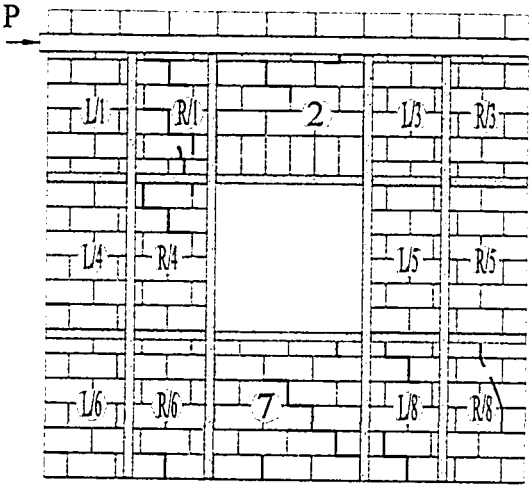

P = 160kN (Wall 4)

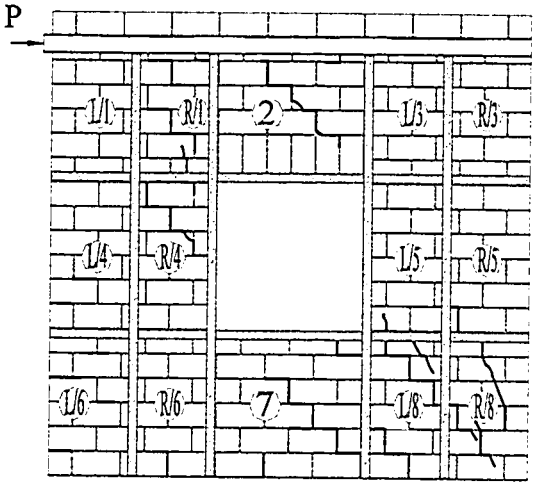

P = 200kN (Wall 4)

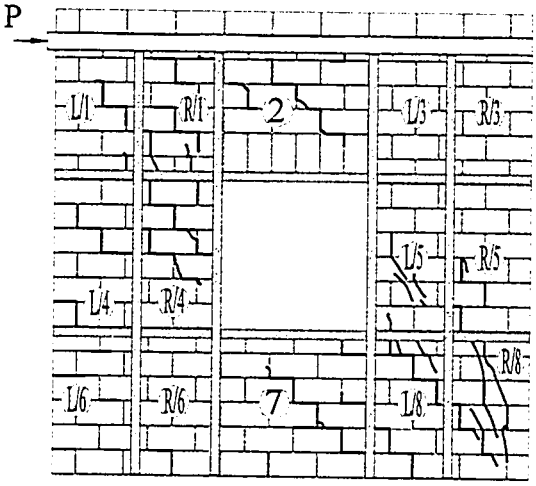

P = 240kN (Wall 4)

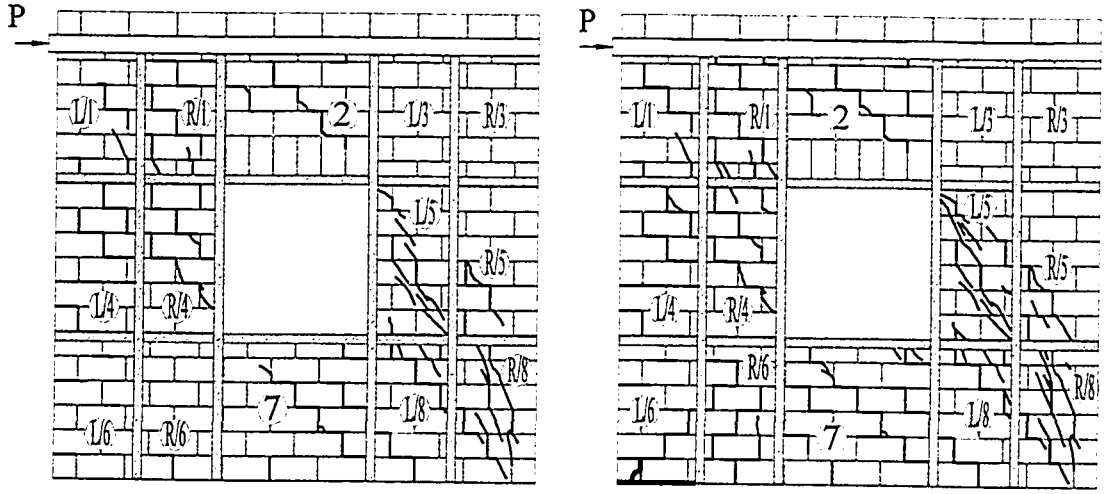

P = 280kN (Wall 4) **P = 330kN (Wall 4)**

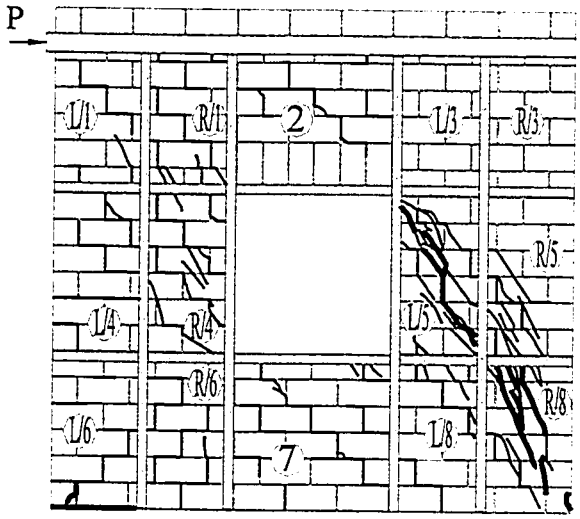

P = 351kN (failure load) (Wall 4)

Figure 4-12 Crack Patterns of Wall 4

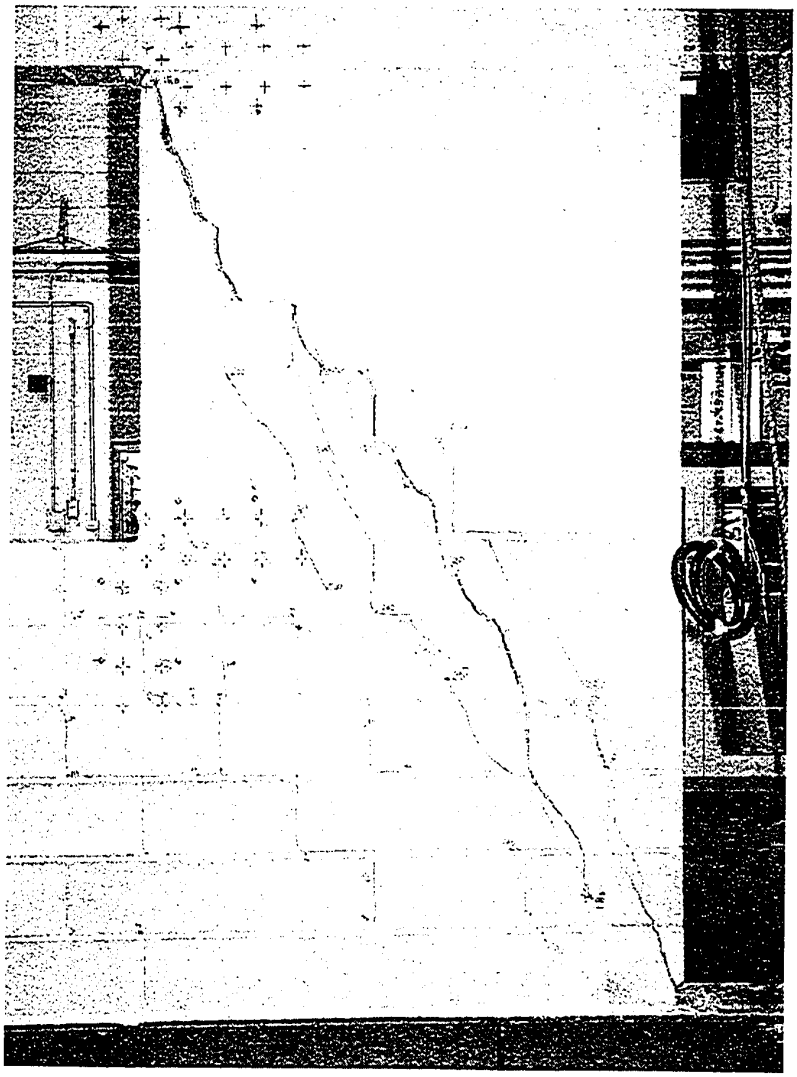

Photo 4-1 Crack Patterns for Wall 1

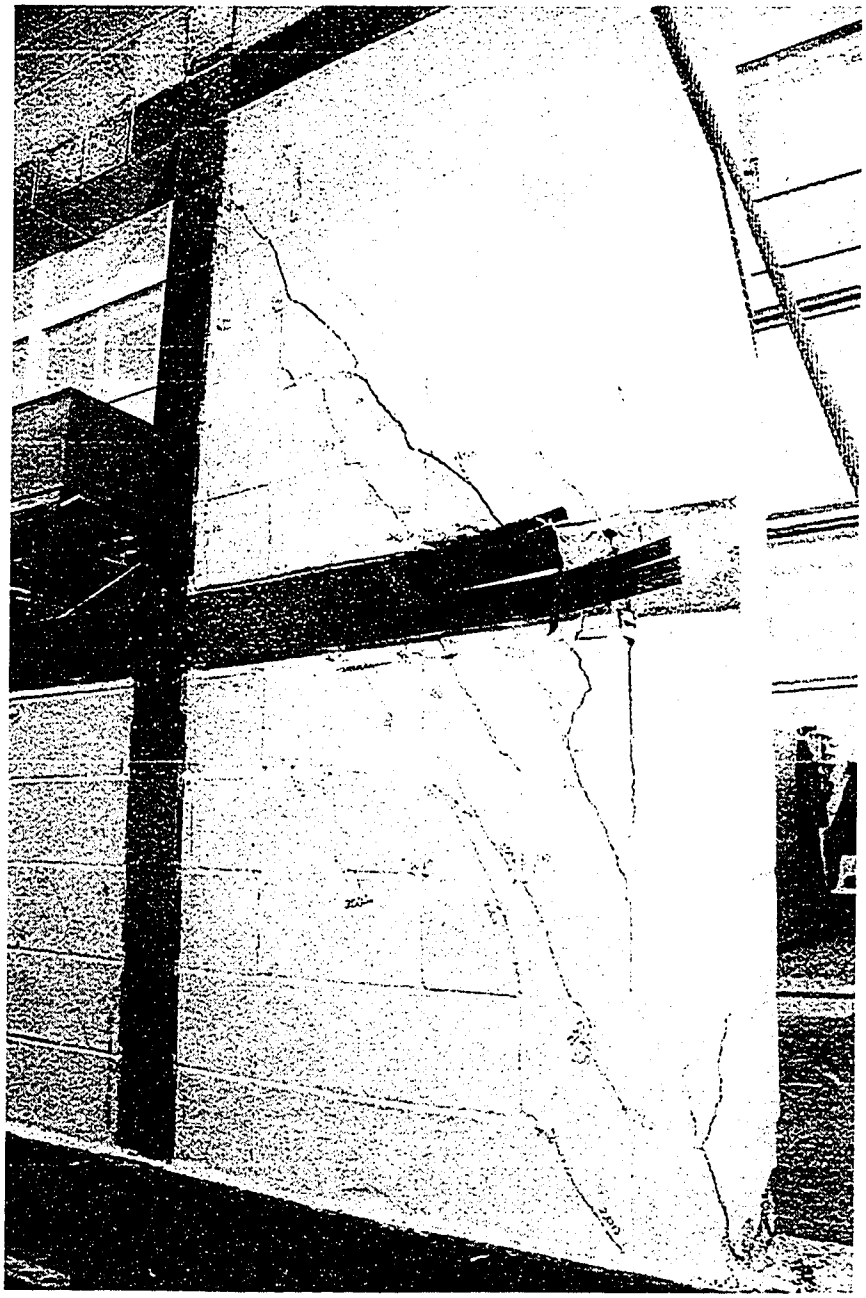

Photo 4-2 Crack Patterns for Wall 2

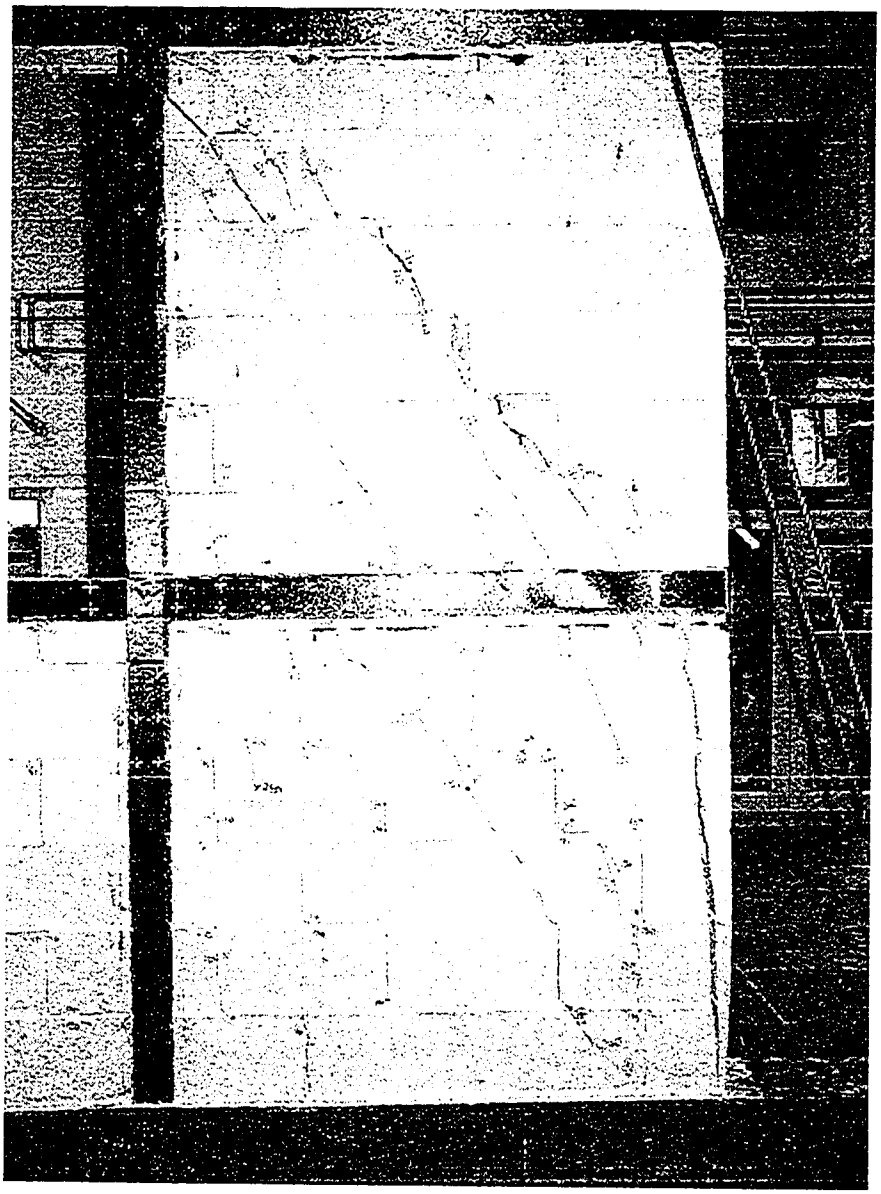

Photo 4-3 Crack Patterns for Wall 3

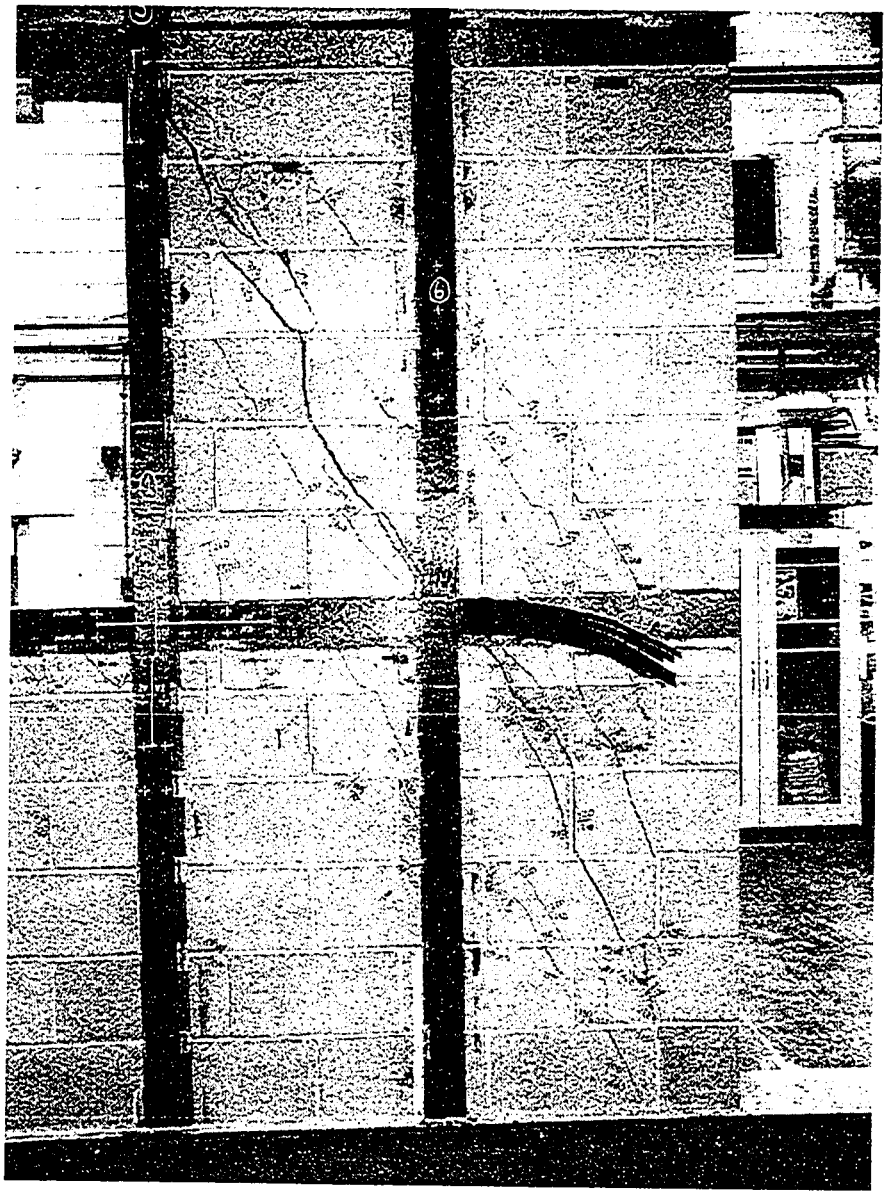

Photo 4-4 Crack Patterns for Wall 4

5. DISCUSSION OF TEST RESULTS AND MACHANICAL MODELS

5.1 Introduction

This chapter presents a comparison between the results of the experimental study and mechanical models. The comparison highlights the effectiveness of using externally bonded Carbon Fiber Reinforcement Sheets as a retrofit method for concrete masonry shear walls with large openings. The comparison of test results is mainly carried out on the basis of the lateral load-displacement behavior and the mechanical stiffness response of the specimens. Several mechanical models to predict the shear contribution of CFRP Sheets to the strengthened walls are investigated. Four mathematical models to estimate the lateral stiffness of wall specimens are also discussed in this chapter.

5.2 Discussion of Test Results

The critical features that evaluate a structural system are its strength, stiffness (or rigidity) and ductility. This section addresses each of these parameters.

5.2.1 Strength Comparison

Since all wall specimens in this experimental program had identical geometric and material properties, the load can be used to investigate the comparative strength. The lateral load-top displacement curves for all walls are presented in Figure 5-1. All curves in Figure 5-1 were obtained by manually removing all the loops and most of sharp but small fluctuations in load before ultimate loads. It can be seen that the curves in Figure 5-1 are clearer for comparative load analysis and they also provide some smooth curves to obtain more accurate mechanical stiffness-displacement curves in next section.

It is apparent that walls strengthened with CFRP Sheets lead to a significant increase in ultimate loads. Wall 1, the control wall achieved a maximum lateral load of 225.1kN. Wall 2 achieved 360.4kN, Wall 3 achieved 330.8kN and Wall 4 achieved 353.1kN. Table 5-1 summarizes the test results of the load capacity (P_u) for each specimen.

Compared with specimen Wall 1, the ultimate loads of Wall 2, Wall 3 and Wall 4 are increased by 60.1%, 47.0%, and 56.9%, respectively. The greater load capacities carried by Wall 2 and Wall 4 than Wall 3 reflect the effect of the amount of CFRP Sheets. The more CFRP strips applied in walls, the greater load capacity obtained. Furthermore, the comparison on load capacity between Wall 2 and Wall 4 illustrates the effect of the layout of CFRP Sheets on the strength is small since these two wall specimens had different arrangement of CFRP Sheets and a great difference on the amount of CFRP strips, while there is a negligible difference in their strengths. Table 5-1 shows the comparisons of strength.

5.2.2 Ductility Comparison

The ductility for each specimen is illustrated and compared by the value of lateral top displacement in Figure 5-1. Table 5-1 shows the lateral displacement capacity (Δ_u) for each wall. Generally, the displacement capacity is considered when the lateral load decreased to 80% of the maximum lateral load. Thus, maximum lateral displacement were observed to be 29.7mm, 56.6mm, 49.1mm, and 62.9mm for Wall 1, Wall 2, Wall 3, and Wall 4, respectively. Compared with Wall 1, the ultimate displacement of Wall 2, Wall 3 and Wall 4 are increased by 90.6%, 65.3% and 111.8%, respectively. It is obvious that in addition to increasing the ultimate loads, CFRP Sheets can remarkably improve the lateral displacement capacity.

By comparing the test results of Wall 2, Wall 3 and Wall 4, it is noticeable that the effect of amount of CFRP reinforcement is more significant in increasing the displacement capacity than in increasing the load capacity. Compared with Wall 3, Wall 2 had only an increase of 8.9% in ultimate load, but an increase of 15% in displacement capacity. Compared to Wall 4, which had four additional lines of CFRP strips in the middle of piers except for the CFRP reinforcement around the opening, Wall 2 achieved a lower value of ultimate displacement although Wall 2 had a greater amount of CFRP reinforcement. This fact shows that the effect of layout of CFRP Sheets is great in increasing the ductility and CFRP reinforcement uniformly distributed provides a larger ductility than CFRP Sheets applied in a concentrated region. Furthermore, it is important

to note that there is no dramatic drop in load for Wall 4 when it achieved its ultimate load unlike the other three walls. This behavior shows relatively more ductile properties in Wall 4. By considering the ultimate displacement as a measure for the wall ductility, it can be concluded that ductility of the shear walls with large openings increases significantly with the increase of the amount of CFRP Sheets around opening, and the CFRP reinforcement uniformly distributed provides a more ductile wall.

5.2.3 Mechanical Stiffness Comparison

Wall stiffness ratio is defined as the force required causing a unit displacement. Figure 5-2 illustrates the mechanical stiffness for each specimen. The mechanical stiffness curves were obtained by dividing the lateral loads by top displacement at the corresponding load of walls. It is found that CFRP Sheets can increase the wall stiffness of perforated concrete masonry shear walls in the later stage of loading due to the action of CFRP system. Wall 1, the control wall had a little higher stiffness at the first loading stage because of the initial setting, but this initial stiffness decreased faster than the other walls strengthened by CFRP Sheets because the CFRP system defer the appearance of diagonal cracks and restricts the development of the cracks. Before achieving the maximum loads, similar mechanical stiffness curves for all strengthened walls indicate that there is a negligible effect of amount and layout of CFRP reinforcement on the stiffness of the walls with large central openings strengthened by CFRP Sheets. Unlike Wall1, Wall 2 and Wall 3, which had a sudden drop in stiffness at the maximum loads, Wall 4 had a very small degradation in stiffness at its ultimate load. It can be explained that the action of the additional CFRP Sheets in the middle of piers better restricts the development of the major diagonal cracks and improves the integrity of the wall in the later loading stage.

It is evident that the effect of CFRP Sheets amount and distribution is more significant in increasing the ductility than in improving the strength. The effect of CFRP Sheets in increasing the wall stiffness is small.

All the conclusions drawn above are based on the vertical CFRP strips. The current state of work did not allow an assessment of the effect of the non-vertical CFRP strips.

5.3 Mechanical Strength

5.3.1 Introduction

Based on the test observations and results, mechanical models are discussed in this section to demonstrate the effectiveness of the CFRP sheets to a masonry shear wall with an opening. This analysis will be based on American and Canadian Codes. To successfully quantify and predict the capacity of the strengthened perforated masonry shear walls with CFRP Sheets, a further discussion on the behavior of the masonry shear walls with opening under combined axial load and in-plane load is presented in the following section.

5.3.2 Behavior of Perforated Masonry Shear Walls

Openings in shear walls often are provided as a matter of functional necessity, such as doors and windows. Introducing openings in a shear wall reduces its flexural and shear strength and alters its deformation characteristics. The analysis of shear walls with openings is difficult because openings introduce complexity in the wall behaviour. One complexity in analyzing perforated shear walls is the effect of the coupling system on strength, ductility and stiffness. When a member that is stiff enough to transfer shear from one segment of the wall to the other wall elements, a coupled shear wall system is created. The connecting elements between coupled shear walls typically require horizontal and vertical reinforcement to transfer shear force. Figure 5-3 and Figure 5-4 shows schemes of coupled and uncoupled shear walls. Hendry (1991) provided several basic methods of analysis of coupled walls in multi-story shear walls and pointed out that coupled wall system had a greater stiffness than the equivalent uncoupled wall system. Corrêa and Page (2003) carried out an experimental study for a one-story wall with openings and concluded that the coupled wall stiffness and strength were both more than double the corresponding stiffness and strength of two isolated walls. So the strength of a

coupled shear wall with openings is not simply a summation of the strengths of either sidewall segments or piers. EI-Shafie *et al.* (1996) summarized the structural analysis of shear walls with openings considering the coupling effects.

Under the action of an in-plane lateral force acting on the masonry shear wall, the wall is subjected to horizontal shear and vertical axial forces as well as moment that cause flexural stresses. Shear causes diagonal tensile stress in wall piers. The preferable failure mode is flexural failure caused by the bending moment since the wall displays much more ductility in this failure mode, while shear failure is a type of brittle failure mode manifested by bed joint slip loss of anchorage, diagonal tension failure and crushing at the toe of the wall in masonry structures. The shear failure is indicated by typical diagonal-tension cracks in the piers. To prevent shear failure, horizontal shear reinforcement is provided. The vertical reinforcement carries the racking load by dowel action that is often neglected in the calculations. The presence of openings in a wall causes the concentration of stresses around the corners of the opening and can precipitate cracks originating from the corners of the openings. Accordingly, reinforcement should be provided both horizontally and vertically near each corner of an opening. It must be mentioned that the axial force increases the shear and bending strength.

5.3.3 Load Capacity of Perforated Masonry Shear wall

Two methods are available to predict the load capacity of the masonry shear walls without CFRP Sheets: ACI code and CSA code. The wall specimens were designed to fail in shear and not in flexure. Thus, only shear capacity calculations will be considered to predict the ultimate loads carried by the walls.

There are four different pier models shown in Figure 5-5 to be constructed in this analysis. In Model (a), the wall was idealized as two cantilevers (pier1 and 2) fixed at the bottom and free at the top and pier 3 fixed at both of ends. Pier 1 and 2 were connected by a non-deformable link provided by spandrel at the top of opening. Model (b) divided wall into four piers. Except for cantilever pier 3 bottom end fixed, the other three piers

were considered fixed both at the top and bottom. In Model (c), the wall was considered as three piers. Cantilever pier 3 was connected rigidly at the bottom with pier1 and 2. While both pier 1 and 2 were two ends fixed and connected by a non-deformable link provided by spandrel under the opening. In Model (d), the wall was idealized as two cantilevers, pier 1 and 2, fixed at the bottom and free at the top and connected by non-deformable links provided by spandrels at the both of top and bottom of opening. Figure 5-5 also showed the values of $\frac{M}{Vd}$ ratio of considered pier 2 for different models. It should be mentioned that the following calculation of load capacity of Wall 1 are based on the capacity of pier 2. Each method used to predict the load capacity for Wall1, the un-strengthened masonry wall with opening is presented in detail below.

MDG-3, Masonry Designers' Guide, Third Edition. The Masonry Society.

MDG-3 is based on Building Code Requirements to Masonry Structures (ACI 530-99/ASCE-5-99/TMS 402-99) and Specification for Masonry Structures (ACI 530.1-99/ASCE 6-99/TMS 602-99). The design procedures of the code are predicated on the allowable stress methods: structural assemblages are designed for service loads using an elastic analysis; and the computed stresses are compared to allowable stresses that represent failure stresses.

This analysis is assumed that all materials are linear elastic; all materials are homogeneous; sections that are plannar before bending remain plannar after bending and strains in the reinforcement are equal to those in the surrounding mortar or grout.

The calculation of shear stresses in MDG-3 is based on "cracked section" properties since the flexural tension is considered for pier. The shear component carried by dowel action of the vertical steel reinforcement is neglected. Therefore the Wall 1 is considered to have no shear reinforcement. Based on clauses 13.1.3.1 in MDG-3 and 2.3.5.2.2 in ACI code, the allowable shear stresses F_v of pier 2 is as follows:

$$F_v = \frac{1}{3}(4 - \frac{M}{V'd})\sqrt{f_m'} \quad , \quad \frac{M}{V'd} < 1.0 \tag{5.1a}$$

But shall not exceed $0.55 - 0.31(\frac{M}{V'd})$ (MPa)

$$F_v = \sqrt{f_m'} \, , \quad \frac{M}{V'd} \geq 1.0 \tag{5.1b}$$

But shall not exceed 0.241MPa

Here, f_m' is the compressive strength of masonry, V' is the shear force, $\frac{M}{V'd}$ is called the shear span shown in Figure 5-5 and F_v is the unit allowable shear stress.

Clearly, the allowable shear stress in each pier model case is given as a function of $\frac{M}{V'd}$ ratio and the square root of f_m'. Shear walls with lower aspect ratios (expressed by $\frac{M}{V'd}$) have higher allowable shear stress.

The calculated shear stress of pier 2 is determined by the relationship

$$f_v = \frac{V'}{bd} \tag{5.2}$$

In which, b is the pier 2 thickness, d is the effective depth and taken 0.8 L_w, and L_w is the length of pier.

This equation is valid for solid masonry shear walls since the quantity of bd stands for the effective area of pier. However for partially grouted wall specimens in this experimental program, the effective area of the wall can be taken as 126950mm^2 based on the Table 4-4 of CSA S304.1.

As it is demanded that the calculated shear stress, f_v dose not exceed the allowable shear stress, F_v, the ultimate shear force, V' carried by the pier 2 considered in this calculation can be computed. Finally, the ultimate lateral load of the whole wall specimen is obtained as twice V'. Table 5-2 shows the predicted results on basis of MDG-3 and ACI code.

S 304.1-94, Masonry Design for Buildings (limit state design), Canadian Standards Association.

S304.1-94 is predicated on the limit states principle to analyze the masonry structures. This code considers the effect of gravity load on the shear capacity, while it neglects the contribution of vertical steel reinforcement to shear stresses.

Based on clause 11.5.3 of S304.1, which provides the factored in-plane shear resistance of a masonry shear wall, the shear capacity of pier 2 is as follows:

$$V = \Phi_m (V_m bd + 0.25P')\gamma_g + \Phi_s (0.6A_v f_y \frac{d}{s}) \tag{5.3}$$

In which, b is the wall thickness, d is the effective depth of pier, P' is the factored dead load, taken 0.85 times dead load, γ_g is a factor to account for partially grouted walls and equals $\frac{A_e}{A_g} \leq 0.5$, A_e is the effective cross-sectional area, A_g is the gross cross-sectional area, and V_m is the shear strength contributed by masonry.

$$V_m = 0.16(2 - \frac{M}{V' d})\sqrt{f_m'} \tag{5.4}$$

In Equation 5.3, the second part of the right side is neglected because there is no structural horizontal shear reinforcement provided in test specimen, Wall 1. The resistance factor for masonry, Φ_m, is ignored in calculating the capacity. In computing the shear capacity of pier 2 for model (b) and (d) shown in Figure 5-5, the self-weight of the pier were considered.

It must be noted that clause 11.5.3.2 in S304.1 provides a calculation equation of the maximum factored shear resistance for low aspect ratio walls ($\frac{h_w}{L_w} < 1$). Where h_w is the pier height and L_w presents the pier length. However this equation is not applied in this research even some considered piers had lower aspect ratios less than 1. That's because the calculation in clause 11.5.3.2 is only applied in the situation where the distribution of shear input to the wall would not lead to failure of a portion of the wall, while the test wall was failed in shear failure model.

Similar to MDG-3, the ultimate lateral load carried by the Wall 1 is twice of the shear capacity of pier 2, V'. The predicted ultimate load based on CSA is present in Table 5-2 also.

Compared with the test results of Wall 1, both the ACI and CSA codes underestimated the capacity of masonry shear walls with openings. This is maybe because that both provisions do not consider the beneficial effects of wall coupling. Corrêa and Page (2003) demonstrated, through an experimental study of masonry walls with openings, the coupling effect provided strength and stiffness more than twice those of a isolated pier. Moreover, the coupled wall exhibited a large elastic phase. Another reason to explain the lower predicted wall capacity is perhaps that the codes neglect the effects of dowel action provided by vertical reinforcement on shear strength. Furthermore, this analysis is mainly based on elastic analysis when considering the connection between isolated piers, while a plastic collapse mechanism is more accurate mechanical model comparing the test observations and results. EI-Shafie *et al.* (1996) provided some basic theories in analyzing perforated masonry shear walls with openings considering coupling effect and plastic collapse mechanism.

Table 5-2 shows that pier model (b) provides a more exact mathematical model. In other pier models, the calculated load capacity is far less than test result. This is because that the load capacity calculations using the other three pier models ignored the great

contribution of spandrels between two isolated piers to load capacity. However, crack patterns of test observations shows that pier model (c) should also be a reasonable mechanical model. Thus a mechanical model for masonry shear walls with openings strengthened by CFRP sheets will be developed using pier models (b) and (c).

5.3.4 Contribution of CFRP Sheets to Shear Capacity Based on Literature

According to modern codes and standards, the shear resistance of a reinforced masonry shear wall (V) is given by two contributing components: the shear resistance of the masonry (V_m) and the shear resistance of shear reinforcement (V_s) provided in the form of horizontal bars that are oriented in the plane of loading. As a result, the contribution from the CFRP sheets (V_{frp}) can be added to reinforced masonry shear walls separately. Thus, the shear capacity of the walls strengthened with CFRP sheets (V) can be given as follows:

$$V = V_m + V_s + V_{frp} \tag{5.5}$$

In this experimental study, only two contributing components of V_m and V_{frp} are considered because there were not structural horizontal bars in the wall specimens. Since the previous sections have analyzed the shear contribution of masonry, this section only discusses the contribution of CFRP Sheets to shear resistance or ultimate lateral load.

The contribution of CFRP Sheets is difficult to quantify. Most of research work available about shear capacity mainly focused on the effect of FRP reinforcement uniformly distributed in walls. The results from these studies (Triantafillou1998, Valluzzi *et al.* 2002 and Belarbi *et al.* 2003) will be used to develop a mechanical model that estimates the contribution of CFRP Sheets to a perforated masonry shear wall. In following calculation, Pier 2 is considered and the total contribution of CFRP Sheets is taken double results from Pier 2.

Method A (Triantafillou 1998)

This analysis of contribution of FRP reinforcement to shear capacity is on the basis of Eurocode 6 format. Figure 5-6 shows the test matrix to be used in developing a mechanical model of FRP-strengthened masonry walls under in-plane shear with axial force. One assumption made here is that the contribution of vertical FRP reinforcement, which is assumed to provide mainly a dowel action effect, is negligible. Therefore, the only shear resistance mechanism left is associated with the action of horizontal laminates, which can be modeled in analogy to the action of stirrups in reinforced concrete beams. Adopting the classical truss analysis, the contribution of the horizontal FRP reinforcement to the shear capacity is given as follows:

$$V_{frp} = \rho_h E_{frp} (\gamma \frac{\varepsilon_{frp,u}}{\gamma_{frp}}) t 0.9d \tag{5.6}$$

In which, ρ_h is the area fraction that is defined as the total cross-sectional area of horizontally placed FRP reinforcement divided by the corresponding area of the wall, E_{frp} is the modulus of elasticity of FRP composite, $\varepsilon_{frp,u}$ is the ultimate FRP tensile strain, γ_{frp} is the partial safety factor for FRP in uniaxial tension approximately and equals to 1.15 for CFRP, γ is a reinforcement efficiency factor, depending on the exact FRP failure mechanism (FRP debonding or tensile fracture), d is the effective depth of pier and can be taken approximately $0.8L$, L is the length of pier, and t is the nominal thickness of the wall.

Thus, Equation 5.6 can be expressed as

$$V_{frp} = 0.7 L t \rho_h E_{frp} \frac{\varepsilon_{frp,e}}{\gamma_{frp}} \tag{5.7}$$

Where, $\varepsilon_{frp,e}$ is an effective FRP strain. $\varepsilon_{frp,e}$ depends heavily on the area of the FRP-masonry debonded interfaces, or, in other words, on the FRP development length, defined as that length necessary to reach FRP tensile fracture before debonding. Moreover, the development length depends on the FRP axial rigidity expressed by the product $\rho_h E_{frp}$. Therefore, the effective FRP strain, $\varepsilon_{frp,e}$, can be proportional to $\rho_h E_{frp}$. The effective FRP strain is expected to decrease as the FRP axial rigidity increases or the laminates become stiffer and thicker. The expression of $\varepsilon_{frp,e}$ has been obtained for concrete members strengthened with FRP in shear and the same expression is adopted for masonry structures.

$$\varepsilon_{frp,e} = 0.0119 - 0.0205(\rho_h E_{frp}) + 0.0104(\rho_h E_{frp})^2 \tag{5.8}$$

Where, E_{frp} is in GPa.

Finally the shear resistance of CFRP without the safety factor can be expressed as

$$V_{frp} = 0.7\rho_h E_{frp} \varepsilon_{frp,e} L_w t \tag{5.9}$$

Table 5-3 presents the comparison between the predicted and experimental values of the contribution of CFRP Sheets to the shear strength of strengthened masonry shear walls with openings. It is noted that the shear contribution of CFRP Sheets in this experimental program is presented by the increase of ultimate lateral loads for strengthened walls. The test results demonstrate that the increase in ultimate lateral load due to the external FRP reinforcement is great: 135.3kN, 105.7kN and 128.0kN for Wall 2, Wall 3 and Wall 4, respectively, compared with Wall 1. While the theoretical predictions provides far less values of contribution of FRP reinforcement: 70.4kN, 37.8kN and 37.8kN for Wall 2, Wall 3 and Wall 4, respectively. This mechanical model ignores the effect of vertical CFRP Sheets, while the rupture and bending deformation of vertical CFRP Sheets at failure observed during testing indicate that the effects of vertical CFRP Sheets externally bonded to walls on the shear capacity is considerable. Clearly, this mechanical model to estimate the shear contribution of CFRP Sheets is not appropriate for this research work.

Method B (Valluzzi et al. 2002)

Like other mechanical models, this model to evaluate the shear strength of strengthened masonry shear walls is predicated on the linear effects superposition, which derives from the implicit assumption of plastic stress redistribution. But the problem is represented by FRP's up-to-failure linear elastic behaviour, which limits the ductility of system. Therefore, the redistribution-derived theory is not properly introduced when dealing with FRP, but at present no more appropriate approaches are available. Thus, the FRP's effect is reduced to take into account different issues descending from their non-ductile behaviour.

$$V_{frp} = 0.7\rho_{frp}E_{frp}\varepsilon_{frp,e}L_w t \tag{5.10}$$

The expression of $\varepsilon_{frp,e}$ is given by Equation 5.11:

$$\varepsilon_{frp,e} = 0.0119 - 0.0205(\rho_{frp}E_{frp}) + 0.0104(\rho_{frp}E_{frp})^2 \tag{5.11}$$

Equation 5.11 was almost same as that in Equation 5.8 except for the FRP ratio. ρ_h in Equation 5.8 only accounts for the effect of horizontal FRP strips, while ρ_{frp} in Equation 5.11 considers the effects of both vertical and horizontal FRP strips. The same difference exists in Equation 5.9 and 5.10.

Comparison between the experimental and the predicted values of shear strength carried by CFRP Sheets is reported in Table 5-3. The expected increase in load capacity is 139.2kN, 70.6kN and 105.6kN for Wall 2, Wall 3 and Wall 4, respectively. Compared with the test results, the theoretical analysis underestimates the effects of CFRP Sheets about 33.2% and 21.2% for Wall 3 and Wall 4, respectively, while overestimates the effects of CFRP Sheets by about 2.9% for Wall 2. Although this model accounts for the effect of vertical CFRP Sheets on shear strength and provides a closer value than the method of Thiantafillou (1998), there are still considerable differences between the

theoretical prediction and experimental results for Wall 3 and Wall 4. In this mechanical model, the effects of both vertical and horizontal FRP reinforcement on shear capacity were considered in the same calculation model, while the test results showed the different failure modes for vertical and horizontal CFRP Sheets: Peel-off (or debonding) failure for horizontal CFRP Sheets, tensile fracture for the vertical CFRP Sheets applied around opening and bending deformation for vertical CFRP Sheets applied in the middle of piers for Wall 4. Therefore a reasonable mechanical model should consider the effects of FRP reinforcement depending on their failure modes and layout.

Method C (Belarbi et al. 2003)

This paper analyzed the contribution of horizontal and vertical FRP rods to shear capacity respectively. Equation 5.12 proposed the horizontal FRP reinforcement contribution, $V_{F,H}$ as

$$V_{F,H} = 0.5nA_f f_f \tag{5.12}$$

In which, n is the number of FRP rods crossing the cracks, A_f is the cross-sectional area of the FRP reinforcement, and f_f is assumed tensile stress in the FRP reinforcement which was half of the ultimate tensile strength.

The contribution of the vertical FRP reinforcement ($V_{F,V}$) to shear strength is provided as follows:

$$V_{F,V} = 2F_1'\xi \tag{5.13}$$

$$\xi = \frac{\sum_{i=1}^{m} d_i^2}{Hd_i} \tag{5.14}$$

Where, i is from 1 to m, m is the total number of vertical FRP rods, d_i is the distance from i^{th} FRP rod to the farthest corner of the wall carrying maximum compression, H is the height of pier, and F_1 'is the force developed in the FRP rod farthest from the bottom compression zone.

Since the vertical CFRP strips were fracture failure, it's reasonable to take F_1 equal to the product of the ultimate tensile strength, f_u, and the total cross-sectional area of FRP reinforcement. Table 5-3 compares the predicted and experimental results of the effect of CFRP Sheets to the ultimate lateral load of masonry perforated shear walls. It's needed to mention that unlike the other two methods discussed in previous two sections, this mechanical model accounts for the effect of aspect ratio, $\frac{\sum_{i=1}^{m} d_i^2}{Hd_i}$. Therefore, there are two different results for pier (b) and (c). Compared with test results analyses, pier model (b) provided more accurate values. Comparing with experimental results, while pier model (b) overestimate the shear contribution of CFRP sheets about 8% and 32.3% for Wall 2 and Wall 4, respectively, while underestimate approximately 25% for Wall 3. The higher difference between prediction and test results for Wall 4 is because that this method assumes all vertical CFRP sheets reach ultimate strength. Observation of the test showed only those vertical CFRP reinforcement around the opening achieved fractured and developed their full capacity. However, there were not enough test data to measure the strain or stress of each CFRP strip at failure.

5.3.5 Proposed Model

The relatively limited test results obtained demonstrated that all above mechanical models are not accurate enough to predict the effects of CFRP Sheets on lateral load capacity of strengthened masonry walls with openings. To address some of the theoretical issues faced by method A, B, and C, it is proposed to use force equilibrium to provide mechanical models shown in Figure 5-7. In this model all vertical CFRP reinforcements are assumed to reach the tensile ultimate stress, while the horizontal CFRP sheets are assumed to take a tensile stress that is half of the ultimate tensile strength (f_u) suggested

by Belarbi *et al.*(2003). Two types of pier models: mode (b) and model (c) are considered. Assumption that the angle of the shear crack is 45° is adopted in pier model (b), while the crack is assumed to be formed from the left top corner of the pier 2 to the right bottom of the pier 2 in pier model (c). The later assumption of crack patterns matches well with the test observations. In this mechanical model, only the resistance of CFRP sheets are considered. The basic equation to calculate the load capacity of CFRP Sheets, V_f, is derived from the moment equilibrium about point O:

$$\sum M_o = 0 \tag{5.15}$$

$$V_f h_1 - F_2 h_2 - F_1 d_1 - qld_3 - F_3 d_2 = 0 \tag{5.16}$$

Where, V_f is the ultimate load carried by pier 2, F_1 is the force developed by vertical CFRP strips around opening, F_2 is the force developed by horizontal CFRP strips at the bottom of opening, F_3 is the force developed by vertical CFRP strips in the middle of the pier, q is the uniformly distributed gravity load, and h_1, h_2, d_1, d_2, d_3 are the moment arms for V_f, F_2, F_1, q and F_3 respectively.

Similarly, the overall increase in ultimate capacity is taken to be twice of the load capacity of CFRP Sheets in pier 2. Table 5-3 shows the comparison between the predicted and experimental results of the contribution of CFRP Sheets to load capacity.

Compared with test results and prediction from other methods, this proposed method provides more accurate prediction for contribution of CFRP Sheets on load capacity of perforated masonry shear walls. In addition, pier model (b) gives a closer value than pier model (c). Although the predicted results based pier model (b) match the test results for Wall 3 and Wall 4 well, it overestimates the effect of CFRP Sheets on load capacity for Wall 2. It is noticeable that, pier model (c) provided more accurate crack patterns, but it provides a value further less than test results. Furthermore, bonding condition should be considered in this analysis. However, bonding is a big issue and it is beyond this research.

5.4 Predicted Stiffness

Stiffness of shear walls with openings is one of important issues in the design process. With rigid diaphragms, shear walls will deflect equally under horizontal load. Consequently, horizontal forces transferred by the diaphragms will be distributed to each shear wall in direct proportion to its stiffness. The stiffness of a shear wall is inversely proportional to its deflection under unit horizontal load. Since the stiffness of a shear wall perforated by openings is relative to the stiffness and deflection of each pier, a kind of solid wall, it is necessary to investigate the stiffness and deflection of a solid shear wall.

The deflection of a solid shear wall is the sum of the deflections due to shear and moment. The moment deflection depends on the boundary conditions of walls. Figure 5-5 presents two common boundary conditions in shear walls: the wall is cantilever from its base or fixed at both the top and bottom of the wall. For a fixed-fixed solid shear wall, the moment deflection (Δ_m) is

$$\Delta_m = \frac{VH^3}{12E_mI} \tag{5.17}$$

For a solid cantilever shear wall, the moment deflection (Δ_m) is

$$\Delta_m = \frac{VH^3}{3E_mI} \tag{5.18}$$

For a solid fixed-fixed or cantilever shear wall, the shear deflection (Δ_v) is

$$\Delta_V = \frac{1.2VH}{G_mA} \tag{5.19}$$

Where, V is the lateral load, H is the height of the wall, A is the wall cross-sectional area and is taken as the product of t and d, t is the wall thickness, d is the length of the wall, I

is the second moment area of wall about the relevant axis and equals to $\frac{td^3}{12}$ for rectangular wall, E_m is the modulus of elasticity of masonry, and G_m is the modulus of rigidity of the masonry and taken as $0.4E_m$.

Thus, the total deflection (Δc) of a rectangular solid cantilever shear walls is obtained by this expression:

$$\Delta = \Delta_m + \Delta_V = \frac{V}{E_m t}\left[4\left(\frac{H}{d}\right)^3 + 3\left(\frac{H}{d}\right)\right] \tag{5.20}$$

The total deflection (Δ) of a rectangular solid fixed-fixed shear walls is obtained by this expression:

$$\Delta = \Delta_m + \Delta_V = \frac{V}{E_m t}\left[\left(\frac{H}{d}\right)^3 + 3\left(\frac{H}{d}\right)\right] \tag{5.21}$$

Finally, the lateral stiffness of the wall (K) is defined as

$$K = \frac{V}{\Delta} = \frac{E_m t}{4\left(\frac{H}{d}\right)^3 + 3\left(\frac{H}{d}\right)} \quad \text{(cantilever boundary)} \tag{5.22}$$

Or

$$K = \frac{V}{\Delta} = \frac{E_m t}{\left(\frac{H}{d}\right)^3 + 3\left(\frac{H}{d}\right)} \quad \text{(fixed-fixed boundary)} \tag{5.23}$$

Realistic estimate of stiffness of masonry shear walls with openings is a complex task because wall stiffness is a primary function of many factors: Wall geometry – wall aspect ratio affects the contribution of shear and bending deformation to the wall rigidity; Boundary conditions – restraint at the top of wall affects wall stiffness; Openings – the

size, location and arrangement of openings dramatically affects wall stiffness; Cracking – the extent of cracking applied to reinforced masonry shear walls.

To estimate the lateral stiffness of masonry shear walls with openings, three conventional methods are being used. This section will investigate the stiffness of tested wall shown in Figure 5-8 using every method. In *method I*, the wall rigidity is obtained by following steps: 1) calculate the deflection of a solid cantilever wall with whole wall length and height; 2) subtract the deflection of a cantilever strip having a height equal to that of the highest opening in the wall; 3) compute the deflection of all composite fixed-fixed piers with openings lying within that strip; 4) add these deflection of the individual fixed-fixed piers to the modified wall deflection obtained in 2) to obtain the final wall deflection. The last step is to take the reciprocal of this compound deflection to obtain the wall stiffness. Using this method the stiffness of specimen wall shown in Figure 5-8 can be calculated with following formulas:

$$K = \frac{1}{\Delta} \tag{5.24a}$$

$$\Delta = \Delta_{solid} - \Delta_{stripA} + \Delta_{1+2} \tag{5.24b}$$

$$\Delta_{1+2} = \frac{1}{k_1 + k_2} \tag{5.24c}$$

$$k_1 = k_2 = \frac{1}{\Delta_1} = \frac{1}{\Delta_2} \tag{5.24d}$$

Method Π to determine the wall stiffness is a rather simplified approach and involves simply a summation of the stiffness of the individual piers (pier 1 and 2) between opening within the wall. Method Π provides results that are comparable to others which are somewhat more precise compared with the test results.

In *Method III*, the wall is divided into piers staked on top of each other in series; the lateral deflection of each pier is added to obtain the total deflection. It needs to mention two different manners to add the pier deflections; consequently, the system stiffness is expressed in different way. When piers are connected in parallel, the system stiffness is given by

$$K = \sum_{i=1}^{n}(k_n) = k_1 + k_2 + \ldots + k_n \tag{5.25}$$

When piers are connected in series, the system stiffness is approximately as

$$K = \frac{1}{\sum_{i=1}^{1}(\Delta_i)} = \frac{1}{\Delta_1 + \Delta_2 + \ldots + \Delta_n} = \frac{1}{\frac{1}{k_1} + \frac{1}{k_2} + \ldots + \frac{1}{k_n}} \tag{5.26}$$

Where, Δ_i and k_i are the deflection and stiffness of a component pier i under the horizontal load P, respectively.

Using this method the rigidity (K) of wall specimen shown in Figure 5-8 can be calculated with following formulas:

$$K = \frac{1}{\left(\frac{1}{k_4} + \frac{1}{k_{1+2+3}}\right)} \qquad \text{(In-series model)} \quad (5.27a)$$

$$k_{1+2+3} = \frac{1}{\left(\frac{1}{k_3} + \frac{1}{k_{1+2}}\right)} \qquad \text{(In-series model)} \quad (5.27b)$$

$$k_{1+2} = k_1 + k_2 \qquad \text{(In-parallel model)} \quad (5.27c)$$

In the last method, the deflection of each pier is calculated assuming a fixed-fixed boundary condition. Figure 5-10 presents and compares these stiffness values resulting from the above three methods and test results. Method III resulted in a higher wall stiffness. This can be explained that this method assumes a fixed-fixed boundary condition for all piers and ignores the rotation at the top of piers which are more applicable for squat walls where shear deflection is the predominant mode to flexural deformation.

Qamaruddin *et.al.* (1998) provided an analysis of the stiffness of shear walls with openings and concluded that method-wise comparison of these stiffness values using conventional methods indicated a wide variation among them depending on wall configuration. Qamaruddin *et.al.* (1998) suggested a new method to estimate the lateral stiffness of the shear walls with openings.

The conventional methods assume that the piers in a shear wall are rigidly fixed to the spandrels against rotation at their ends. The new method assumes a partially fixed boundary condition at the junction of the pier and the spandrel. Figure 5-9 shows the rotational deformation of the spandrel and this deformation is assumed to induce vertical stresses in the element *abcd* just in line with the pier. Considering a rectangular pier with $I = \frac{tL^3}{12}$ and the Poisson's ratio, $\upsilon = 0.25$, the lateral stiffness of a pier, k, is obtained by the expression:

$$k = \frac{E_m t}{\left(2pq'^3 + 3q'\right)} \tag{5.28}$$

Where,

$$p = \frac{p_1}{p_2}$$

$$p_1 = 2q'r' + q'^2 + 2q's' + 3r's'$$

$$p_2 = q'r' + 2q'^2 + q's'$$

$q' = \frac{h}{d}$, the aspect ratio of the pier

$r' = \frac{h_1}{d}$, the aspect ratio of the top spandrel

$s' = \frac{h_b}{d}$, the aspect ratio of the bottom spandrel

Finally, the lateral stiffness of a masonry shear wall with a large opening can be estimated by summing up the stiffness of the various piers in the wall. It's noticeable that this relationship is valid for lateral loads at the top of the shear wall. Table 5-4 shows this calculation process and results.

Figure 5-10 compares the predicted and experimental results of test wall stiffness. Generally, predicted stiffness is much higher than test results. Figure 5-10 also shows the comparison of stiffness between a corresponding solid wall and test perforated walls. It can be seen that only Method I provides a lower stiffness than that of solid wall, while other methods results in a stiffer wall with a large opening than a wall without an opening. Clearly, Method I provide a more accurate determination than other methods in this experimental program. The predicted wall stiffness based on Method III is close to the prediction of Method I. That's because both Method I and Method III consider more accurately the influence of the portion of the wall both above and below the openings. Method II is a most simplified and least accurate approach to predict the stiffness of perforated masonry walls since it only involves the rigidities of those vertical piers framed between openings in the wall. New Method mainly considers the influence of spandrels on boundary condition used in Method II, while it only accounts for the influence of part of spandrels that have the same length as that of relative openings in calculation. Consequently, the value of stiffness resulting from New Method is lower than that of Method II and higher than that of Method III.

5.5 Conclusion

A total of four mechanical models used in calculating the CFRP contribution to lateral load capacity of masonry shear walls with openings were presented in this section. However, the comparison between predicted values and experimental results shows that there are no appropriate mechanical methods available to estimate the effects of CFRP reinforcement on perforated masonry shear walls. Therefore, further research is needed in this area. In those mechanical models, the contribution of FRP reinforcement to shear resistance is idealized analogous to that of shear steel reinforcement. This assumption should be refined because the FRP composite is external, while the steel reinforcement is internal, thus the effects of FRP cannot be reduced to a simple question of localization. To understand the resistance mechanisms in masonry walls with openings, experimental research should provide enough data on strain measurement on FRP and steel reinforcements. In all mechanical models discussed in this research, the contribution of FRP reinforcement is simply added to the original contribution of masonry walls, which are maintained. In fact, application of FRP sheets improved the contribution of masonry blocks since FRP sheets alter the load transfer path and alleviate the high overstress around opening. Moreover, FRP reinforcement defers and restrains the development of cracks and improves the integrity walls. Furthermore the coupling effects should be considerable due to application of FRP reinforcement around opening. Therefore, an appropriate mechanical model to predict the behaviour of perforated masonry shear walls strengthened by FRP reinforcement should treat such walls as one wall with a large opening by considerable coupling effect.

This section also discussed the stiffness of masonry shear walls with openings and studied four methods to estimate wall elastic stiffness. Although some of these methods provide accurate prediction of relative stiffness, comparative analysis illustrated that none is accurate enough to predict the absolute stiffness for a masonry wall with a large opening.

The effective stiffness of masonry shear walls with opening is more important since it accounts for cracked section behaviour. In addition to those factors discussed in this

section which affect the stiffness of shear walls with openings, EI-Shafie *et al.* (1996) mentioned several other factors affecting wall stiffness including masonry tension-stiffening, wall reinforcement, axial stress, wall configuration and level of applied load. Usually the effective stiffness of reinforced masonry shear walls is calculated using cracked moment of inertia modified by a factor to account for tension stiffening. The effect of axial stress is generally neglected and this may lead to inaccurate stiffness estimation. The effective stiffness of reinforced masonry shear walls with openings has not been fully investigated and further research is also required to study the effect of FRP reinforcement on the effective stiffness of such walls.

Table 5-1 Comparison of Test Results

Specimens	P_U (kN) value	Increase	Δ_U(mm) value	Increase
Wall 1	225.1		29.7	
Wall 2	360.4	60.1%	56.6	90.6%
Wall 3	330.8	47.0%	49.1	65.3%
Wall 4	353.1	56.9%	62.9	111.8%

Table 5-2 Predicted Load Capacity of Wall 1

	P_U (kN)	
	ACI Code	CSA Code
Pier Mode a)	61.2	102
Pier Mode b)	96.5	146.8
Pier Mode c)	61.2	103.2
Pier Mode d)	61.2	102

Table 5-3 Comparison between Predicted and Test Shear Contribution of CFRP Sheets

Specimens	Predicted Results (kN)						Test Results (kN)
	Method A	Method B	Method C		Proposed Method		
			Pier Model (b)	Pier Model (c)	Pier Model (b)	Pier Model (c)	
Wall 2	70.4	139.2	149.5	93.2	156.0	115.0	135.3
Wall 3	37.8	70.6	76.6	47.8	100.7	84.8	105.7
Wall 4	37.8	105.6	165.4	98.5	130.2	87.6	128

Note: The test results in this table were obtained by load capacities of wall 2, wall 3, and wall 4 subtracting the load capacity of wall 1 for wall 2, wall 3 and wall 4, respectively.

Table 5-4 Predicted Wall Stiffness Using New method

Pier	H(mm)	h_t(mm)	h_b(mm)	d(mm)	q'	r'	s'	k_i
1	1210	1126	1200	1390	0.87	0.81	0.86	$0.19E_mt$
2	1210	1126	1200	1390	0.87	0.81	0.86	$0.19E_mt$
					$K=\sum k_i=$	$0.38E_mt$	=759688	N/mm

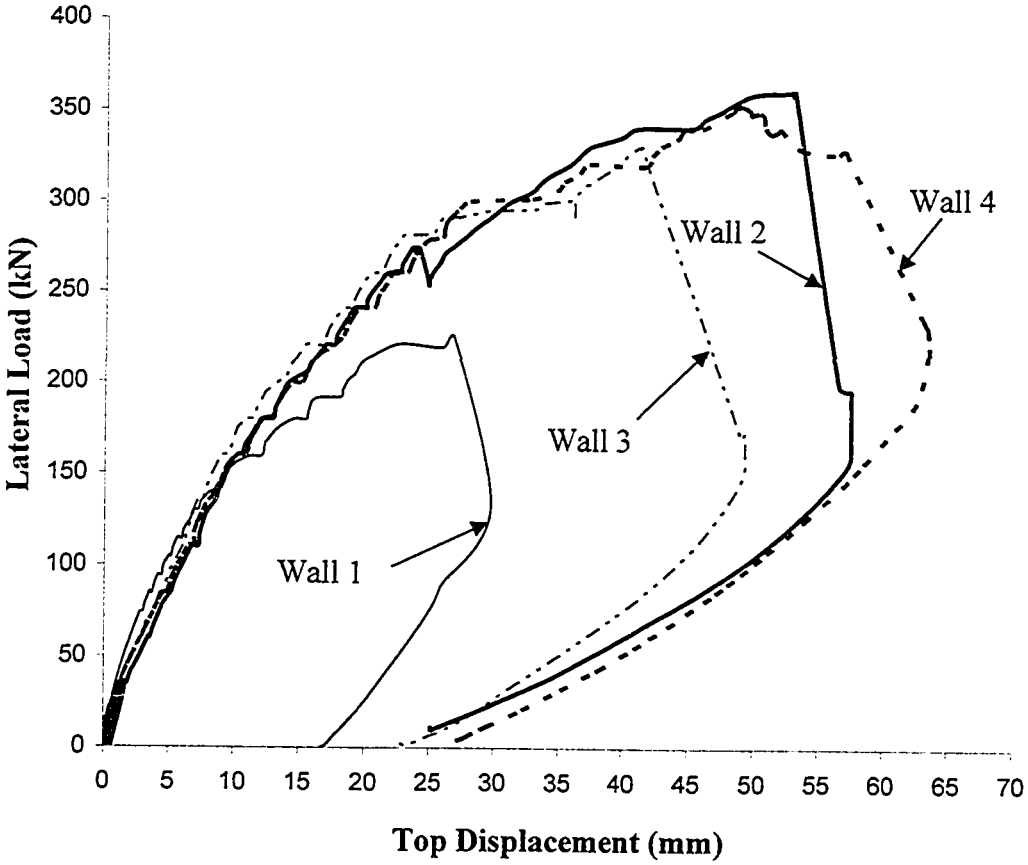

Figure 5-1 Lateral Load Vs. Top Displacement

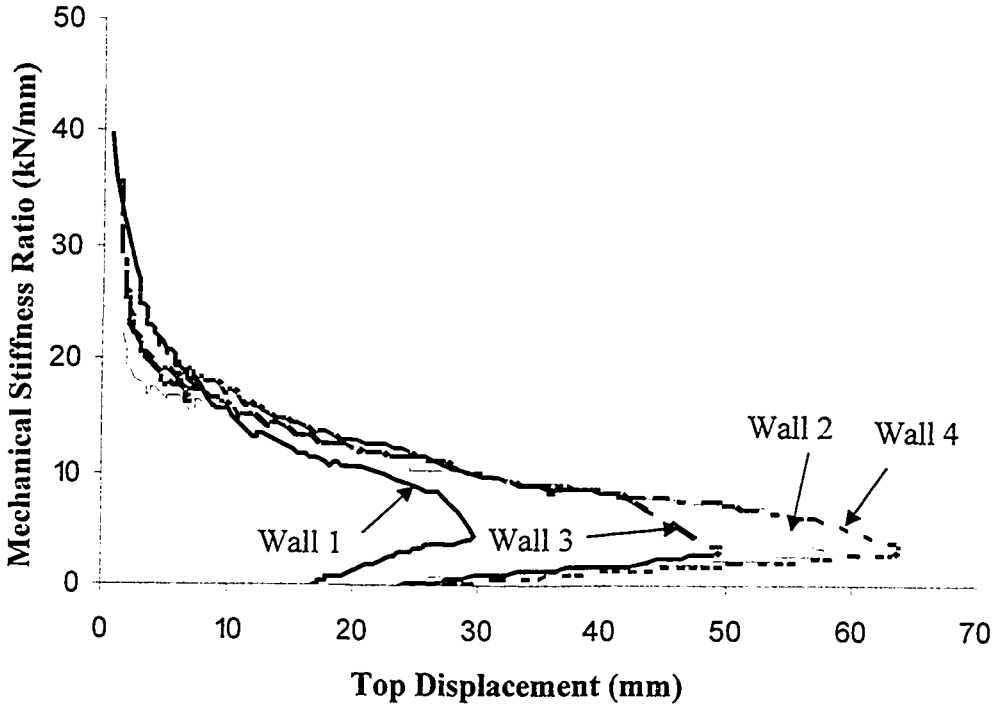

Figure 5-2 Mechanical Stiffness Ratio Vs. Top Displacement

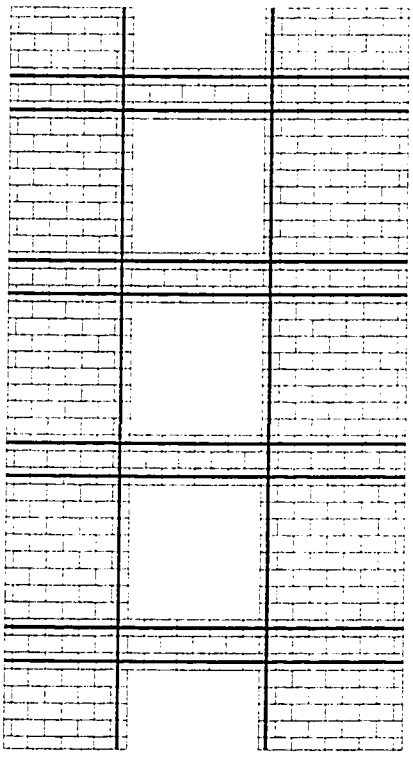

Figure 5-3 Coupled Shear Walls

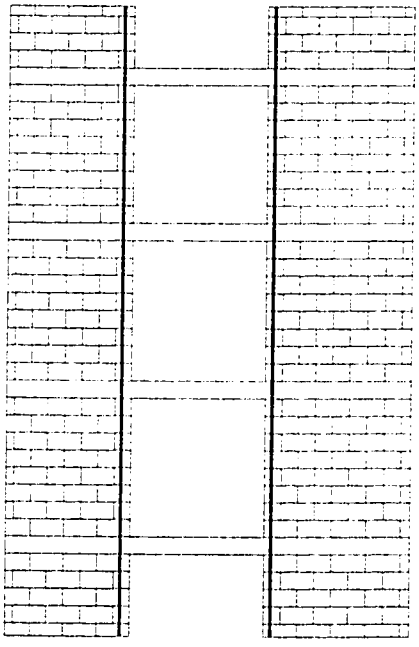

Figure 5-4 Noncoupled Shear Walls

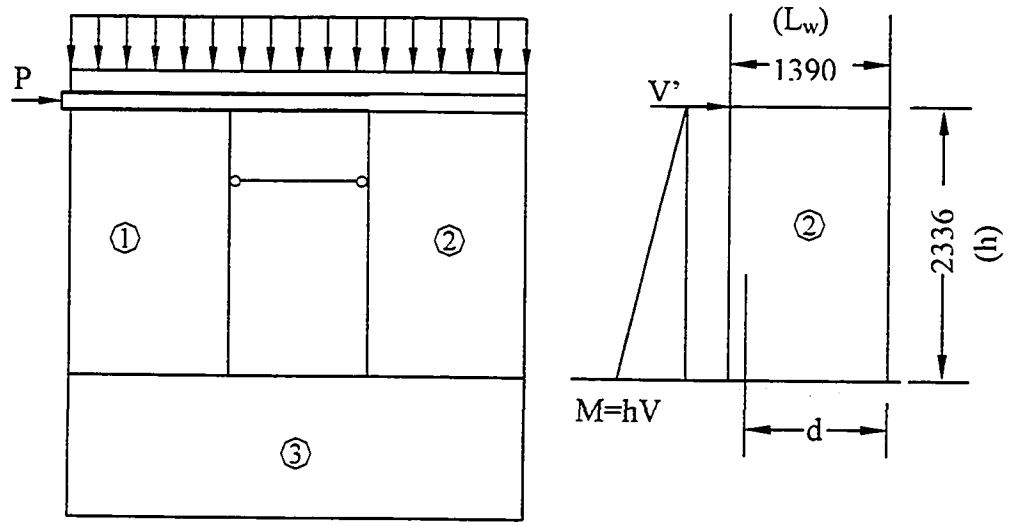

$M/(Vd)=(hV)/(Vd)=h/(0.8L_w)=2.10$

Pier Model (a)

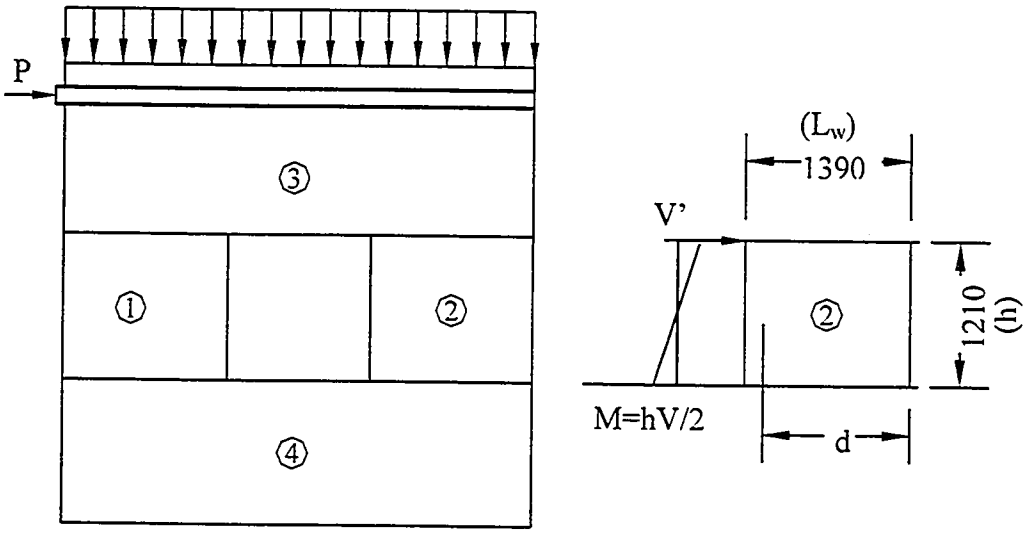

$M/(Vd)=(hV)/[2(Vd)]=h/[2(0.8L_w)]=0.54$

Pier Model (b)

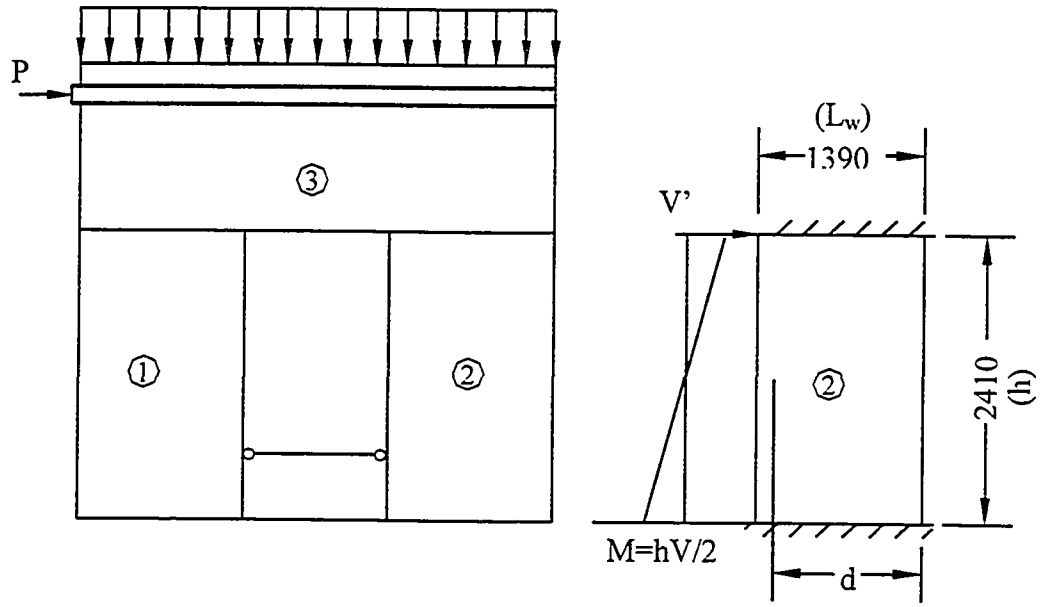

$M/(Vd)=(hV)/[2(Vd)]=h/[2(0.8L_w)]=1.08$

Pier Model (c)

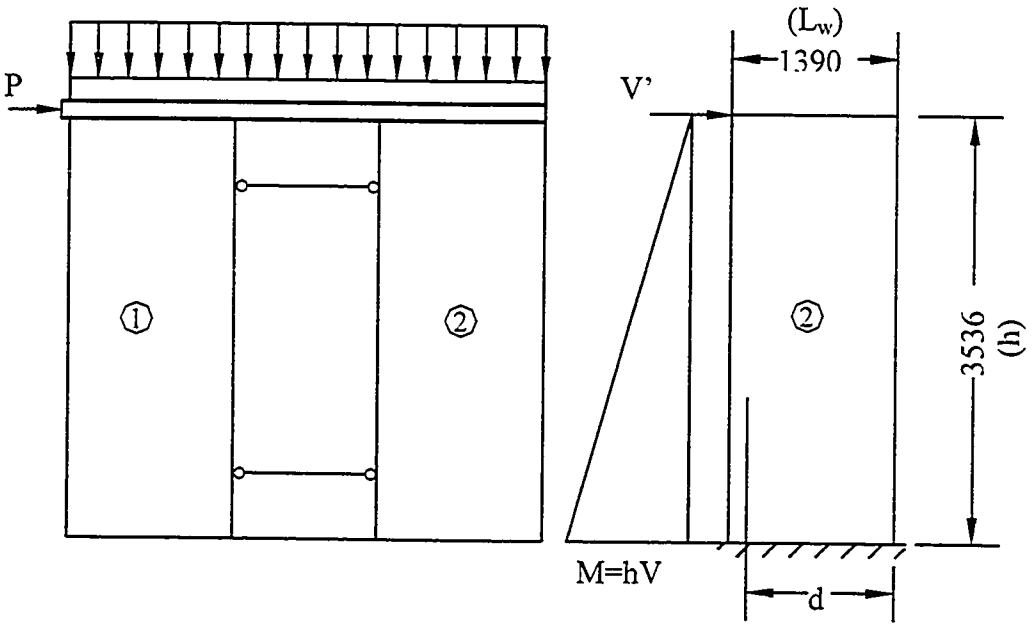

$M/(Vd)=(hV)/(Vd)=h/(0.8L_w)=3.18$

Pier Model (d)

Figure 5-5 Pier Models for Load Capacity Calculation

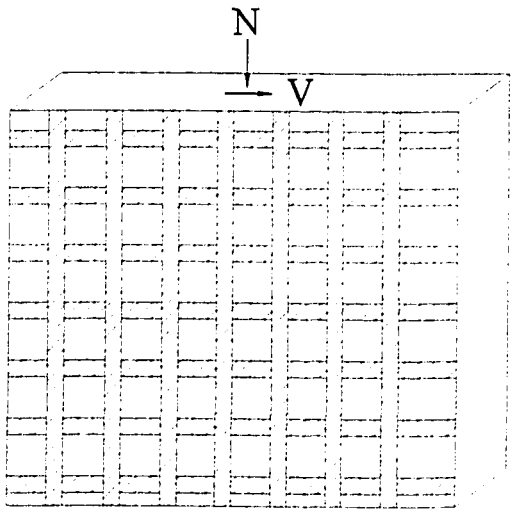

Figure 5-6 FRP-Strengthened Masonry Wall Subjected to In-plane Shear with Axial Force

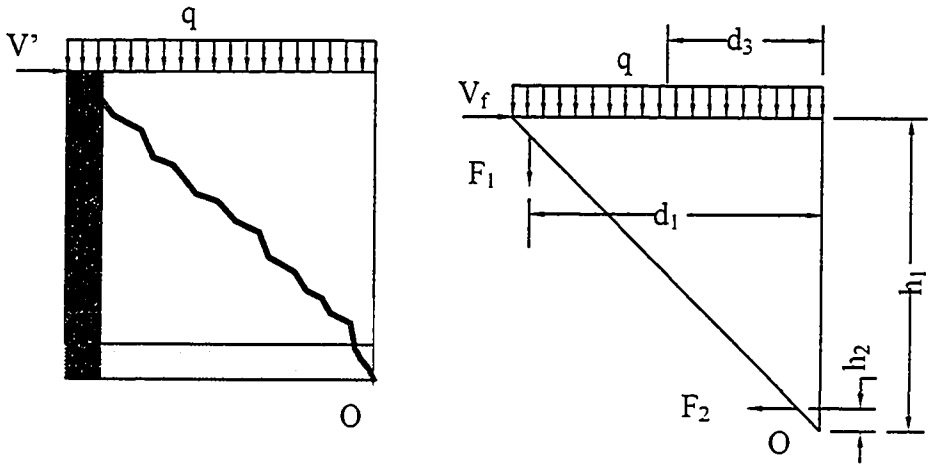

Free-Body of a Cracked Pier 2 in Model (b) for Wall 2 and Wall 3

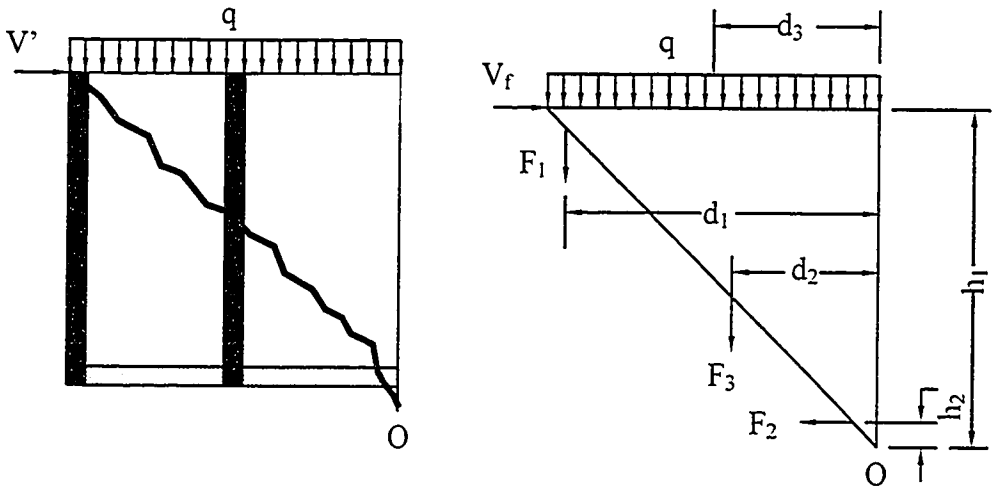

Free-Body of a Cracked Pier 2 in Model (b) for Wall 4

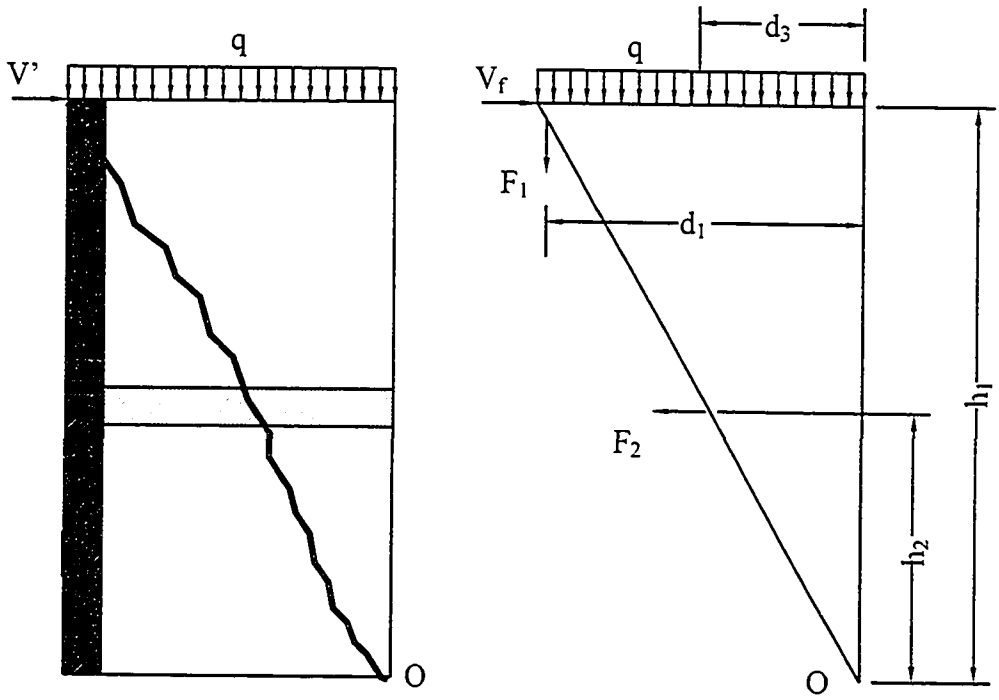

Free-Body of a Cracked Pier 2 in Model (c) for Wall 2 and Wall 3

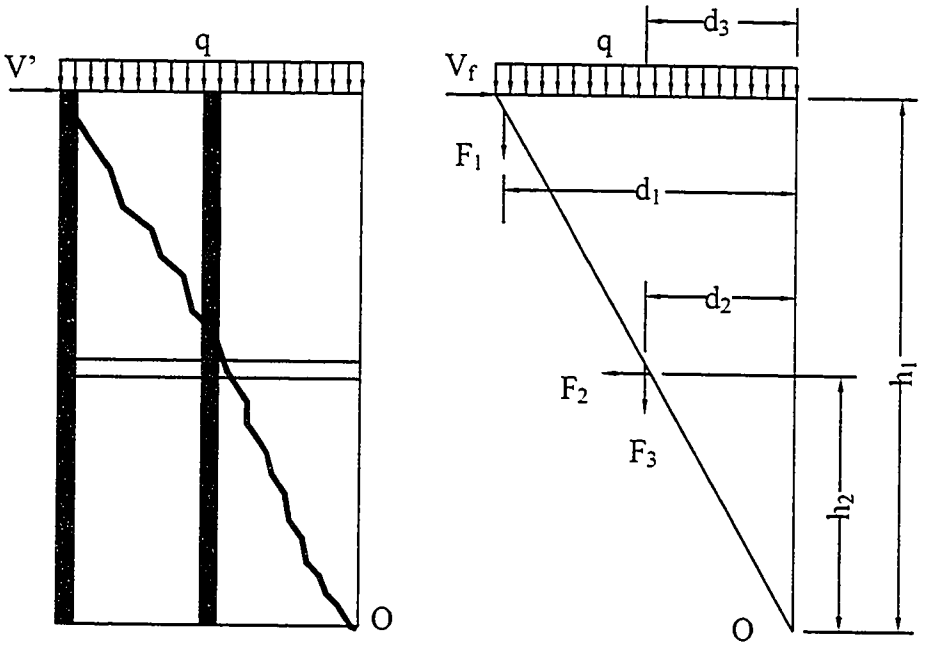

Free-Body of a Cracked Pier 2 in Model (c) for wall 4

Figure 5-7 Analytical Model to Estimate Shear Contribution of CFRP Sheets using Proposed Method

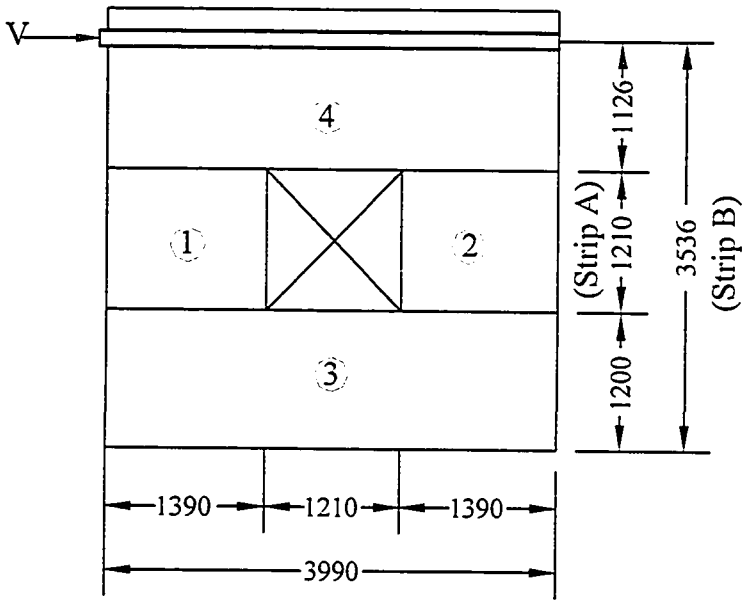

Figure 5-8 Pier Model for Stiffness Calculation

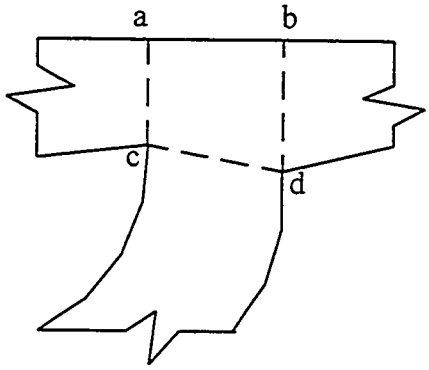

Figure 5-9 Deformation at Pier-spandrel Junction

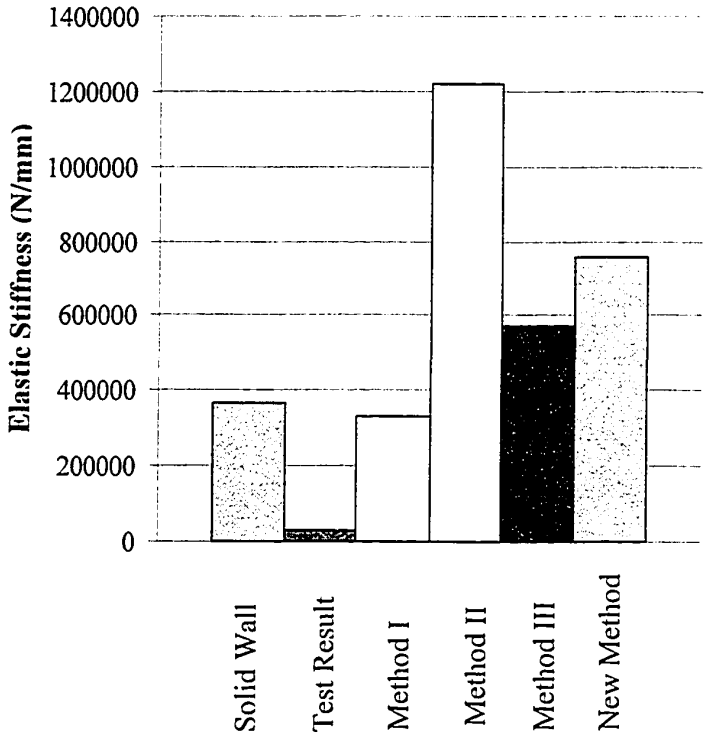

Figure 5-10 Predicted and Experimental Wall Stiffness

6. SUMMARY, CONCLUSIONS AND RECOMMENDATIONS

6.1 Summary

Many of existing masonry buildings has suffered from the accumulated effects of inadequate construction techniques and materials. Compared with traditional retrofitting techniques, the application of FRP reinforcement is an effective and convenient method. Literatures demonstrated that the structural capacity (strength, ductility and stiffness) of shear walls could be significantly increased when strengthened with FRP composites. However, there is a lack of information about the behavior of perforated masonry shear walls strengthened with FRP. In order to obtain the beginning information or data about this subject, an experimental program was presented in this thesis.

Four full-scale wall specimens were designed and constructed. Wall 1 was constructed without a retrofit scheme and acted as the reference wall. Walls 2 through Wall 4 were strengthened with externally epoxy-bonded CFRP Sheets. All walls had identically designed geometric, material and strength properties. Each wall specimen was tested under combined uniformly distributed constant vertical load and monotonic in-plane lateral load. Two major parameters were investigated: amount and layout of CFRP Sheets.

The behavior of walls during the testing was studied based on their lateral load versus top displacement response, failure mode, cracking patterns, stiffness and ductility. Finally several mechanical models were discussed to evaluate the load capacity of un-strengthened perforated masonry shear wall and estimate the shear contribution of CFRP Sheets to the strengthened masonry walls perforated by an opening. Compared with the test results, these mechanical models, available and derived from the analysis for solid shear walls, cannot provide a good evaluation of the effects CFRP Sheets on the perforated masonry shear walls. Four methods were also studied to predict the wall stiffness.

6.2 Conclusions

The experimental results indicate that the strengthening method of perforated masonry shear walls with CFRP Sheets is convenient, effective and reliable. Compared with the un-strengthened wall, the load capacity and ultimate displacement of the walls strengthened with CFRP Sheets are increased remarkably. The CFRP Sheets also improves the effective stiffness of walls at the later loading stage.

The overall behaviours of specimens were similar. All walls failed in a shear mode and the wall behaviours were governed by diagonal tensile cracking. While the strengthened walls have a higher first crack load comparing with the control wall. The mechanical stiffness was shown to continually degrade as the lateral loads increased and cracks developed. It's noticeable that Wall 4 was more stable after reaching the load capacity and showed more ductile than the other walls. This is a very important factor to avoid injuries or loss of human life.

Test observations showed approximately identical CFRP Sheets failure modes for all strengthened wall specimens. Except for the tensile rupture of vertical CFRP strips at the top corner of opening where the major diagonal cracks went through the whole wall thickness, debonding of CFRP strips occurred at the end of horizontal CFRP strips at the bottom of opening. The amount of CFRP Sheets influenced the increase of load capacity and ultimate displacement of walls, but not proportionally. The layout of CFRP Sheets greatly affected the ductility behaviour of walls, However, the effects of layout of CFRP Sheets to lateral load capacity of perforated masonry shear walls was small.

Results of mechanical models derived from the solid shear structures showed that an appropriate mathematical method to evaluate the behaviour of perforated masonry shear walls strengthened with CFRP Sheets should analyze the whole wall considering the coupling effect. It's not reasonable to simply add the contribution of CFRP to the strengthened walls like the action of steel reinforcements.

6.3 Recommendations

Strengthening of opening for masonry shear walls using externally epoxy-bonded CFRP Sheets has been confirmed to be a highly effective technique in this research. To develop a full understanding of the strengthened perforated masonry shear wall, further work is required.

All test specimens in this experimental program had the same grid set-up CFRP arrangement. Since test crack patterns show that diagonal arrange of CFRP reinforcement is predicted more effective retrofit scheme, it is recommended to test walls with diagonal configuration of CFRP reinforcement.

Since peeling-off (debonding) failure is proved to be important and common failure model for CFRP reinforcement, a peeling-off test is required to evaluate the values of shear and normal (peeling-off) stresses at the masonry-CFRP interface. Moreover, further tests need to be carried out to investigate the tension stiffening effect of the sheets on the unit shear strength of masonry.

In this experimental program, strains were obtained using Demec instrument and thus data inaccuracy of strains were introduced because of the factors: reading error and measurement error. Furthermore, this measurement method cannot record all important or critical strain behaviours during testing including strains at failure. Moreover, there is a lack of strain information about steel reinforcement rebars. To understand the effects of CFRP Sheets and steel reinforcement rebars on the capacity of walls, more strain data are required.

Mechanical models to estimate the load capacity of walls divided the perforated masonry walls into several isolated piers and neglected the effects of coupling system. Further research in mechanical models should consider the perforated wall as one wall panel using equivalent frame model. Moreover an accurate mechanical model should account for the positive effect of extra concentrated load from the external hold-down system.

Finally, a finite element study should be performed to predict the behaviour of wall specimens. An accurate finite element study should be based on enough information about each material and bond characteristics between masonry surfaces and CFRP Sheets.

REFERENCES

Alberta, M.L., Cheng, J.J. R., and Elwi, A.E. (1998). "Rehabilitation of Unreinforced masonry Walls with Externally Applied Fibre Reinforced Polymers", Structural Engineering Report No.226, Department of Civil & Environmental Engineering, University of Alberta, Edmonton.

American Society for Testing and Materials Standard D3039/D 3039M-00 (2000). "Standard Test Method for Tensile Properties of Polymer Matrix Composite Materials". American Society for Testing and Materials, West Conshohocken, Pennsylvania.

American Society for Testing and Materials Standard A 370-02 (2002). "Standard Test Methods and Definitions for Mechanical Testing of Steel products". American Society for Testing and Materials, West Conshohocken, Pennsylvania

Amos, K.A.and Waugh, L.M. (1986). "Behaviour of Perforated Masonry Shear Panels in A Steel Frame". The 4TH Canadian Masonry Symposium, University of New Brunswick, Vol.2,1986, pp.569-580.

Belarbi, A., Silva, P.F. and Li, T. (2003). "An Experimental Evaluation of In-Plane URM Walls Strengthened with FRP Composites", The Ninth North American Masonry Conference, June 1-4, 2003, Clemson, South Carolina, USA, pp. 1101-1112.

Building Code Requirements for Masonry Structures (ACI 530-02/ASCE 5-02/TMS 402-02). ISBN 1-929081-13-8 (2002). Masonry Stands Joint Committee (MSJC)

Canadian Standards Association A179-94 (1994). "Mortar and Grout for Unit Masonry". Canadian Standards Association, Rexdale(Toronto), Ontario.

Canadian Standards Association A165 Series-94 (1994). "CSA Standards on Concrete Masonry Units". Canadian Standards Association, Rexdale(Toronto), Ontario.

Canadian Standards Association CAN/CSA-A369.1-M90 (1990). "Method of Test for Compressive Strength of Masonry Prisms". Canadian Standards Association, Rexdale(Toronto), Ontario.

Corradi, M., Borri, A. and Vignoli, A. (2002). " Strengthening Techniques tested on Masonry Structures Struck by the Umbria-Marche earthquake of 1997-1998". Construction and Building materials, Vol.16, Issue 4, June 2002, pp. 229-239

Corrêa, M.R.S., and Page, A.W. (2003). "Experimental Study of Masonry Walls with Openings". The ninth North American Masonry Conference, Clemson, South Carlina, USA, June 1-4, 2003, pp.896-907

Cosenza, E., Manfredi, G. and Nanni, A. (2001). "Composite in Construction: A Reality". American Society of Civil Engineers, Reston, Virginia, pp.203-212.

Ehsani, M.R., Saadatmanesh, H. and AI-Saidy, A. (1997). "Shear Behaviour of URM Retrofitted with FRP Overlays". Journal of Composites for Construction, Vol.1, No.1, February 1997, pp.17-25.

EI-Shafie, H., Hamid, A., Okba, S. and EI-Sayed, N.(1996). "Masonry Shear Walls with Openings: State-of-The-Art Report". The Seventh North American Masonry Conference, South Bend, Indiana, USA, June 2-5, 1996, pp. 638-653.

Foo, S., Naumoski, N. and Cheung, M. (2003). "Research and Application of Seismic Retrofit Technologies –Experience of PWGSC". Annual Conference of the Canadian Society for Civil Engineering, Moncton, Nouveau-Brunswick, June 4-7,2003, pp.GCF-501-1-10.

Ghanem, G.M., Essawy, A.S. and Ahmad A. Hamid (1992). "Effect of Steel Distribution on the Behavior of Partially Reinforced Masonry Shear Walls". The 6TH Canadian Masonry Symposium, Saskatoon, Canada, June 15-17, pp. 365-376.

Glanville, J.I., Hatzinikolas, M.A. and Ben-Omran, H.A. (1996). "Engineering Masonry Design", CSA Standard S304.1, Winston House, Winnipeg.

Hendry, A.W. (1991). "Reinforced and Prestressed Masonry". Concrete Design & Construction Series, New York, the United States

Hiotakis, S., Lau, D.T., London, N., Lombard, J.C. and Humar, J.L. (2003). "Retrofit and Repair of Reinforced Concrete Shear Walls with Externally Epoxy Bonded Carbon Fibre Sheets". Annual Conference of the Canadian Society for Civil Engineering, Moncton, Nouveau-Brunswick, June 4-7,2003, pp.GCU-523-1-10.

Hollaway, L. (1993). "Polymer Composites for Civil and Structural Engineering". Blackie Academic & Professional, Bishopbriggs, Glasgow.

Kuzik, M.D., Elwi, A.E., Cheng, J.J.R. (1999). "Cyclic Behaviour of Masonry Walls with GFRP". Structural Engineering Report No. 228, Department of Civil & Environmental Engineering, University of Alberta, Edmonton.

Lourenco, P.B. and Rots, J.G.(1997). "Multisurface Interface Model for Analysis of Masonry Structures". Journal of Engineering Mechanics, July 1997, pp. 660-668.

Matthys, J.H. (2002). "Masonry Designers' Guide" (Third Edition). The Masonry Society, Bulder Colorado, America.

Mobeen, S.S. (2002). "Cyclic Tests of Shear Walls Confined with Double Head Studs". Thesis in Structural Engineering, University of Alberta, Edmonton, Alberta.

Qamaruddin, M., Al-Oraimi, S. and Hago, A.W. (1998). "New Method for Lateral Stiffness of Shear Walls with Openings". The 8Th Canadian Masonry Symposium, Jasper, Alberta, May31-June 3, pp.435-446.

Taly, N. (2001). "Design of Reinforced masonry Structures". McGraw-Hill, New York SanFrancisco Washington, D.C. Auckland Bogotá.

Triantafillou, T.C. (1998). "Composites: A New Possibility for the Shear Strengthening of Concrete, Masonry and Wood". Composites Science and Technology, Vol.58, Issue 8, August 1998, pp.1285-1295.

Triantafillou, T.C. and Member, ASCE (1998). "Strengthening of Masonry structures Using Epoxy-Bonded FRP Laminates". Journal Of Composites For Construction, Vol. 2, No. 2, May, 1998. pp. 96-104.

Valluzzi, M.R., Tinazzi, D. and Modena, C. (2002). "Shear Behaviour of Masonry Panels Strengthened by FRP Laminates". Construction and Building Materials, Vol.16, Issue 7, October 2002, pp 409-416.

Zhao, T., Xie, J. and Li, H.J.(2003). "Strengthening Of Cracked Concrete Block Masonry Walls Using Continuous Carbon Fibre Sheet", The 9th North American Masonry Conference, June 1-4, 2003, Clemson, South Carolina, USA, pp. 156-167.